Universidade de Brasília
Instituto de Geociências
Programa de Pós-graduação em Geologia

Processos de Enriquecimento de Magnetita em Depósitos de Fe-Skarns do Núcleo Arqueano São José do Campestre, Rio Grande do Norte, Nordeste do Brasil

Magnetite Enrichment Processes in Fe-Skarns Deposits of the Archean Nucleus of São José do Campestre, Rio Grande do Norte, Northeast of Brasil

Heriscarth Marcell Dantas Pinheiro

Dissertação de Mestrado Nº 497

Orientador: Prof. Dr. Elton Luíz Dantas

Brasília, 14/09/2022

Universidade de Brasília
Instituto de Geociências
Programa de Pós-graduação em Geologia

Processos de Enriquecimento de Magnetita em Depósitos de Fe-Skarns do Núcleo Arqueano São José do Campestre, Rio Grande do Norte, Nordeste do Brasil

Magnetite Enrichment Processes in Fe-Skarns Deposits of the Archean Nucleus of São José do Campestre, Rio Grande do Norte, Northeast of Brasil

Heriscarth Marcell Dantas Pinheiro

Dissertação apresentada ao Programa de Pós-Graduação em Geologia – Instituto de Geociências – IG da Universidade de Brasília – UnB como requisito parcial obrigatório para a obtenção do título de Mestre em Geologia.

Área de concentração: Geologia Econômica e Prospecção

Orientador: Prof. Dr. Elton Luíz Dantas

Comissão Examinadora:

Prof. Dr. Elder Yokoyama (IG/UnB);
Prof. Dr. David Lopes de Castro (DGeo/UFRN);
Prof. Dr. Maria Emília Schutesky (Suplente IG/UnB).

Ficha catalográfica elaborada automaticamente,
com os dados fornecidos pelo(a) autor(a)

AGRADECIMENTOS

RESUMO

O Núcleo Arqueano São José do Campestre, situado no extremo nordeste do Brasil, possui um contexto tectono-estrutural complexo, apresentando rochas situadas geocronologicamente, que vão desde o paleo-arqueano ao cambriano. Esse ambiente favoreceu a formação de rochas ricas em magnetita com potencial metalogenético. Tais rochas não possuem gênese bem definida e estão associadas ao Complexo Serra Caiada. Em paralelo, técnicas convencionais, especialmente as que envolvem amostragem e análises químicas (rocha total e química mineral), são caras. Nesse sentido, técnicas indiretas como geofísica podem se mostrar bons guias prospectivos, quando associadas a outras informações de cunho geológico. O presente trabalho se propõe a investigar o enriquecimento em magnetita nessas rochas, através de geofísica terrestre. Para entender melhor as relações entre os corpos mineralizados e as rochas encaixantes, técnicas de realce foram aplicadas e um modelo geofísico foi gerado (inversão 3D). As técnicas de realce utilizadas, Amplitude do Sinal Analítico e Primeira Derivada Vertical, forneceram um mapa de intensidades com 3 Domínios estabelecidos, os quais aumentam em intensidade de Oeste para Leste; além de um mapa de estruturas magnéticas, com predominância de direções NE-SW e influência de estruturas rasas. O modelo gerado, acusou dois corpos mineralizados em subsuperfície, *Target* 1 (em forma de dique) e *Target* 2 (em forma de pipa), com direções N-S e NE-SW, respectivamente. Os resultados geofísicos foram associados a informações geológicas (análises petrográficas e observações de campo), físicas (Susceptibilidade Magnética) e geoquímicas (SATMAGAN). Análises petrográficas ajudaram a delimitar e classificar 4 zonas ou faciologias, de acordo com a paragênese mineral progradante: Piroxênio Anfibólio Skarn, Piroxênio Skarn, Granada Piroxênio Skarn e Magnetita Skarn; além de correlacionar as rochas encaixantes com o contexto geológico regional. Análises estatísticas em conjunto com dados geoquímicos (Fe total, CaO, FeO) reforçam as faciologias e apresentam uma zona de alteração hidrotermal - marmorização. Resultados de SATMAGAN apresentaram valores entre 3,68 e 53,68% de magnetita, e medidas de susceptibilidade magnética portátil forneceram valores entre 91,25 e 2.867,25 x 10^{-3} SI para os corpos mineralizados. Tais números são compatíveis com os resultados obtidos na inversão 3D, entre 95 e 1.591,8 x 10^{-3} SI. Os resultados

são similares a parâmetros de literatura, os quais classificam tal mineralização como do tipo Fe-Skarn. Por fim, a integração dos resultados obtidos permitiu a interpretação de retrabalhamento crustal das rochas pré-existentes e remobilização de Ferro proveniente de silicatos, como piroxênios, e óxidos e solubilizados como magnetita em bolsões e lentes, onde o principal conduto seriam diques graníticos.

Palavras-chave: Geofísica Terrestre; Susceptibilidade Magnética; SATMAGAN; Inversão 3D; Núcleo Arqueano São José do Campestre.

ABSTRACT

The Archean Nucleus of São José do Campestre, located in the extreme northeast of Brazil, has a complex tectono-structural context, comprising geo-chronologically situated rocks ranging from Paleo-Arquean to Cambrian. This environment favored the formation of magnetite-rich rocks with metallogenetic potential. Such rocks do not have well-defined genesis and are associated with the Serra Caiada Complex. In parallel, conventional techniques, especially those involving sampling and chemical analyses (whole rock analysis and mineral chemistry), are expensive. In this sense, indirect techniques such as geophysics can prove to be good prospective guides when associated with other geological information. The present work aims to investigate magnetite enrichment in these rocks, through terrestrial geophysics. To better understand the relationships between mineralized bodies and host rocks, enhancement technics were applied and a geophysical model was generated (3D inversion). The enhancement techniques, Analytical Signal Amplitude and First Vertical Derivative, provided an intensity map with 3 established domains, which increase in intensity from West to East; in addition to a map of magnetic structures with predominance of NE-SW directions and influence of shallow structures. The generated model accused two mineralized bodies in subsurface, Target 1 (dike-shaped) and Target 2 (pipe-shaped), with N-S and NE-SW directions, respectively. The geophysical results were associated with geological (petrographic analyses and field observations), physical (Magnetic Susceptibility) and geochemical (SATMAGAN) Petrographic analyses helped to delimit and classify 4 zones or faciologies, according to the prograding mineral paragenesis: Pyroxene Skarn Anfibolium, Pyroxine Skarn, Piroxênio Skarn and Magnetite Skarn; in addition to correlating the host rocks with the regional geological context. Statistical analyses with geochemical data (Total Fe, CaO, FeO) reinforce these zones and present a zone of hydrothermal alteration – marbleization. SATMAGAN results showed values between 3.68 and 53.68% of magnetite, and measurements of portable magnetic susceptibility provided values between 91.25 and 2,867.25 x 10^{-3} SI for mineralized bodies. These numbers are compatible with the results obtained in 3D inversion, between 95 and 1,591.8 x 10-3 SI. Results are similar to published parameters, which classify such mineralization as Fe-Skarn type. Finally, the integration of the

obtained results allows the interpretation of crustal reworking of pre-existing rocks and remobilization of Iron from silicates, such as pyroxenes, and oxides and solubilized as magnetite in pockets and lenses, where the main conduit would be granitic dikes.

Keywords: Ground Geophysics; Magnetic Susceptibility; SATMAGAN; 3D inversion; Archean Nucleus of São José do Campestre

LISTAS DE ILUSTRAÇÕES

<u>Dissertação</u>

<u>Artigo</u>

LISTA DE TABELAS

SUMÁRIO

CAPÍTULO 1 - INTRODUÇÃO

1   INTRODUÇÃO

1.1   Apresentação e justificativa

O Núcleo Arqueano do Maciço São José do Campestre (NASJC), no Nordeste Oriental do Brasil, apresenta um contexto geológico bastante complexo, reunindo em seu empilhamento tectono-estratigráfico, desde rochas antigas (da ordem de 3,4 Ga) a suítes graníticas ediacaranas (entre 630 e 542 Ma). Nesse âmbito, rochas ricas em magnetita ocorrem pertencendo ao Complexo Serra Caiada (Dantas et al., 2004; Roig e Dantas, 2013), que engloba ainda anfibolitos e rochas metabásicas; além de intercalações de níveis de rochas calcissilicáticas com scheelita, mármore e quartzitos micáceos. Trabalhos anteriores em áreas próximas (Moraes, 2020; Abrahão-Filho et al., 2016; Figueiredo, 2012; Silva-Filho, 2012) apresentaram essas rochas ricas em magnetita como Formações Ferríferas Bandadas, porém com uma associação muito próxima a Anfibolitos, Piroxenitos e Mármores, além de variações destas com granada e níveis calcissilicáticos. Essas ocorrências de rochas portadoras de magnetita estão localizadas na porção Centro-Oeste do Núcleo Arqueano de São José do Campestre e são objeto de pesquisa por empresas de Exploração Mineral, ressaltando o potencial metalogenético da região. Estes prospectos se apresentam como lentes ou faixas dispostas internamente em um pacote de rochas que inclui mineralogia diversa composta por predominância de piroxênio, granada, anfibólio e mármores impuros.

Baseado em suas assinaturas geoquímicas, duas hipóteses são sugeridas em relação à origem de Formações Ferríferas da região central do NASJC, a saber: enriquecimento supergênico ou alteração hidrotermal de rochas máficas e granulitos (Abrahão-Filho et al., 2016). Moraes (2020) também estudou as ocorrências de Ferro no NASJC e advoga por duas hipóteses sendo uma delas formações ferríferas modificadas por hidrotermalismo e a outra hipótese atrelada a magnetititos hidrotermais associados a zonas de cisalhamento ou a Fe-Skarns. A hipótese de ocorrência de um depósito de Fe-Skarn será discutida neste projeto.

O presente trabalho se propõe a delimitar e classificar um depósito de Ferro, bem como explicar, através de geofísica terrestre e dados de susceptibilidade magnética, o enriquecimento de magnetita na porção central do NASJC, integrando magnetometria terrestre a relações geológicas de campo

(mapeamento e sondagem diamantada), petrografia, geoquímica de elementos maiores, susceptibilidade magnética portátil e quantificação de magnetita por Análisador por Saturação de Magnetização (SATMAGAN, acrônimo para "*Saturation Magnetization Analyser*") e análise estatística multivariada dos dados.

A organização da dissertação ocorre em três capítulos. O capítulo 1 introduz e apresenta o trabalho, aponta a localização da área de estudo, pontua a metodologia de pesquisa e mostra o contexto geológico regional. O capítulo 2, diz respeito ao artigo *"3D Magnetic modeling applied in the investigation of a small unconventional Fe-Skarn deposit in the extreme NE of Brazil"*, o qual discorre sobre dados geológicos, petrográficos, geofísicos e petrofísicos no depósito de Fe de Bandeiras, Sítio Novo, estado do Rio Grande do Norte. Finalmente, o capítulo 3 aborda as discussões finais e conclusões.

1.2 Objetivos

1.2.1 Objetivo Geral

O objetivo principal deste trabalho é explicar o processo de enriquecimento em magnetita de rochas na porção centro-oeste do Núcleo Arqueano do Maciço São José do Campestre, apresentar uma classificação do depósito mineral, bem como, sugerir uma fonte para a mineralização, utilizando dados geológicos, geofísicos e físicos.

1.2.2 Objetivos Específicos

1. Caracterizar geológica, petrográfica e fisicamente os corpos mineralizados e as rochas encaixantes;

2. Caracterizar faciologicamente o depósito de Ferro através da integração de dados geológicos (mapeamento de superfície, sondagem diamantada e petrografia), geofísicos (levantamento terrestre – Magnetometria) físico (medidas de Susceptibilidade Magnética com dispositivo portátil, em amostras de testemunho de sondagem) e geoquímicos (análises do minério por SATMAGAN);

3. Integrar os dados obtidos para entender as relações entre rochas encaixantes e corpos mineralizados, interações de fluídos e alterações hidrotermais de modo a sugerir um controle para esta mineralização.

1.3 Localização

A área de estudo está localizada a cerca de 90 km a SW de Natal, Capital do Estado do Rio Grande do Norte, NE do Brasil (Figura 1). O acesso é feito pela BR-304 até o trevo no fim da reta Tabajara. A partir daí segue-se pela BR-226 até o município de Tangará onde toma-se a RN-093 com destino a área rural do município de Sítio Novo, mais precisamente na localidade de Bandeira.

Figura 1 – Localização e vias de acesso da área de estudo na base cartográfica do Instituto de Geografia e Estatística do Brasil (IBGE).
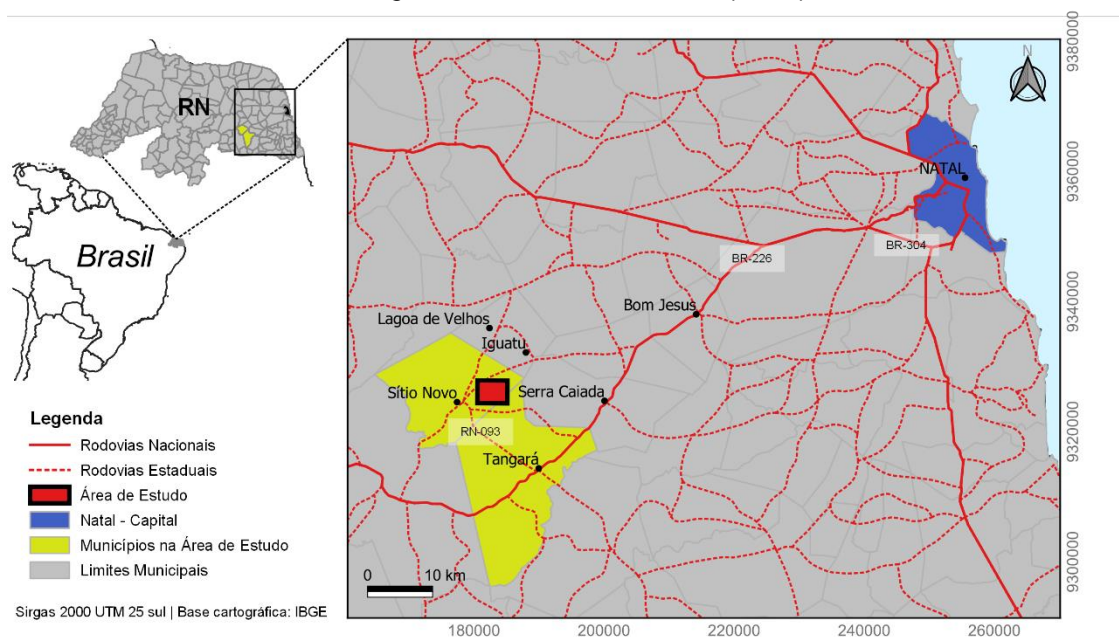
1.4 Materiais e Métodos

1.4.1 Mapeamento

A área foi mapeada em malha com linhas de 4 km, espaçadas a cada 250 metros em escala de 1:25.000. A coleta de informações geológicas se deu ao longo das linhas, com pontos de GPS registrados a cada 100 m ou onde ocorressem afloramentos. A malha foi ajustada para interceptar os corpos mineralizados ortogonalmente.

1.4.2 Dados de Sondagem

Este trabalho possui dados geológicos de 26 furos de sondagem diamantada com profundidade média de 90 m. A malha foi ajustada para interceptar os corpos mineralizados ortogonalmente em atitude média de 132/60°. A partir dos testemunhos de sondagem foram coletadas amostras destinadas a análises químicas e análise de saturação da magnetização, assim como para petrografia.

1.4.3 Petrografia

Para petrografia, foram coletadas 04 amostras de superfície e mais 22 amostras de 04 furos de sonda. As amostras foram extraídas em pontos específicos dos testemunhos de sondagem e afloramentos. Essas amostras foram descritas destacando sua mineralogia, microtexturas e microestruturas, possibilitando uma interpretação em detalhe dos corpos mineralizados e suas interações com as rochas encaixantes.

1.4.4 Analisador por Saturação de Magnetização (SATMAGAN)

O Analisador por Saturação de Magnetização – SATMAGAN (*SATuration MAGnetization ANalayser*) é um equipamento do tipo balança magnética que quantifica indiretamente fases minerais ferro- e ferri-magnéticas. Utiliza o método de pesagem de Faraday em campos magnético e gravitacional. O princípio de funcionamento consiste em determinar o momento magnético de amostras pulverizadas (até 105 μm) através de submissão a um forte campo magnético que permita a saturação magnética do material (Stradling, 1991).

Amostras coletadas nos testemunhos de sondagem foram enviadas ao Laboratório ALS para determinação da quantidade de magnetita por SATMAGAN.

O procedimento compreende a coleta de 20 a 25 gramas da amostra pulverizada e inserção em um medidor de susceptibilidade magnética, em frequência estabelecida para magnetita, utilizando-se de padrões certificados.

1.4.5 Geoquímica

Foram utilizadas análises químicas prévias realizadas em testemunhos de sondagem diamantada, realizadas no Laboratório ALS. O pacote (ME-XRF21u) contempla Elementos maiores (12 elementos) e menores (12 elementos) analisados por Fluorescência de Raios X, além de Perda ao fogo por calcinação (LOI, "Loss On Ignition").

As amostras foram britadas a -3 mm, pulverizadas a 150 micras e retiradas cerca de 2 gramas para confecção de pastilha fundida com Borato de Lítio para enfim serem analisadas por Fluorescência de Raios X (24 Elementos).

A técnica de LOI foi realizada em mufla a 1000°C.

A determinação do FeO por volumetria foi realizada coletando 1 g da amostra pulverizada e digerida por uma combinação de Ácido Sulfúrico e Ácido Clorídrico. Tal solução contendo Ferro ferroso é titulada em um recipiente com uma mistura de Ácido Sulfúrico, Ácido Ortofosfórico e Ácido Bórico com Dicromato de Potássio.

As análises químicas dos analitos Fe total, CaO e FeO foram utilizadas na correlação com dados Petrográficos, de Sondagem, de Susceptibilidade e de porcentagem de magnetita por Satmagan.

1.4.6 Susceptibilímetro Portátil KT-20

Medidas de Susceptibilidade Magnética foram realizadas utilizando um dispositivo portátil KT-20. O Susceptibilímetro KT-20 possui as funções de coleta de susceptibilidade magnética e quantifica a porcentagem de magnetita na amostra. Possui ainda, funções de medidas pontuais e por varredura. A configuração também permite que se escolha entre o modo *Borehole* (furo de sonda), agrupando pontos em uma sequência e em determinados intervalos, que também podem ser selecionados no menu do dispositivo.

As medidas foram coletadas em espaçamento de 20 em 20 centímetros, no método "*Borehole*/*point*", utilizando o diâmetro do furo (Ø=69 mm) e a unidade 10^{-3} SI.

1.4.7 Análise Estatística

Uma Análise Exploratória de Dados foi divulgada apresentada como tabelas estatísticas e gráficos como scattergrams e boxplots. Procedimentos técnicos estatísticos de regressão linear múltipla - MLR (Landim, 2011) foram aplicados com o objetivo de testar os níveis de dependência cumulativa de suscetibilidade magnética (k), contra as concentrações de Fe total, FeO, óxido de cálcio (CaO) e o teor de magnetita (Mt).

Um modelo estatístico multivariado testou os intervalos.

A relação geral do modelo segue:

$$k = a + b1.Fetotal_\% + b2.FeO_\% + b3.CaO_\% + b4.Mt_\% + error \text{ (Equação 01).}$$

Testes probabilísticos paramétricos foram executados para avaliar a adequação do modelo, a saber:

I.   Teste de Shapiro-Wilk (Shapiro and Wilk, 1965) para avaliar se os resíduos têm distribuição normal a 95% do nível de confiança.

II.   além disso, teste de variância ANOVA (Storch and Zwiers, 2003) para avaliar o nível de significância dos parâmetros estimados a 95% do nível de confiança para cada variável independente.

Ambos os testes foram realizados no software© R, v. 3.6.0.

1.4.8 Magnetometria Terrestre

O presente trabalho faz uso de dados de levantamento de magnetometria terrestre, realizado pela Geo Téc Estudos Geológicos Ltda em abril de 2014. Foram utilizados dois magnetômetros GSM-19 v6, sendo um instalado em uma estação base, com medições cíclicas de 10 segundos, e o outro como unidade móvel (estação rover) para aquisição de dados ao longo das linhas de pesquisa com resolução de 0,01 nT e faixa entre 20.000 e 95.000 nT. O levantamento foi realizado com espaçamento de 200 m entre as linhas e a direção foi no sentido NW-SE (310 Az) (Figura 2). As medições foram espaçadas a cada 10 metros. A altura média do sensor era de 2 m e era orientada na direção E-W.

Figura 2 – Mapa de Linhas de Aquisição dos dados de
Magnetometria Terrestre.
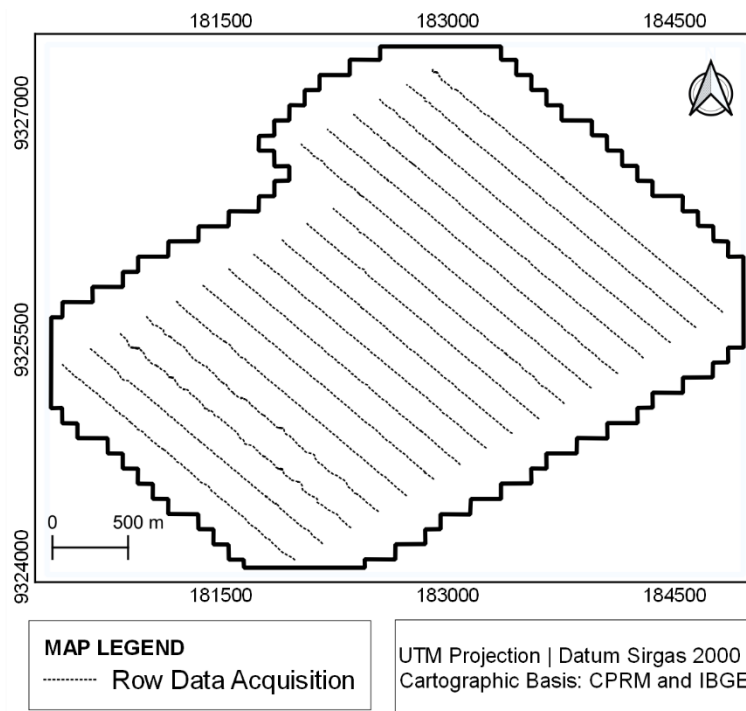
Os dados foram processados para gerar um mapa de Anomalia Magnética reduzido ao polo (Figura 3) no qual foram aplicados filtros de realce de anomalias (Dentith & Mudge, 2014), tais como:

- Amplitude do Sinal Analítico (*Analytic Signal Amplitude*): utilizado para realçar domínios de anomalias magnéticas, em alguns casos, estruturas como falhas;
- Primeira Derivada Vertical (*Vertical Derivative*): utilizado para realçar domínios de anomalias magnéticas e estruturas como falhas e fraturas.

A aplicação dos filtros acima apresentados foi utilizada para destaque das anomalias principais em escala local, assim como as principais estruturas que as influenciam.

O mapa de anomalia magnética também gerou uma inversão por susceptibilidade magnética utilizando VOXI Earth Modelling. Para isso foi gerado um modelo digital de terreno a partir de imagens de satélite *Advancced Spaceborne Thermal Emission and Reflection Radiometer – Global Digital Elevation Model Version 3 (ASTGTM)* obtida do sítio do *Land Processes*

Distributed Active Archive Center (LP DAAC)/United States Geological Survey (USGS) (https://lpdaac.usgs.gov/products/astgtmv003/), e a carta geológica da CPRM/Serviço Geológico do Brasil SB.25-Y-A-I São José do Campestre, escala 1:100.000 (Roig e Dantas, 2013).

Figura 3 – Mapa de Anomalia Magnética reduzido ao polo, com suas linhas de aquisição.
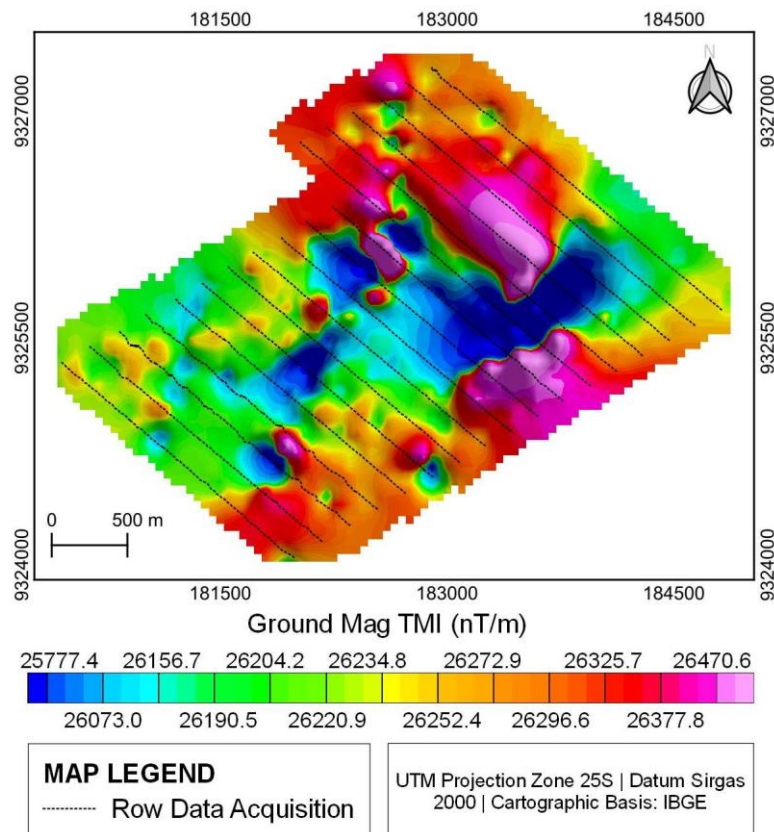
O método de inversão apresentado no trabalho é o de Susceptibilidade Magnética (Magnetic Susceptibility/MS). A inversão cobriu toda a área de estudo e utilizou células com tamanhos X, Y e Z em 100, 100 e 25 m, respectivamente, com profundidade máxima de base para a fonte magnética em 730 m. Uma vez que a inversão foi realizada, um ponto de corte, com base em dados de susceptibilidade magnética de campo e de literatura, foi assumido para geração de iso-superfícies, com valores de k acima de 90 x$^{10-3}$ SI, equivalentes a valores publicados para Fe Skarns. Para centralizar, melhorar a delimitação dos corpos magnéticos e refinar a estrutura de inversão geofísica, foi utilizado o filtro "*Iterative Reweighting Inversion*" + 2 (IRI 2+). Os corpos magnéticos modelados

foram interpretados, quanto a geometria interna, utilizando Gorczyk & Vogt (2018).

Os dados foram tratados por meio de software especializado, *Seequent Oasis Montaj.*

1.5 Contexto Regional

1.5.1 *Província Borborema*

A Província Borborema (Almeida *et al.*, 1977) representa uma grande região do nordeste brasileiro, disposta em mosaicos de blocos crustais de idade arqueana a paleoproterozóica, os quais definem o embasamento gnáissico-migmatítico a granulítico, sotoposto discordantemente a rochas supracrustais paleo a neoproterozóicas de fácies xisto verde a granulito (Jardim de Sá, 1994; Vauchez *et al.,* 1995). Tais blocos foram organizados com base em expressivas descontinuidades crustais e têm seus limites caracterizados por extensas zonas de cisalhamento transcorrentes, associadas a atividade plutônica, geradas durante o Brasiliano (Jardim de Sá, 1994; Medeiros, 2004; Medeiros et al., 2017). Estudos geofísicos indicam que zonas de subducção estão presentes através de estruturas que delimitam os principais domínios da Província, como as zonas de cisalhamento Patos e Pernambuco (Padilha et al., 2014; Correa et al., 2016; Padilha et al., 2016; Padilha et al., 2017; Oliveira & Medeiros, 2018).

Esta província foi bastante afetada pela orogênese Brasiliana ocorrida no final do Neoproterozóico, além de apresentar um elo de correlação com a África ocidental (Faixa Trans-Sahara) (Jardim de Sá, 1994; Brito Neves *et al.,* 2001). Uma complexa cronologia metamórfico deformacional inclui os eventos Jequié (>2,7 Ga), Transamazônico (2,2 – 1,8 Ga), Cariris-Velhos (1,0 Ga) e Brasiliano (620 – 570 Ma) (Almeida et al., 1981; Brito Neves et al., 2014). Assim sendo, estabelecem-se os seus limites geológicos, a sul pelo Cráton São Francisco, a oeste pelas rochas sedimentares paleozóicas da Bacia do Parnaíba e a norte e a Leste por sedimentos costeiros mesocenozóicos (Jardim de Sá, 1994; Brito Neves *et al.,* 2000) (Figura 4).

No modelo atual, o Rio Grande do Norte foi, geologicamente, subdivido nos domínios Rio Piranhas-Seridó e São José do Campestre (Angelim et al., 2006).

Figura 4 – O Domínio São José do Campestre, localizado no contexto da Província Borborema (modificado de Medeiros et al., 2017).
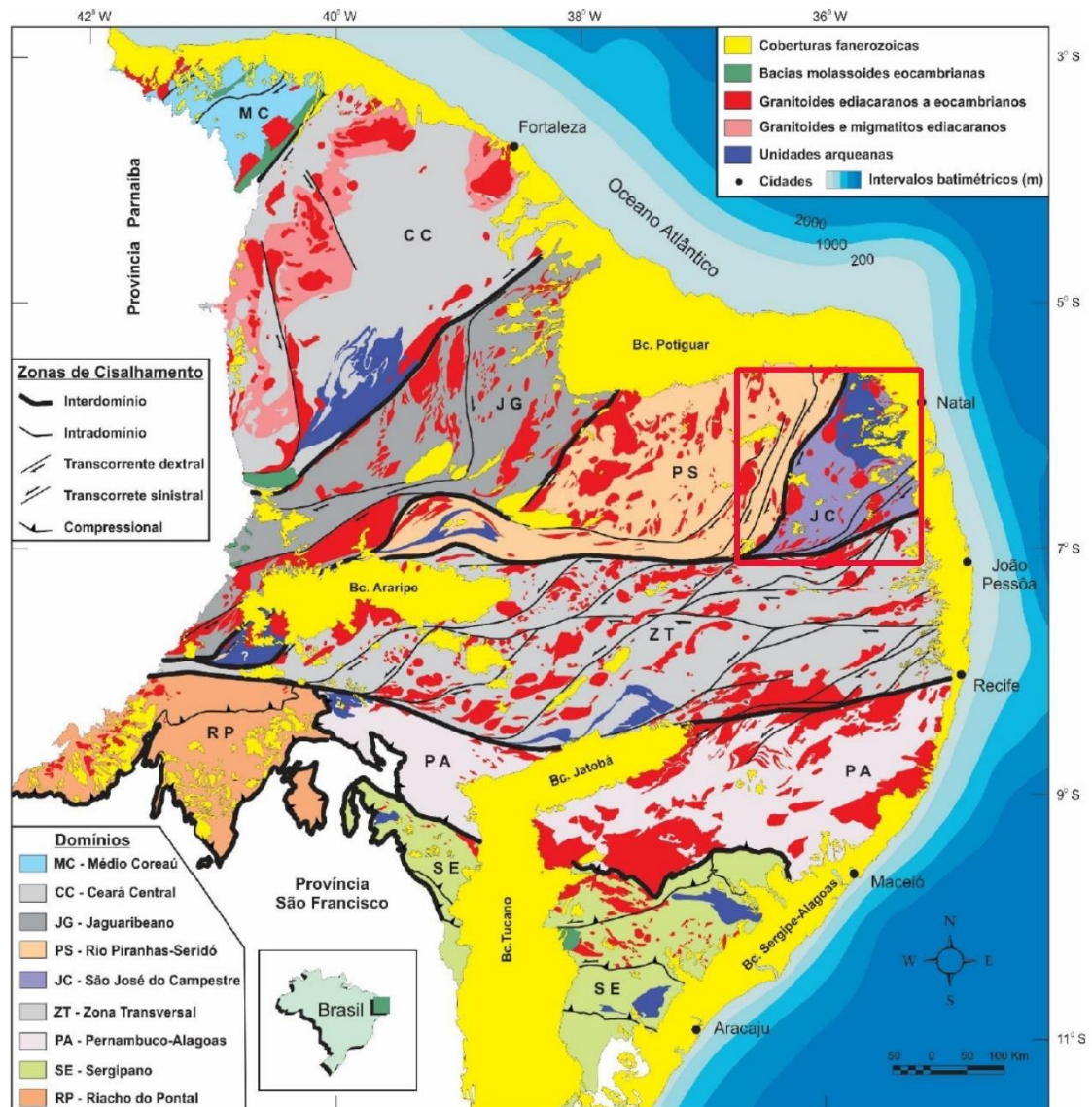
1.5.2 Domínio São José do Campestre (DSJC)

O termo Domínio São José do Campestre (Angelim et al., 2006) é atribuído à porção leste do Domínio Rio Grande do Norte, limitado a sul pela Zona de Cisalhamento Patos, a Oeste pela Zona de Cisalhamento Picuí-João Câmara e a leste e norte por formações fanerozóicas. O arcabouço geral engloba assembléias litoestratigráficas de idades arqueanas a paleoproterozóicas, rochas intrusivas neoproterozóicas relacionadas à orogênese Brasiliana e

rochas vulcânicas básicas associadas ao magmatismo cenozóico de abertura do Oceano Atlântico.

Pelos menos sete eventos de geração de crosta em ambiente convergente são atribuídos à evolução arqueana no DSJC, durante o intervalo entre 3,41 Ga e 2,66 Ga (Dantas et al., 2004, 2013; Souza et al., 2016). Tais eventos de acresção no arqueano acabariam por formar um microcontinente, o qual teria relações com escudos africanos (Arthaud et al., 2008; Dantas et al. 2013, Neves, 2015).

Neves (2011) advoga que, após um período relativamente calmo, importantes eventos de acresção de terrenos ocorreram durante o Paleoproterozóico, no que incluiria o Bloco São José do Campestre-Nigéria, quando da formação do continente Atlantica. Sob essa hipótese, um arco de ilha teria se formado (Neves, 2015) apresentando pulsos magmáticos do tipo cálcio-alcalino de alto K e TTG (Souza et al., 2007; Souza et al., 2016).

Por fim, a Orogênese Brasiliana (ca. 601 e 530 Ma.) atuou de forma expressiva na região retrabalhando as rochas existentes e gerando plutonismo entre 600 Ma e 575 Ma (Brito Neves et al., 2014; Ganade de Araújo et al., 2014; Archanjo et al., 2013; Souza et al., 2016).

1.5.3 Núcleo Arqueano São José do Campestre (NASJC)

Dantas (1997) reconheceu a presença de um núcleo arqueano entre as cidades de Bom Jesus, João Câmara e São José do Campestre, no estado do Rio Grande do Norte (Figura 5). Devido à intensidade deformacional e de metamorfismo, durante o Brasiliano, as litologias são de difícil diferenciação em campo. Portanto, Dantas et al. (2004) definiram as idades dos litotipos, principalmente por estudos isotópicos.

Para Dantas et al. (2004), o reconhecimento e a distinção entre afloramentos particularmente paleoproterozoicos ou arqueanos, na zona de contato com o NASJC, é de difícil caracterização. Assim, evidências de idades arqueanas para o NASJC, derivadas principalmente de estudos isotópicos, possibilitaram o reconhecimento de vários episódios de acreção crustal e pulsos magmáticos refletidos por uma ampla variedade de litologias. Esta litoestratigrafia é apresentada a seguir.

Figura 5 - Mapa Geológico do NASJC (modificado de Dantas et al. 2004 e Abraão Filho, 2016)
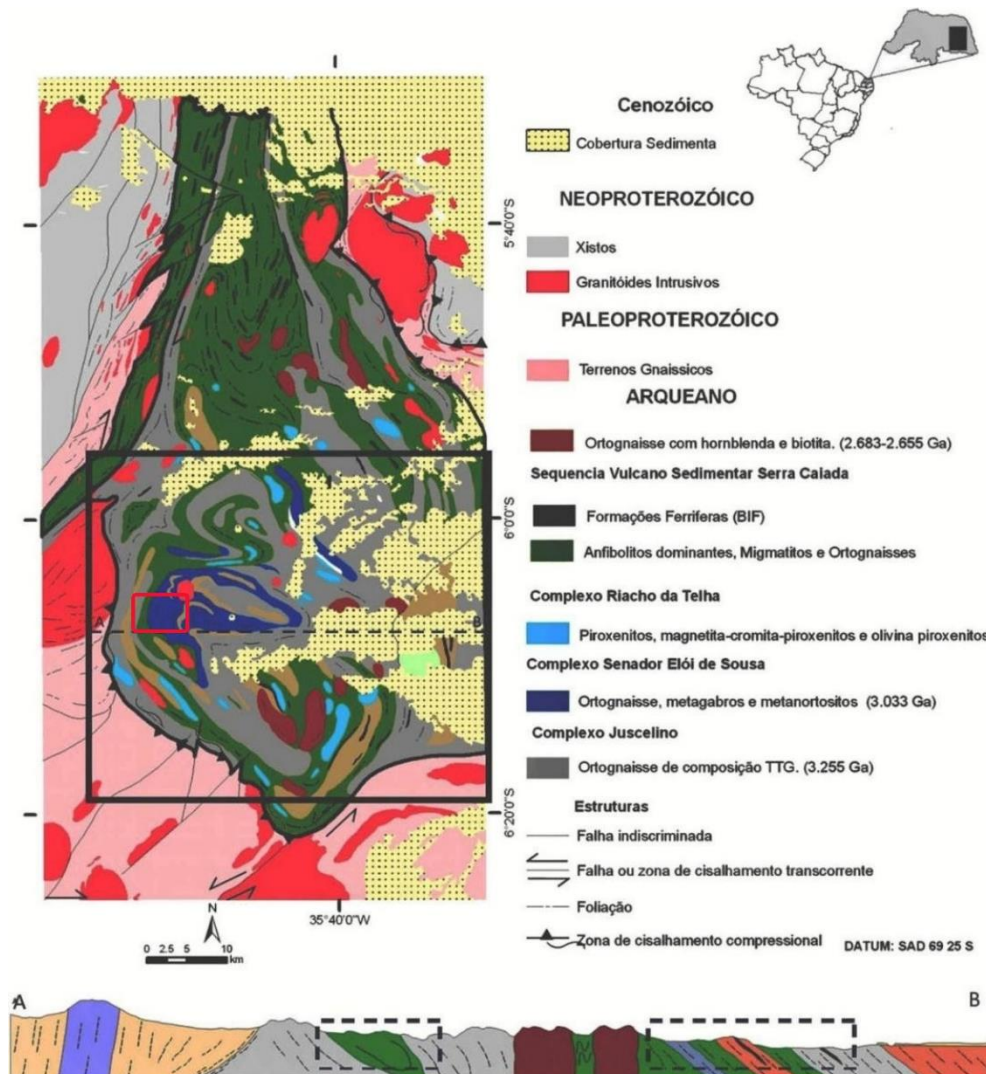
1.5.3.1 Unidade Bom Jesus – 3,41 Ga

Esta unidade é constituída por ortognaisses tonalíticos, ocupando a porção central do NASJC. A mineralogia principal apresenta plagioclásio, quartzo e hornblenda. Encraves máficos estão presentes de maneira boudinada obedecendo a foliação principal. A geoquímica indica predominância metaluminosa com origem relacionada a reciclagem crustal ou fusão parcial de manto enriquecido. Configura como a unidade mais antiga da região apresentando idades de cristalização U-Pb da ordem de 3412 ± 8 Ma (Dantas, 1997; Dantas et al., 2004, 2013; Souza et al., 2016).

1.5.3.2 Complexo Serra Caiada – 3,36 Ga e 3,21 Ga

Litotipo composto por ortognaisses granodioríticos a graníticos, por vezes com xenólitos de ortognaisses tonalíticos. Apresenta mineralogia básica composta por biotita ± diopsídio ± hornblenda (Dantas et al., 2013). A geoquímica apresenta tendência peraluminosa a metaluminosa e sub-alcalina (Dantas, 1997). Dois eventos magmáticos importantes são marcados por datação U-Pb em zircão, em ca. 3,36 Ga e 3,21 Ga (Dantas et al., 2004, 2013; Souza et al., 2016). Estas rochas estão associadas a mármores em um ambiente próximo a fumarolas hidrotermais (Silva Filho, 2012). Abrahão Filho (2016) considera como parte desta unidade uma sequência vulcanossedimentar, de ca. de 2683 Ma, englobando também formações ferríferas bandadas.

1.5.3.3 Complexo Brejinho – 3,4 Ga e 3,2 Ga

Unidade composta por ortognaisses de composição TTG, com biotita ± diopsídio como máficos principais. Datações U-Pb em zircão indicam que este magmatismo ocorreu entre 3333 ± 77 Ma e 3178 ± 8 Ma (Dantas et al., 2004). Valores de εNd(t) são predominantemente positivos (+1,20 a +1,40), indicando um magmatismo juvenil, com idade modelo TDM entre 3,6 a 3,2 Ga (Dantas et al., 2013).

1.5.3.4 Complexo Riacho das Telhas – 3,1 e 3,06 Ga

Constitui uma associação de rochas máficas-ultramáficas intrusivas no embasamento arqueano, com características geoquímicas que incluem magmas tholeiíticos ricos em Fe com assinatura de EMORB (Abrahão Filho, 2016). Engloba piroxenitos, localmente enriquecidos em cromita e magnetita, lherzolitos, wherlitos, gabros e anfibolitos (Jesus, 2011; Abrahão Filho, 2016). Datações U-Pb em zircão, indicam que este magmatismo se estabeleceu entre 3083 ± 17 Ma e 3041 ± 23 Ma (Jesus, 2011; Abrahão Filho, 2016). Valores de εNd(t) levemente positivos (+0,41 a +6,41), indicam um episódio de magmatismo juvenil através de fusão de um manto empobrecido (Jesus, 2011).

1.5.3.5 Complexo Senador Elói de Souza – 3,04 Ga

Compõe uma associação de corpos alongados segundo a direção NW-SE, consistindo em diopsídio-grossulária anortositos, granada

metagabros/noritos, intrudindo os paragnaisses do Complexo Serra Caiada (Dantas et al., 2013). Datações U-Pb em zircão indicam uma cristalização em 3033 ± 3 Ma para estas rochas (Dantas, 1997). A geoquímica aponta um caráter cálcio-alcalino e metaluminoso, com valores de εNd(t) negativos (-2,87) e idade modelo TDM em torno de 3,6 Ga, indicando crosta arqueana retrabalhada (Dantas, 1997).

1.5.3.6 Magmatismo Neoproterozoico

Na região estudada, várias suítes intrusivas compõem o magmatismo neoproterozóico no embasamento Arqueano-Paleoproterozóico, apresentando idades U-Pb em zircão entre 601 Ma e 530 Ma (Archanjo et al., 2013; Souza et al, 2016), com predominância de plutonismo granítico cálcio-alcalino de alto K sob a forma de batólitos (Cavalcante et al., 2014; Antunes, 2000; Dias, 2006). Diques e Stocks de leucogranitos equigranulares com hornblenda, de caráter metaluminoso a peraluminoso, intrudem o NASJC (Dantas, 1997). Os diques estão associados aos estágios finais do evento Brasiliano (Ediacarano), com alojamento em nível de crosta superior (Pinheiro, 2009).

1.5.3.7 Magmatismo Meso-Cenozóico

Durante o Aptiano, a Província Borborema teve sua porção norte atingida por um vulcanismo básico extenso, sob a forma de *plugs*, diques e derrames, relacionado ao desmembramento do supercontinente Gondwana e a abertura do Oceano Atlântico (Misuzaki et al., 2002). O Enxame de Diques Rio Ceará-Mirim marca o início deste magmatismo. Apresentam direção preferencial E-W com inflexão para NE-SW nas proximidades da Bacia do Parnaíba. Possuem caráter toleítico, constituídos por basaltos com plagioclásio, clinopiroxênio e olivina, (Ngonge et al., 2016). Araújo et al. (2001) e Souza et al. (2003) encontraram idades 40Ar/39Ar entre 136 Ma e 111 Ma para este evento magmático. Hollanda et al. (2019) correlacionam a este magmatismo, soleiras de idade similar na Bacia do Parnaíba e sugerem a existência de uma Grande Província Ígnea (*Large Igneous Province* – LIP) na região, a qual denominaram de Província Magmática Atlântico-Equatorial (*Equatorial Atlantic Magmatic Province* – EQUAMP).

1.5.3.8 Skarns e Depósitos de Fe-Skarns

Skarn é uma rocha definida por sua mineralogia rica em minerais calcissilicáticos como granada e piroxênio (Meinert et al., 2005) e, geralmente, são formadas pela substituição de rochas carbonáticas durante o metamorfismo regional ou por processos metassomáticos de contato relacionados a intrusões ígneas (Pirajno, 2009).

Processos na gênese de *skarns* no mundo (Einaudi et al. 1981; Einaudi & Burt 1982; Ray & Webster 1991; Meinert 1992; Meinert et al. 2005; Bucher & Grapes 2011; Hao et al. 2014; Nadoll et al. 2014) e na Província Borborema (Sousa Neto et al. 2008; Parente et al. 2015, Hollanda et al. 2017, Corrêa et al., 2020 e Corrêa et. al, 2021), são relacionados a rochas contendo piroxênio e granada, associados à atividade hidrotermal e metamorfismo de contato por plutonismo (Figura 6). Sumarizando, pode-se dizer que *skarns* se formam a partir de processos de: i) recristalização isoquímica de rochas carbonáticas como resultado de metamorfismo regional ou metamorfismo local a partir do contato com rochas graníticas; ii) reações metassomáticas localizadas entre diferentes litologias, como argilitos e calcários; iii) metassomatismo de infiltração envolvendo fluidos hidrotermais de origem magmática ou metamórfica.

Assembleias minerais, constituídas de piroxênios, granada, anfibólios, quartzo e magnetita na fase progradante e de escapolita, calcita, apatita, biotita e sulfetos na fase retrogradante, são típicas de *skarns*. (Einaudi et al. 1981; Einaudi & Burt 1982; Meinert 1992; Meinert et al. 2005; Frisch & Herd 2010; Bucher & Grapes 2011). As assembleias minerais se dividem em zonas onde a predominância em piroxênios é classificada como distal e a zona rica em granada, se classifica como proximal. Nos ambientes de formação de *skarns*, é comum a correlação espacial e genética entre rochas máfico-ultramáficas, rochas calcissilicáticas, mármores e formações ferríferas (Meinert et al, 2005).

Mineralizações em skarns são variadas em termos de bens minerais (Fe, Cu, Zn, Sn, W, Mo, Au, Elementos Terras Raras etc.) e estão presentes em quase todos os lugares do mundo e em quase todas as eras geológicas. Os depósitos de Fe-Skarn são brevemente apresentados a seguir.

Figura 6 – Tipos de Formação de Skarn (Compilado de Meinert et al., 2020): a) O metamorfismo isoquímico envolve a recristalização e mudanças na estabilidade mineral sem transferência significativa de massa além da escala de grãos. (b) A reação de skarn resulta do metamorfismo de lithologies intercamadas, como xisto e calcário, com transferência de massa entre camadas em escala local (bimetasomatismo). (c) Skarnito resulta do metamorfismo de litologias impuras com alguma transferência de massa local por movimento de fluidos de pequena escala. (d) O skarn metasomático dominado por fluidos é tipicamente grosso e, em grande parte, não reflete de perto a composição ou textura do protólito.
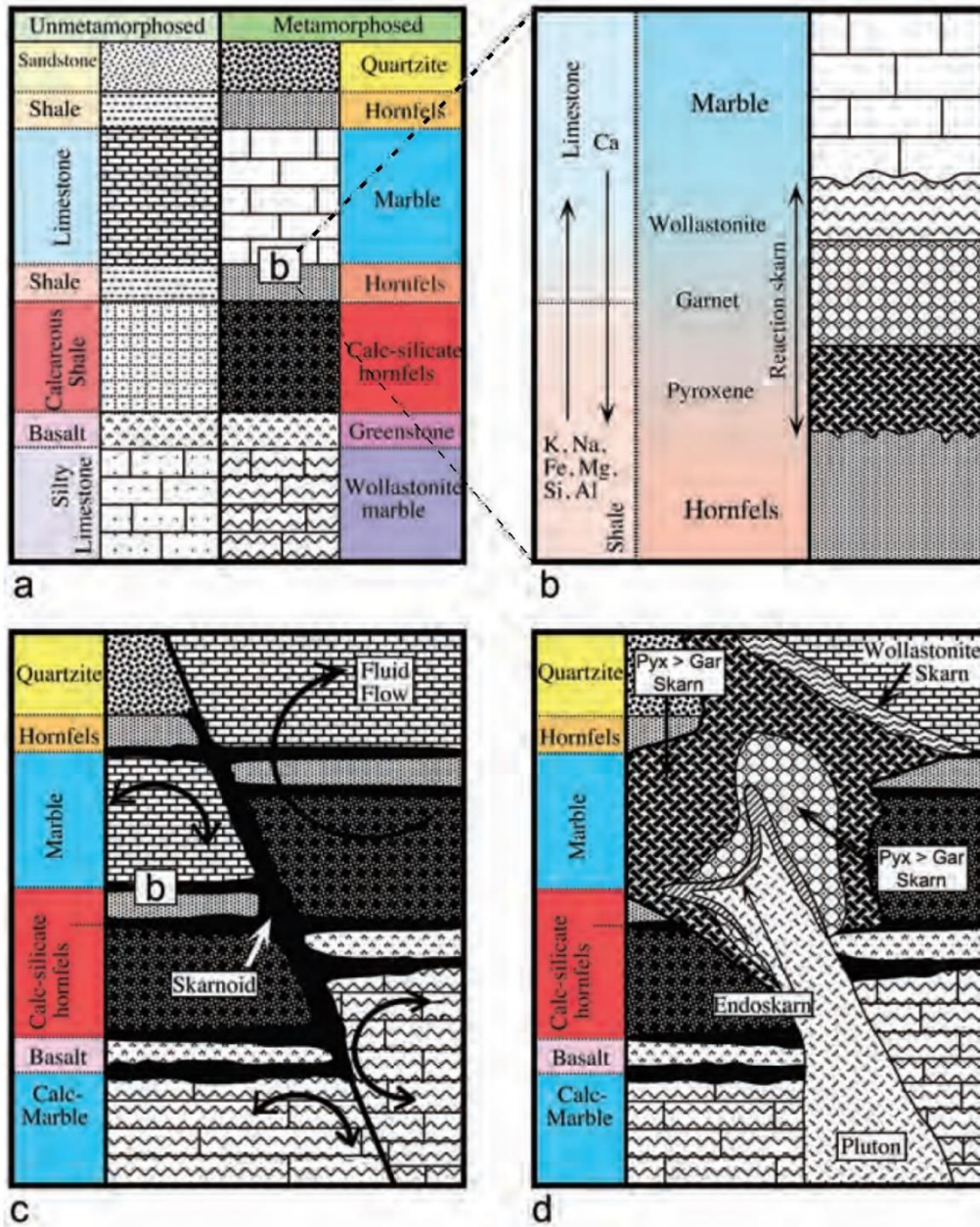
1.5.3.8.1 Depósitos de Fe-Skarn

Os depósitos de Fe-*Skarn* são os maiores depósitos de *Skarn* (Meinert et al., 2005). São minerados principalmente pela quantidade de magnetita e o Fe é

a *comodity* comumente recuperada (Meinert et al., 2005 e Pirajno, 2009). São divididos em Fe-*Skarns* Cálcicos e Fe-*Skarn* Magnesianos (Meinert et al., 2000).

Fe-*Skarns* Cálcicos estão relacionados a plutons enriquecidos em Fe, intrudidos em rochas carbonáticas e rochas vulcânicas, ocorrendo em ambientes de arcos de ilha. As rochas intrusivas são geralmente dioritos, com sienitos e gabros subordinados. Em alguns depósitos, a faixa de Endoskarn pode ser maior que a faixa de Exoskarn (Meinert et al., 2005). A mineralogia básica predominante no estágio progradante consta de ferrosilita, salita, magnetita, granada grandita, epidoto e actinolita, todos ricos em Fe (Purtov et al., 1989). o Estágio retrogradante apresenta assembleia mineral contendo anfibólio, clorita e ilvaita. Magnetita é o mineral minério de maior expressão, por vezes acompanhado de sulfetos em quantidades menores. Em rochas ígneas ocorre alteração com vasta substituição e veios de albita, ortoclásio e escapolita, além do endoskarn (Meinert et al., 2005 e Pirajno, 2009).

Por outro lado, Fe-*Skarns* Magnesianos se apresentam relacionados a uma variedade de plutons (a maioria de composição granodiorítica) formando pequenos *stocks*, diques, brechas e *sills*, e em ambientes tectônicos diversos, sendo a característica unificadora a quantidade de rochas encaixantes ricas em Mg como dolomito (Meinert et al., 2005 e Pirajno, 2009). A assembleia mineral principal nesse tipo de *skarn* não contém muito Ferro, e é composta de forsterita, diopsídio, periclásio, talco e serpentina. O Fe disponível em solução forma magnetita ao invés de andradita ou hedenbergita (Hall et al., 1988). Uma associação mineralógica típica é espinélio-piroxênio-forsterita-calcita, desenvolvendo zonas distintas entre o granito e o mármore fonte.

Sobreposição entre *skarns* cálcicos e *skarns* magnesianos é relatada em muitos depósitos na Rússia (Sokolov e Grigorev, 1977; Aksyuk e Zharikov, 1988). Corpos de natureza estratiforme ricos em magnetita de *skarns* magnesianos podem atingir grandes dimensões em comprimento e espessura e são encontrados na Rússia apresentando teores de 33-35 % de Fe e com reservas de até 234 Mt (Einaudi et al. 1981 e Meinert et al., 2005).

CAPÍTULO 2

3D Magnetic modelling applied in the investigation of a small unconventional Fe-Skarn deposit in the extreme NE of Brazil.

CAPÍTULO 2 - ARTIGO

3D Magnetic modelling applied in the investigation of a small unconventional Fe-Skarn deposit in the extreme NE of Brazil

[1]Heriscarth Marcell Dantas Pinheiro*

http://orcid.org/0000-002-4874-4899

[1]Elton Luiz Dantas

https://orcid.org/0000-0002-7954-5059

[1]Postgraduate Program in Geology (PPG) of University of Brasília – Brasília (DF), Brazil.

* Corresponding author: heriscarth@gmail.com

Abstract

Indirect investigation techniques, such as terrestrial geophysics, can result in an efficient mineral prospecting guide when integrated with geology information, reflecting less expense and low risk of environmental damage. Furthermore, terrestrial geophysics offers a degree of detail that helps in the determination of features and delimitation of small mineral deposits as skarn-type deposits. This study investigates a small unconventional Fe-Skarn deposit in the Archean Nucleus of São José do Campestre (ANSJC – NE Brazil), using magnetic processing modelling techniques to delimit mineralized iron ore bodies and determine their shapes and geometries. Measurements magnetic susceptibility, SATMAGAN data, geochemical data, and petrographic analysis of drill core samples, in addition to field observations, were used in the validation and geological interpretation of the geophysical model. To integrate that information, an exploratory data analysis was released combined to multivariate data analysis. Parametric Probabilistic tests were performed to assess statistical proceedings. Analytical Signal Amplitude and First Derivative of magnetic data show two anomalies with NE-SW direction and 3 main magnetic domains, presenting an increase in intensity from West to East. The magnetic model reveals two mineralized bodies, Target 1 and Target 2, in depth, dipping NW and presenting Dike- and Pipe-shaped, respectively. Target 1 and Target 2 bodies showed Magnetic Susceptibility values (95 - 1591 x 10-3 SI) compatible with data obtained by Magnetic Susceptibility Measurements in fieldwork (91.25 - 2,867.25

x 10-3 SI). These results are comparable to those obtained in the literature for Fe-Skarn deposits. Finally, the integration of geophysical, physical and geological information helps classifying the studied Fe Skarn deposit, attributing to granite dikes participation in the enrichment of magnetite.

Keywords: Archean Nucleus of São José do Campestre, Fe-Skarn, 3D Magnetic Inversion, Magnetic Susceptibility, Ground Magnetic.

1   INTRODUCTION

Several mineral exploration indirect techniques have been used for research in detail of mineral occurrences, such as, aerial, and terrestrial geophysics When integrated with additional geology information, are widely used in this area of activity (e.g., Raju & Kumar 2020, Sheibi et al. 2018, Fries et al. 2020, McGladrey et al. 2017), and may result in a prospecting guide. Geophysics work is generally at low cost compared to other techniques (e.g., excavations, trenching and drill core), and are not destructive, meaning low risk of environmental damage, including reduced bureaucracy with environmental permits.

In cases where the mineral studied has magnetic properties and its occurrences are small, a detail scale is necessary, and ground magnetic data could offer good results allowing the enhancement of magnetic anomalies related to iron ore occurrences. Some techniques like Analytic Signal Amplitude and First Vertical Derivative are very useful, especially when associated with Magnetic Susceptibility Inversion (Miller and Singh 1994; Nabighian et al. 2005; Verduzco, Fairhead and MacKenzie 2004). Magnetic inversion displays itself a tool to assessing some deposits spatially, and it is often used to inform depth of magnetic source (Al Macky et al. 2020; Jiang et al. 2020, Pilkington & Bardossy, 2015). In addition, auxiliary techniques, such as the use of magnetic susceptibility measurements in rocks, can improve the classification of different rock types, and developed correlation tables values of magnetic susceptibility to density measurements (Clark & Emmerson,1991; Hunt et al. 1995; Kim et al. 2015; Khesin et al. 2005). Nielsen & Rasmussen (2002) and Markowski et al. (2006) used these methodologies in several studies, aiming to refine or supporting their classifications.

These techniques when used in isolation have good results. To date some of these techniques are used in mineral exploration in an integrated way, but not all (McGladrey et al. 2017; Fruchting 2017). Saturation Magnetization Analyser (SATMAGAN) which provides a quantitative analysis of Magnetite content, is a technique which is more used in geometalurgical studies, specifically to help understanding the ore features and identifying the best route for mining processes in the future (Anderson et al. 2014, Lischuk et al. 2019 A, Lischuk et al. 2019 B, Pérez-Barnuevo, Lévesque & Bazin, 2018, Shafiei & Shahabpour, 2008). In the early stages of a mining project, SATMAGAN data can, along with Magnetic Suscepbility, Geological and Petrographic data assist in the delimitation of magnetite rich iron ore bodies, and eventual quantification of resources (reserves). Some of these mineralizations may be related to Skarns, in its origin.

Mineral deposits of Skarn are largely known around the world and are explored due to a variety of chemical elements that are related to W, Cu, Pb, Zn, Mo, Au, Ag, U, REE, F, B, Sn and Fe. Fe-skarns can be found in Archean terrains (Mueller 1997), which genesis are related to be formed during regional or contact metamorphism through metasomatic processes involving fluids of magmatic or regional metamorphic events, (Meinert et al. 2005). Diagnostic features of these deposits include a peculiar zonation in the distal phase (exoskarn) and proximal phase (endoskarns), where the main mineralization is present; The mineral paragenesis of these rocks includes garnet, pyroxenes, and wollastonite in progradational stages; whereas in the retrogradational phase, amphibole, chlorite, idocrase, or a pyroxene can also occur (Meinert 1992; Barton & Johnson, 1996).

The use of geophysic studies in this type of deposit allows identifying and delimiting mineralized zones, body size, geometry, and depth of sources (Yang et al, 2011; An et al. 2018, Sun & Chen 2016; Mazhari et al. 2017). Despite the existence, in the international literature, of these studies in mineral deposits of the Skarn type, most are performed by aerial surveys, which does not offer good detail.

Generally, studies of detail are restricted because they are onerous. These studies use local scales for metallogenetic, and prospective

research aimed at mining. In this context, Ground magnetic surveys employed systematically (taking measures in regular grid) provides good results about spatial evaluation of mineral deposits. In addition, when associated with to field data such as sampling and mapping, among others, it can serve as a prospective guide (e.g., Pereira et al. 2019, Lino et al. 2018, Gonçadrey & Sampaio 2013, McGladrey et al. 2017). Exceptionally, few studies integrate these methods into skarn type deposits.

Rare is also the integration of all the above techniques with geophysical modeling. 3D Magnetic Inversion has been successfully used in the investigation of mineralized bodies (Liu et al. 2018, Honsho et al. 2016). However, most of the studies are also carried out through aerial surveys.

In extreme eastern of Brazilian NE region, there are W, W-Mo, W-Au, and Au well known Skarn deposits, ocurring restricted to the Seridó Mobile Belt. Those deposits have been exploited intermittently since the 1940s (Souza-Neto et al. 2008). Other occurrences of Skarn deposits into Borborema Province were unknown until Parente et al. (2015) had indicated a deposit of Fe-Cu Skarn type in the magmatic arc of Santa Quitéria, NW portion of Borborema Province.

The Archean Nucleus of São José do Campestre (ANSJC) (Dantas 1997, Dantas et al. 2004) is a crustal block located in the extreme NE of Brazil that has a diversity of mafic/ultramafic rocks, with high economic potential in mineral occurrences, mainly Iron ore. Currently, the region has been receiving mineral exploration companies to find potential deposits due the occurrence of magnetite-bearing rock deposits with no origin defined.

Recently, Brazilian Geological Survey has undertaken some airborne geophysical surveys that enhanced those rocks which were synthetized in two geological maps (Roig & Dantas 2013). These works have based studies more focused on regional and global geotectonic contexts, contemplating compartmentalization and characterization of crustal blocks, large lineaments, and main structures (Gonçalves 2009; Araújo 2012; etc.), but not investigating metalogenetic features.

Previous studies about ANSJC have already adressed the occurrence of iron ore deposits associated with magnetite minerals

(Moraes 2021, Abrahão Filho 2016, Figueiredo 2012, Silva-Filho 2012). Abrahão (2016) indicated a possible Skarn reaction origin for occurrences of Fe eastward. Moraes (2021) presents an alternative of BIF origin for these rocks but presenting features of mixing through the geological eras.

The present study investigates one of these iron ore deposits in the WSW part of the ANSJC, with the objective of analyzing the influence of metamorphic and orogenetic events in magnetite-rich rocks in Archaean terrain using magnetic data processing and modelling. For this purpose, a lithogeophysical map of the region was elaborated using terrestrial magnetic data, surface geological mapping, and a 3D magnetic inversion is presented to delimit the mineralized body internal geometry. Internal geometry of causative sources of anomalies were delimited using Gorczyk & Vogt (2018) methodology, in a proxy way to classify the anomalies bodies. Magnetic susceptibility measures, Saturation Magnetization Analysis, geochemistry data in drill holes, in addition to statistical exploratory data analysis and a statistical multivariate analysis were used to enrich and to validate geophysical information. Finally, an interpretation of the model was made considering features of interaction between the host rocks and the magnetite-bearing rocks, leading to a discussion about the classification/origin of the iron ore deposits.

2   GEOLOGICAL SETTINGS

The study area is in the Central region of the Archean Nucleus of São José do Campestre, Northern of Borborema Province, which extends about 6.000 km² (Figure 1). In the Borborema Province, there is a complex orogenic system from Neoproterozoic age with a presence of several mobile belts which display continuity with another African mobile belts (Santos & Medeiros 1999, Brito-Neves et al. 2000, Archanjo et al. 2008, Santos et al. 2017).

Figure 1 –Geological map of the study area. This map shows Archean Nucleus of São José do Campestre in NE Borboreme Province (modified from Roig and Dantas 2013, and, Medeiros et al., 2017).
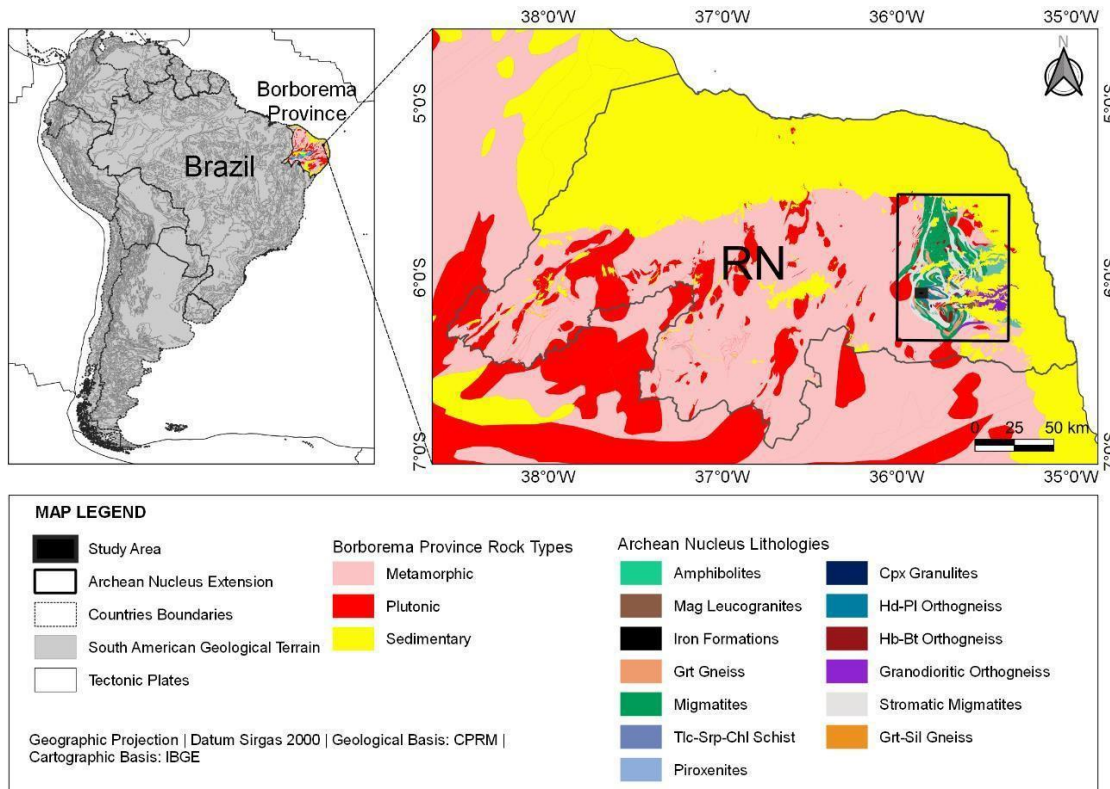
Borborema Province is one of the main structural provinces in South America. It is featured by a mosaic of Domains and Terrains from Paleo to Neoproterozoic ages and Archean Nuclei (Dantas et al. 2013, Costa et al. 2015, Santos et al. 2015, 2017, Lima et al. 2019) comprising high grade and metassediments basement rocks. This sequence is completed with Neoproterozoic Metassediments and Volcanoesedimentary sequences intruded by Ediacaran plutonic rocks linked to the Brasiliano Orogeny (Van-Schmus et al. 1995, 2008, 2011, Brito-Neves et al. 2000, 2014, 2016, Neves et al. 2006, Sial & Ferreira 2016, Bastos et al. 2019, Santos et al. 2018).

The Archean Nucleus of São José do Campestre is characterized by a history of crust generation episodes in a convergent environment (Dantas et al., 2004, 2013; Souza et al., 2016). Such events of accretion formed a microcontinent, which would have dismembered from the Nigerian or Cameroon Shield (Arthaud et al., 2008; Dantas et al., 2013; Neves, 2015).

Archean Nucleus of São José do Campestre presents characteristics of several magmatic events between the ages of 3.45 and

2.65 Ga., with the formation of orthogneisses and a unit of supracrustal rocks. Dantas (1997) divided these rocks into five units, as follows in Table 1.

*Table 1 - Lithotype Units of the Archean Nucleos of São José do Campestre, with information of Rocks Assembly and Ages according to Dantas (1997) and **other** researchers.*

Unity Name	Age	Rocks Assembly
Bom Jesus	3.45 Ga.	Tonalitic to Granodioritic Orthogneisses. (Dantas, 1997)
Presidente Juscelino Complex/Serra Caiada	3.35-3.12 Ga.	Monzogranitic orthogneisses with Tonalite-Trondjemito-Granodiorito (TTG) geochemical affinities, related to older magmatic events. (Dantas; 1997)
Riacho das Telhas Complex	3.1 a 3.06 Ga	Pyroxenites, magnetite-chromite pyroxenites, olivine pyroxenites, lherzolites, werlites, olivine gabbros, gabbros and amphibolites. (Dantas et al. 2004, Jesus, 2011; Abrahão; 2016)
Senador Elói de Souza Complex	3.04 Ga	Gneisses of granulite facies and rocks with a high-grade metamorphism constituting Hedenbergite-orthogneisses, meta-mafic rocks, mafic pyroxene and felsic granulites, associated with calcisilicatic rocks and Hornblende - Pyroxene Orthogneisses (Dantas et al. 2004).

Serra Caiada Meta-Vulcanossedimentary Sequence	~ 2.68 Ga	Meta-Volcanoessedimentary sequence Magnetite rich rocks associated with amphibolites, metabasic to metaultrabasic rocks, intercalations of calcisilicate rocks, marbles and quartzites, among others. (Dantas et al., 2013; Roig & Dantas; 2013)

Serra Caiada Meta-Volcanoesedimentary Sequence was classified and described by Abrahão Filho (2016) as a rock package including mostly quartz-feldspatic gneisses, cherts, metasandstones, schists, marbles, calcissilicate rocks, pyroxenitic rocks and iron formations. According to the author, all these lithologies were stabilized in the Amphibolite to Granulite facies and were intruded by granites.

Pyroxenitic and Calcsilicatic Rocks are found in the study area (Figure 2) associated with magnetite-rich rocks, which were first called Banded Iron Formations. Previous studies about that region have already discussed the occurrence of iron deposits associated with magnetite minerals (Abrahão Filho 2016, Figueiredo 2012, Silva-Filho 2012). Abrahão Filho (2016) attributed to these rocks two hypotheses based on studies of isotope and mineral chemistry:

1. Magnetite-rich BIF's, originated from Volcanoe-Metasedimentary environment of Archaean age, as deposits of Volcanogenic Massif Sulfides.

2. Magnetite enrichment in rocks was originated by Hydrothermal and Metassomatic activities from Skarnitic reactions.

Moraes et al. (2021) studied the same Magnetite enriched rocks and obtained another hypothesis, in which BIF's would have been formed in the Archean and would have been reworked throughout the geological era.

Figure 2 – Geological map detailing the area of study (adapted from Roig & Dantas, 2013).

3   MATERIALS AND METHODS

The rocks, which are referred to in this work as Skarns, present significant regional geophysical anomalies indeed good percentage of magnetite and intermediate iron grade. A good response of ground magnetic survey also drawn attention. Based on the anomalies, new occurrences of Magnetite-rich rocks in the Southwest portion of the Archean Nucleus São José do Campestre are addressed. The study makes use of the integration of ground magnetic data, with field observations and physical data, mainly Magnetic Susceptibility, and Saturation of Magnetization analyses from drill core samples, to provide an interpretation of geologic context. The integration of all data generated an Magnetic Susceptibility inversion and a simple 2D model (geological and

geophysical) for the two main anomalies in the study area.

3.1 Magnetic Susceptibility – Measurement and Analysis

Magnetic Susceptibility data in drill cores were obtained using a TerraPlus KT-20 Susceptibility Meter over 26 core drillholes (2,100 measurements in total). The device was calibrated to the diameter of the drill core (HQ = 63.3 mm) and its unit of measurement in 10^{-3} SI. Measurements were taken every 25.0 cm for all drill holes' extension; average of 03 measurements were performed in a regular interval referring to one sample (usually 1.00 m). For this parameter, once factors such as air heat, weathering of the rocks and mineral granulation are important for a good measurement, they have been controlled by keeping daily periods of assay, which were realized indoor, in addition to macroscopic petrographic observations. Air heat conditions were avoided when undertaking those readings just like weathered rocks were not read just because the imprecision in measurements. Mineral granulation was calibrated adjusting the susceptibility meter device.

3.2 Saturation Magnetization Analyzer (SATMAGAN)

SATuration MAGnetization ANalayser – SATMAGAN is a magnetic type of balance equipment that quantify indirectly magnetic mineral phases. Uses Faraday weighing method in magnetic and gravitational fields. The operating principle is to determine the magnetic moment of powdered samples (up to 105 µm) through submission to a strong magnetic field that allows the magnetic saturation of the material (Stradling, 1991).

The content of Magnetite in 700 rock samples was measured by Saturation Magnetization Analyzer, which is often used to determine and quantify Magnetic Mineral Phases in rocks, specifically Magnetite, often employed in Geometalurgy. Analysis had been performed by ALS Labs and consisted in 25 g of drill core crushed sample submitted to the SATMAGAN 135 device. Its results were correlated with Magnetic Susceptibility to identify patterns in the 3D Magnetic Inversion.

3.3 Petrography

A total of 26 drillholes were described macroscopically and using a hand magnifying glass. The results were systematized in a geological log, supported by photographs. Furthermore, 20 thin sections were made, contemplating not only host rocks but also mineralized zones - 15 of them extracted from drill cores - and described under a petrographic microscope using transmitted light. The petrographic data collected provided information on mineralogy, intergranular texture and microstructures that helped to better classify the lithotypes.

3.4 Geochemical data

Major elements geochemical analysis was applied to 741 samples of fresh rocks in 26 drillholes. Analytical package (ME-XRF21u) was performed by X Ray Fluorescence method in ALS Labs and included SiO_2, TiO_2, Al_2O_3, Cr_2O_3, Fe, Mn, CaO, MgO, Na_2O, K_2O, BaO, P, beside the minors As, Cl, Co, Cu, Ni, Pb, S, Sn, Sr, V, Zn, Zr and LOI (Loss on Ignition). FeO was determined by volumetric methodology (FE-VOL05) also in ALS Labs.

This work used Fe, CaO and FeO results with magnetite percentage by SATMAGAN and Magnetic Susceptibility as the best parameters to classify Skarn Rocks and a Hydrothermal alteration zone.

3.5 Statistical Analysis

An Exploratory Data Analysis was released presented as statistic tables and graphs like scattergrams and boxplots. Statistical technical procedures of multiple linear regression - MLR (Landim, 2011) were applied aiming to test cumulative dependence levels of magnetic susceptibility (k), against concentrations of Fe total, FeO, calcium oxide (CaO) and the content of magnetite (Mt).

A multivariate statistical model tested the ranges.

The general relation of model follows:

$$k = a + b1.Fetotal_\% + b2.FeO_\% + b3.CaO_\% + b4.Mt_\% + error \text{ (Equation 01).}$$

Parametric probabilistic tests have been run to assess model adequacy, as namely:

(i)   Shapiro-Wilk (Shapiro and Wilk, 1965) test to evaluate if residuals have normal distribution at 95% of confidence level.

(ii)   in addition, ANOVA (Storch and Zwiers, 2003) variance test to evaluate the significance level of estimated parameters at 95% of confidence level for each independent variable.

Both tests were proceeded in R© software, v. 3.6.0.

3.6 Ground Magnetic Data Acquisition and Processing

The ground magnetic survey was carried out by the company Geo Téc Estudos Geológicos Ltda. during April 2014. Two GSM-19 v6 magnetometers were used, one installed in a base station with cyclic measurements of 10 seconds and the other as a mobile unit (rover station) for the acquisition of data along the survey lines with a 0, 01 nT resolution and Range between 20,000 and 95,000 nT; spaced 200 m from each other. The survey direction along these lines was NW-SE (310 Az). The measurements were spaced every 10 meters. The average height of the sensor was 2 m and it was oriented in E-W direction.

The data acquired in the base and rover stations, i.e., Magnetic Anomaly, were processed and generated into Seequent Geosoft Oasis Montaj software and had the corrections for diurnal variations and the International Geomagnetic Reference Field IGRF (NOAA, 2019) undertaken. To apply the diurnal corrections, a constant reference level was used based on the average reading values of the base station for the area, aligned with the reference values of the regional magnetic field. The value established for Datum was 26,250 nT.

Data processing took place using data interpolation by the minimum curvature method (Bridges, 1974) to generate Magnetic Anomaly grid (Figure 3). Reduction to Magnetic Pole technique is more indicated for low latitudes such as Northeast of Brazil and was applied to Magnetic Anomaly grid to adjust the center of anomalies, as such as, Butterworth Filter also applied to reduce the effect of noise on the products. From the Magnetic Anomaly grid, Analytical Signal Amplitude (SA3D) and First Vertical

Derivative (1DZ) filters were applied. Finally, pseudo-illumination maps were made for SA3D and 1DZ representation, with 45 ° direction and 45 ° inclination angles of light source.

Figure 3 – Magnetic Anomaly Map, reduced to pole, and showing the acquisition lines.
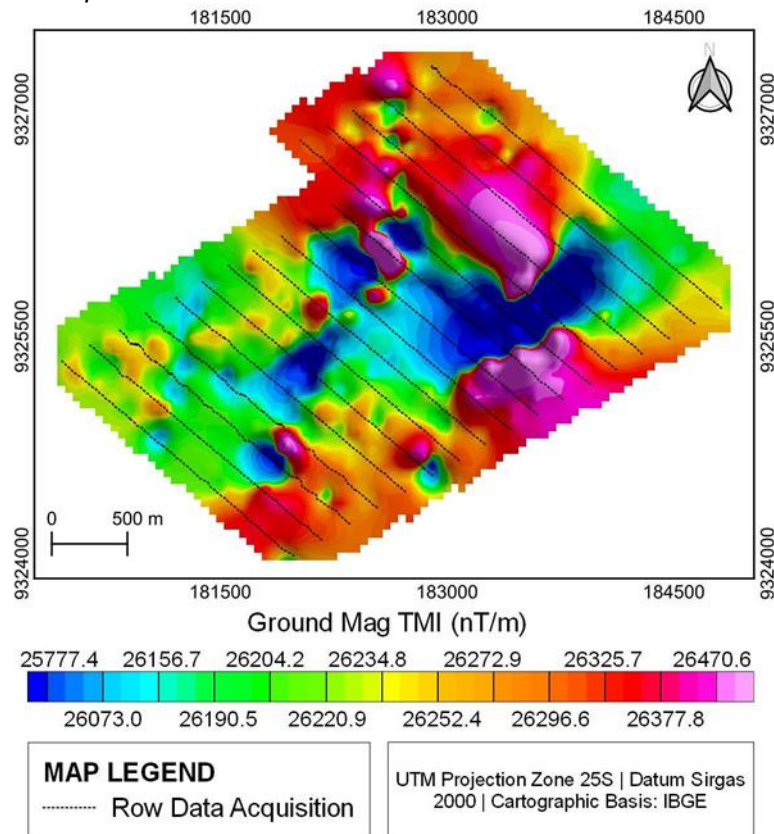
3.7 3D Magnetic Inversion

It was performed an inversion of magnetic Susceptibility from the Magnetic Anomaly grid. The inversion was made using Voxi Earth Modelling by Geosoft Oasis Montaj. The process is detailed below.

Magnetic anomaly map generated an inversion by magnetic susceptibility using VOXI Modelling. For this a Digital Elevation Model was generated from satellite images Advancced Spaceborne Thermal Emission and Reflection Radiometer – Global Digital Elevation Model Version 3 (ASTGTM) obtained from the site of Land Processes Distributed Active Archive Center (LP DAAC)/United States Geological Survey (USGS) (https://lpdaac.usgs.gov/products/astgtmv003/), and the geolgical chart of

CPRM/Serviço Geológico do Brasil (*Geological Survey of Brazil*) SB.25-Y-A-I São José do Campestre, in the 1:100.000 scale (Roig e Dantas, 2013).

The inversion method presented in this study is the Magnetic Susceptibility (MS) method. The entire área of study was covered by the inversion and the size of the cells X, Y e Z used was 100, 100 e 25 m, respectively, with maximum base in depth 730 m for the magnetic source. Once the inversion was performed a cut-off point based in magnetic susceptibility field and published data, was assumed for the generation of isosurfaces, with k values above 90 x10-3 SI, equivalent to published values for Fe Skarns. Iterative Reweighting Inversion + 2 (IRI +2) was used to centralize, better delimitate the magnetic bodies and refine the structure of geophysical inversion. The magnetic bodies modelled were interpreted, as its internal geometry, using Gorczyk & Vogt (2018).

After this, it was generated one section with NW-SE direction, in central part of the area, to display the main magnetic sources in depth.

Whole study process is showed in a flowchart for better understanding (Figure 4).

Figure 4 – Methodology Flowchart describing the proceedings for Geophysical Data Process in this study.
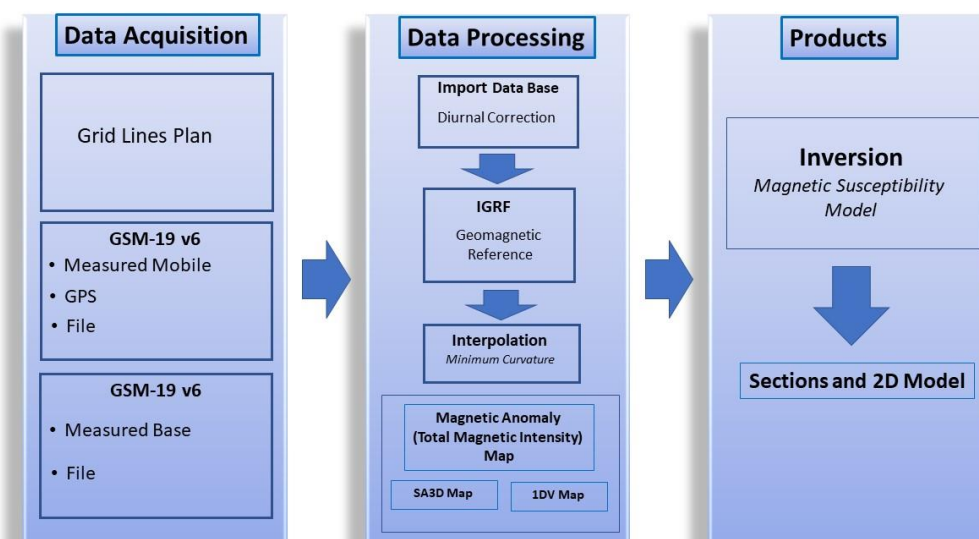
4   RESULTS AND DISCUSSION

First, geophysical maps and profiles were associated, generating a

magnetic model. Afterward, those data were integrated with petrographic and magnetic susceptibility to create a geological model for the area.

4.1 Geophysical analysis

The analysis was performed using the 1DZ and Analytical Signal Amplitude maps. One section was made from a magnetic inversion applied to the ground geophysical Magnetic Anomaly/Total Magnetic Intensity Field in an area of 21,96 km^2, East of Sítio Novo Village.

Two analyses were elaborated using the 1DZ and SA3D filters: Contour Analysis and Direction of Anomalies, besides Analysis of Magnetic Lineament Directions. By the products made it is possible to extract some features and perceive trends.

SA3D filter contours map (Figure 5) better delineate anomalous bodies. The southeast and central anomalies are visible and delineate a belt of NE-SW direction contend all small anomalies. Thus, 4 different levels of magnetic intensity (Intensity bar code, Figure 5) were individualized, where it is possible to distinguish 3 Domains (A, B and C) characterized by a more eastern part (Domain C), presenting strongest anomalous values; and, by a central band around 300 meters wide and extending over 1200 m, limited by expressive magnetic alignments, showing very high anomalous portions in the core (Domain B). The most western part is a band of lower intensity anomalies (Domain A). It is possible to notice that those anomalies obey an intensity degree from West to East.

Figure 5 – Analytical Signal Amplitude Contour map showing magnetic anomalies in a scale of intensity (nanoTesla/m), in a qualitative analysis where Red is the Higher Intensity and Dark Green is the lower. From the intensity level analysis, 03 Domains were individualized showing strike directions NE-SW. It is possible to notice there is a graduation of anomalies intensity and volume from West to East.
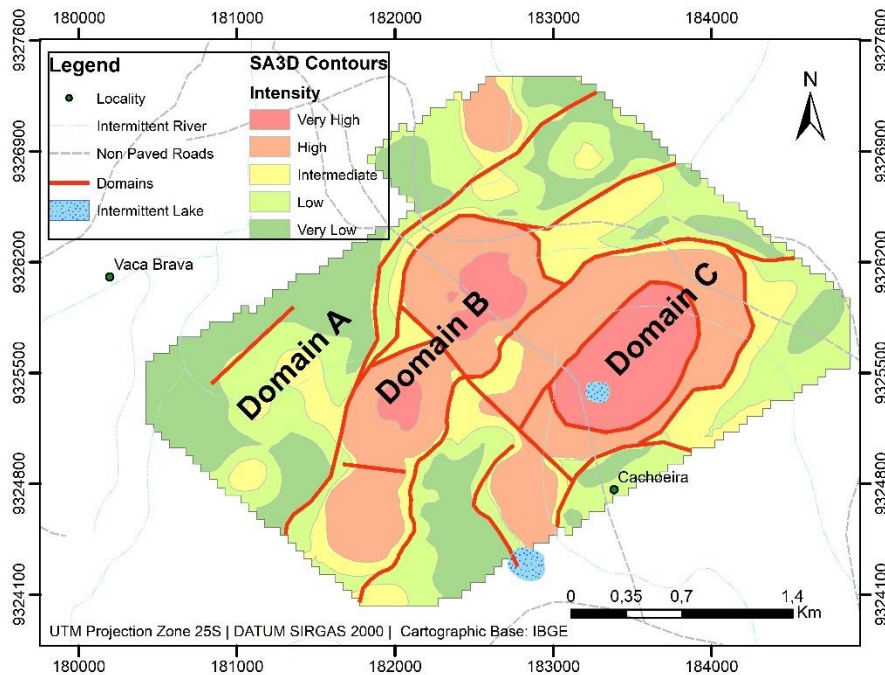
The 1DZ lineaments map (Figure 6) shows most of the magnetic lineament siting predominantly in NE-SW direction (Lineaments A). Lineaments B, red straight lines, is supposed to show shallow and recent structures. A corridor, forming a small belt, is observed in the central part (Lineaments C, thick line in blue, Figure 6) where the highest values is displayed.

Figure 6 - Vertical Derivative Magnetic Lineaments maps showing magnetic lineaments in various intensity ranges (in nanoTesla/meter): a) Vertical Derivative map with lineaments where it is possible to see a group of anomalies forming a small belt; and b) The same map with only the lineaments.
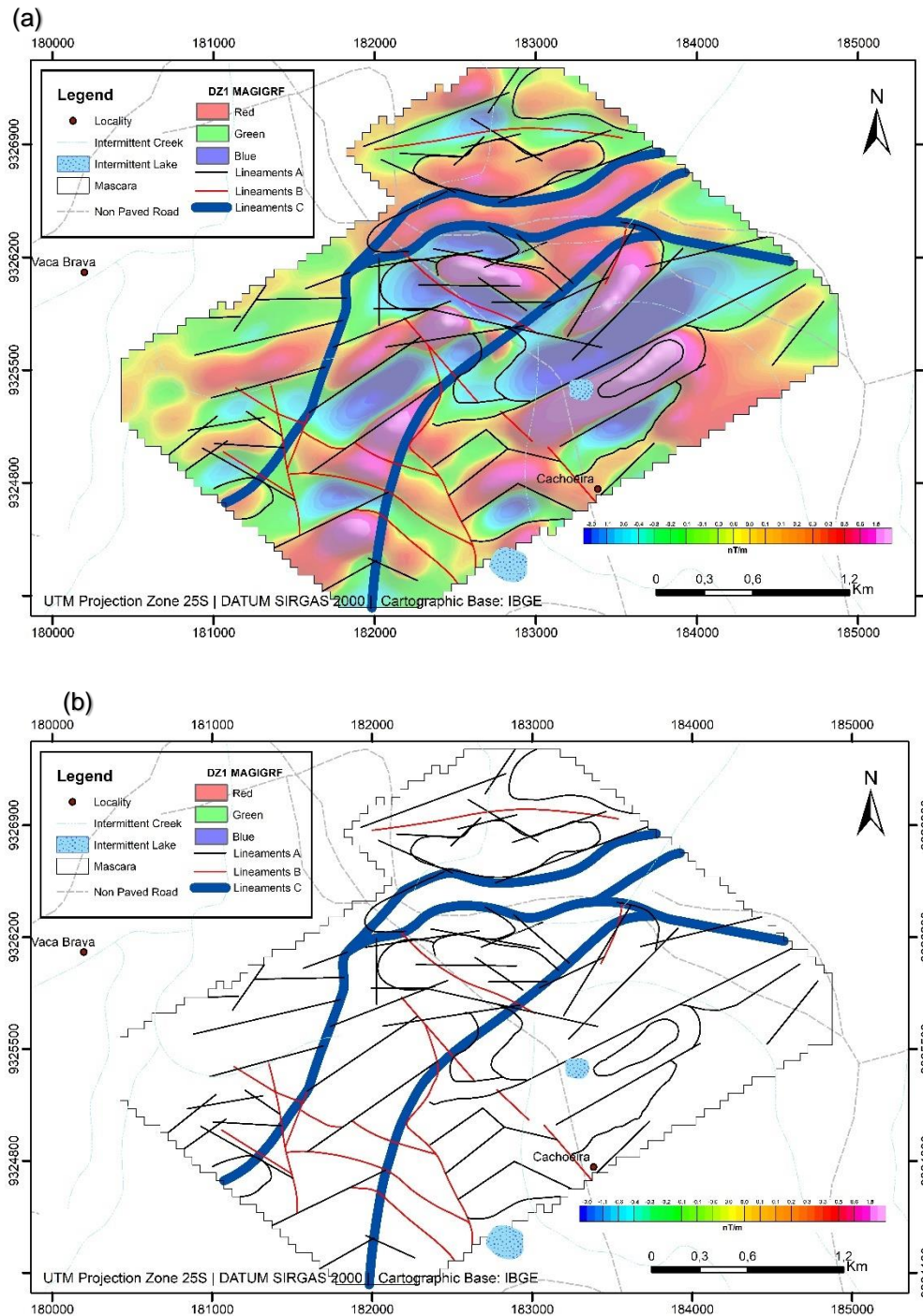
The SA3D Lineaments Map (Figure 7) enhance the lineaments, mainly in direction NE and showing displacements patterns in NW-SE direction, which could represent posterior faults and or shalowest, from brittle character, which fragments the oriented main bodies in regional ductile foliation (Dantas

et al., 2004). In the Northwest portion of the area, it is possible to notice lineaments with almost E-W direction (ENE-WSW) that may be linked to Brasiliano Orogeny.

Figure 7 – Analytical Signal Amplitude Magnetic Lineaments map showing magnetic lineaments in the edge of the anomalous bodies (in black) indicating some brittle structures (in white).
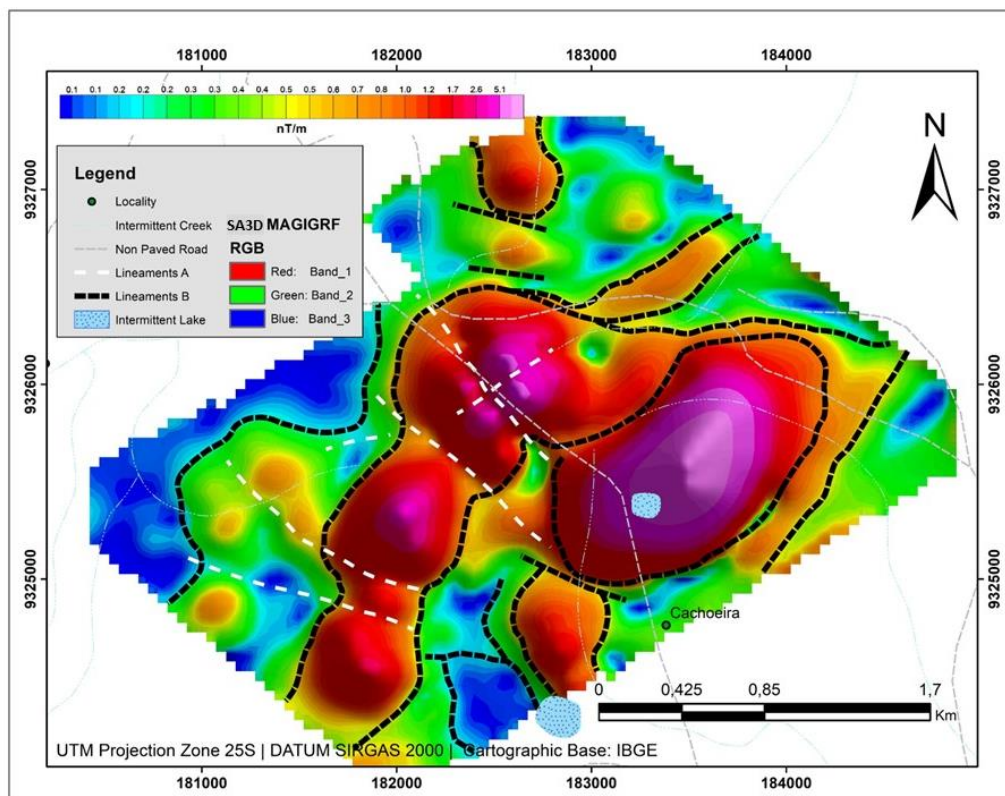
The lineament directions found are compatible with results obtained in previous studies indicating shallow magnetic components (up to 1 km deep) (Lacerda, 2012). The coexistence of these two directions of lineaments may indicate a reworking process of these rocks, with reactivations of NW-SE structures and reorientation of these structures in E-W.

4.2 Geology and Petrographic Analysis

There are two sequences of magnetite-bearing rocks with several zones of hydrothermal alteration in the study area, which are embedded in several gneisses, marbles, and metabasic rocks. Some rocks rich in pyroxenes and garnet (i.e., areas of hydrothermal alteration), presenting features of skarns, were grouped into rocks of the Serra Caiada Complex.

The decision to correlate magnetite-bearing rocks with the third unit of the Serra Caiada Complex despite of those from Elói de Souza Complex is mainly due to the occurrence of rocks known belonging to the first complex. However, it is necessary to develop more accurate studies about these lithological relations.

Some host rock gneisses are attributed to the Senador Elói de Souza Complex because it contains amphibole and pyroxene in its modal composition.

Geological map and profile (Figure 8) were drawn based on previous data by Brazilian Geological Survey (CPRM), in addition to ground magnetic survey data and geological observations on the field.

*Figure 8 – Geological **map** of study area with the borehole locations in (a), and a schematic profile showing lithologies in subsurface (b).*
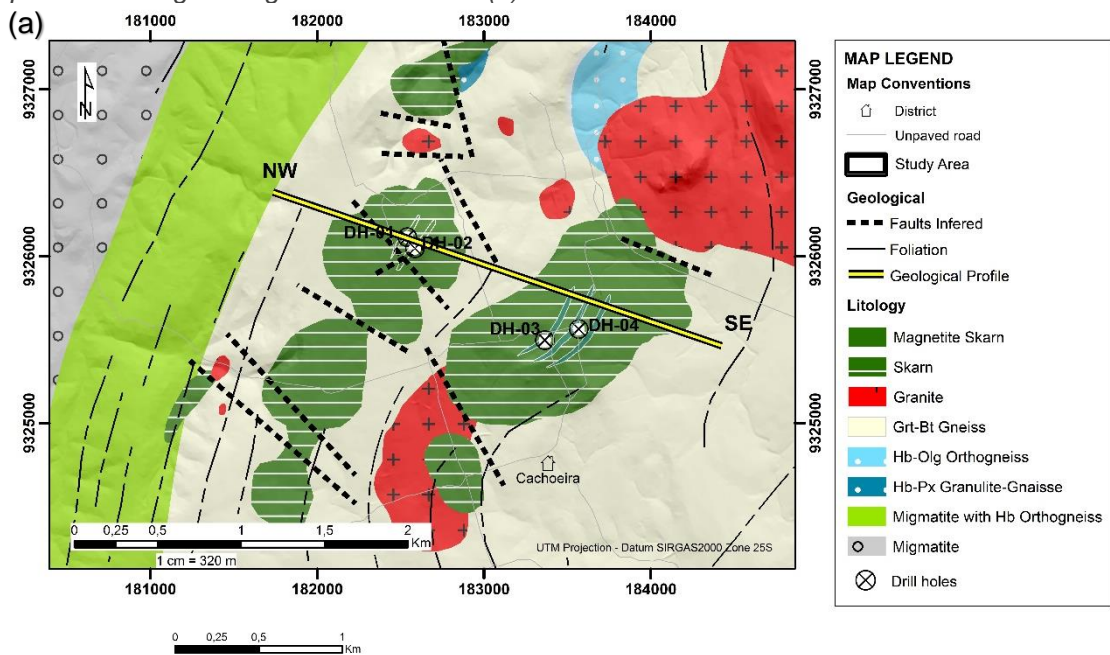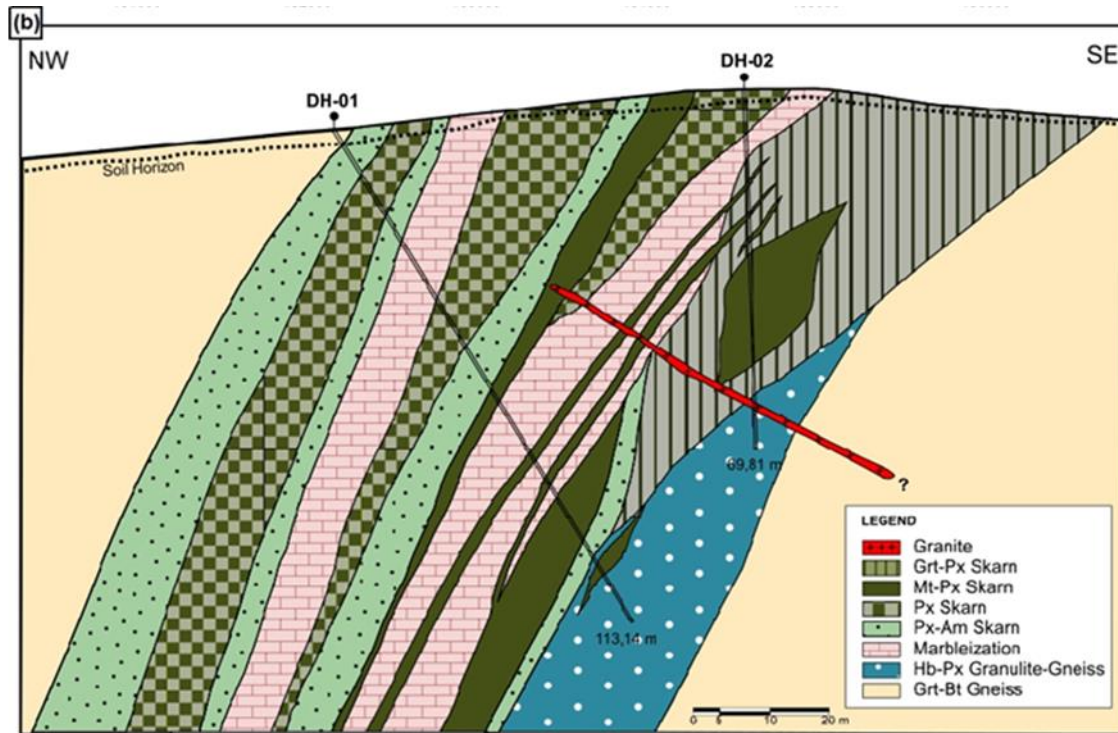
A brief description of the recognized lithologies follows.

4.2.1 *Senador Elói De Souza Complex*

This unit is represented by mafic, coarse grain, and grey to green coloured gneisses containing hornblende and pyroxene. Structurally, they are found in dip of low to medium intensity, to NW direction. Outcrops of this rock are found in the NW portion of the study area. In this work, this lithotype has correlation to the Senador Elói de Souza Complex of MesoArquean age. Dantas (1997) suggests associations of this unit with calcissilicatic rocks. They present a certain quantity of magnetite and portions rich in garnet. The gneisses found can be classified as Amphibole-pyroxene-gneisses.

The thin sections corroborate and refine this classification. They are homogeneous and granulation rocks varying from thin to thick (crystal size varying from ≤ 0.01 mm to 5.00 mm), presents granoblastic, lepidoblastic, and nematoblastic textures, in general, and more than one texture can be found in the same sample.

The basic mineralogy comprises quartz (Including veinlets, 20-28%), k-feldspars (orthoclase and microcline, 3-4%), plagioclase (24-26%),

53

pyroxenes (ratings of CPX – 1-4%, is greater than OPX – 8%), amphiboles (which may occur as pyroxene alterations, 5-32%), biotite (9-25%), and opaque minerals (sulphides and oxides, 4-6%). Secondary minerals are apatite (trace), clay minerals (trace), chlorite (trace-1%), white mica (trace-2%), iron hydroxide (trace-1%), allanite (trace), epidote (trace), and zircon (trace).

It presents a foliation Sn defined by the arrangement of recrystallized aggregates of plagioclase and subordinately quartz and K-feldspar associated with films and aggregates of amphibole, clinopyroxene, and biotite crystals. Typically, they present a diffusive compositional banding, defined by the alternation of millimetric levels, subparallel to each other and sometimes composed mainly by recrystallized aggregates of feldspar and quartz, or by aggregates of pyroxene ± amphibole ± biotite crystals, associated to the recrystallization of feldspars and quartz (Figure 9).

Figure 9 – Hornblende-Pyroxene Granulite Gneiss presenting an alteration from pyroxene to hornblende into a foliation Sn, which is arranged by recrystallized blasts of quartz, plagioclase, pyroxene and amphibole. It is also noticed a banding marked by the same blast's aggregates. (A) Image of a Drill hole DDH01 (Depth between 103,65 m and 106,41 m, drill hole inclined in 60° SE; (B) Detail of Gneiss from thin section in parallel nicols (obj. 10x) and crossed nicols (obj. 10x).
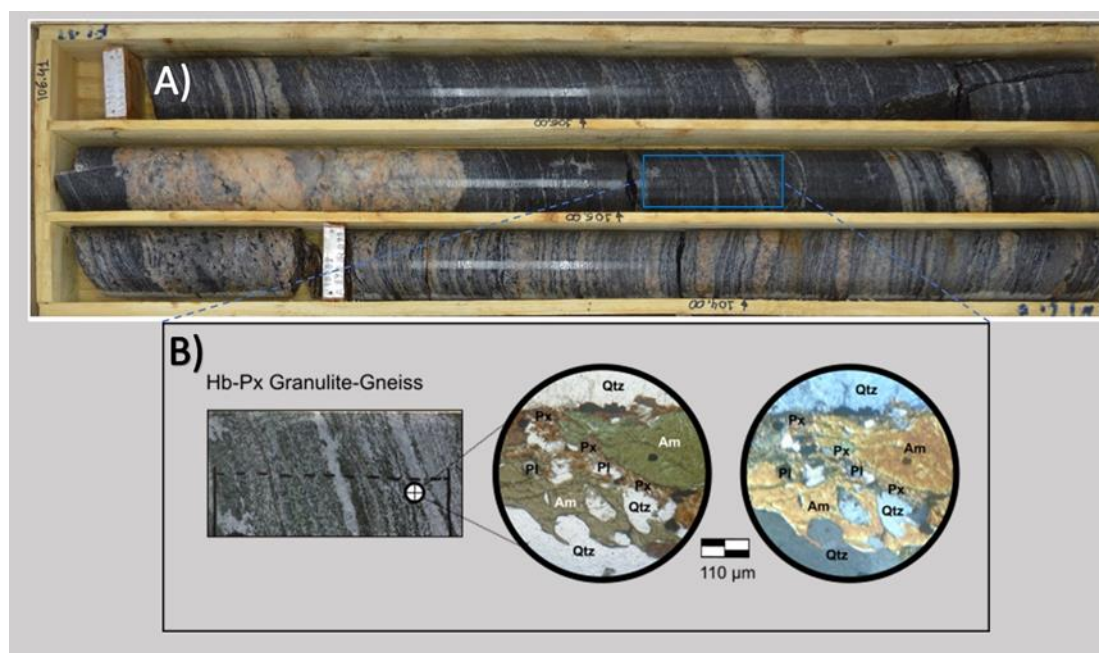
4.2.2 Serra Caiada Complex
4.2.2.1   Biotite Gneisses with Garnet

These lithologies constitute the most occurrence of the study area. They are leucocratic gneisses, sometimes migmatized, with quartz-feldspatic composition, granomatoblastic texture, in addition to foliation with medium to gentle dips and direction between NW and SW (Figure 10).

Figure 10 – Macro aspect of Biotite Gneiss present in area. Mineralogy content is biotite, quartz and feldspars. Locally is noticeable a few garnet blasts.

Micropetrographically, this lithotype shows granulation ranging from thin to medium (crystal size ranging from ≤ 0.01 mm to 3.00 mm, some crystals can reach 1.50 cm). There are granoblastic and lepidoblastic textures.

The basic mineralogy comprises quartz (27%), k-feldspar (27%), biotite (13%), plagioclase (25%), and opaque minerals (oxides and sulphides, trace). The sample also has garnet (3%) and titanite (2%) in its composition.

The association of plagioclase + K-feldspar + garnet + biotite suggests this lithology reached amphibolite facies. The occurrence of chlorite, formed from the biotite, indicates stabilization up to the green schist facies. The occurrence of deformed twining, undulating extinction, and broken crystals may evidence the occurrence of brittle deformations.

4.2.2.2   Metacarbonates/Marbles

Small exposures of marble are concentrated in the western portion of the study area, where dark red and clay soil develop over them (Figure 11).

A white, coarse-grained, and isotropic type of marble was observed. The white marble has portions with apparently monotonic mineralogy, with the presence of carbonate (calcitic or dolomitic) and quartz, rarely being observed accessory minerals. These bodies are associated with mineralization. This rock is composed by >80% of calcite and dolomite mixture (observation by lenses and HCl test and predominance of calcite) with accessories minerals like apatite (~5%), olivine (~5%), biotite/phlogopite (~5%), and magnetite (trace).

Figure 11 – Calcitic/dolomitic marble located on NW portion of study area.

4.2.2.3   Skarns

This unit was registered on surface just like a straight lens in W portion, and in E of the study area, on sigmoid shape. Both present SW-NE strikes direction. Apparently, this unit occurs associated to marbleization forming a package with four types of skarns.

The saprolitized conditions of the exposures and the scarcity of outcrops are the main obstacles for surface observations.

Those rocks are greenish color, with varying tones, fine to medium granulation, isotropic, either massive or with structure like banding, but not

consistent, and granoblastic macrotexture. It was possible to observe carbonate in lenses (10 to 15x magnified), pyroxene, amphibole, garnet, biotite, and white mica, in addition to varying amounts of magnetite. In drill core samples, it is possible to observe practically monomineral zones, mainly (metric) zones rich in pyroxene, occasionally (decametric) zones with garnet and smaller amounts of pyroxene.

In thin sections, those rocks display an arrangement with the following mineral contents clinopyroxene (hedenbergite – 40-80%), garnet (8-35%), plagioclase (andesine – 3-22%), epidote (zoisite – 0-6%), quartz (1-5%); amphibole (actinolite – 1-5%), opaques (magnetite – 1%). It was possible identify scapolite (32%) that maybe have relationship with marble contact and fluids exchange by metassomatism (Deer, Howie and Zussman, 2005).

The skarns found in the region suggest their origin from interactions of calcissilictic rocks, metacarbonates, pegmatites, and granites. Structures with aspects of Skarnoids (or Hydrothermal Breccias) occur in the N and NE portions and in subsurface of the study area and reflects these interactions among the lithologies. Also, such features seem to be related to structural faults.

In drill core samples, it is possible to identify decimetric to metric zones of hydrothermal alteration, such as carbonation/marbleization (with the presence of carbonate venules and its dissemination) and silicification. Centimetric to metric area with garnets varying in granulation are also observed, as well as areas with dominance of pyroxene and magnetite. Pictures of the features and lithologies observed in the field represents the above discussed (Figure 12a,b,c,d).

Figure 12 – (A) Skarnoid feature at NE of study area. SiO2 rich fluid involving mafic rock. (B) Relation between Metamafic rock of fine granulation, intruded by SiO2 rich rock. These rocks with skarnoids aspects are found at W, N, and NE of the area. (C) Skarnoid feature at NE of study area. Pegmatite intrudding mafic rock bringing some xenoliths of it. (D) Metamafic rock with gneiss aspect, containing pyroxene (green), plagioclase (white) and garnet (brown redish) (inconsistent) bands. Small Outcrop located in the N of the area.

The drill cores of these lithologies appear as a complex plot of lithotypes, alternating in short intervals, presenting subtle and gradational contacts. With the help of the thin sections, it was possible to delineate the contacts between these rocks and their zones of hydrothermal alteration.

Their basic mineralogy content show pyroxene, amphibole, biotite, and quartz. In addition, there are variable amounts of garnet, magnetite, plagioclase, carbonates, chlorite, sulphides, apatite, zircon, clay mineral, titanite, and allanite. K-feldspars occur in some portions. Skarns also present opaque minerals defined as oxides and sulphides, with predominance of oxides, mainly magnetite. This mineralogy will be detailed forward.

Skarns and carbonatic alteration in drill cores has been detailed and classified by mineralogy such as Pyroxene-Amphibole Skarn, Pyroxene Skarn,

Garnet-Pyroxene Skarn, Marbleization, and Magnetite-Pyroxene Skarns. Their aspects and interactions will be explained coming up.

4.2.2.3.1 Pyroxene-Amphibole Skarns

The drill cores show this lithology intrinsically connected to the Pyroxene Skarns, being very difficult to distinguish and to individualize them, due to their alternation in thin bands or small portions. The differentiation of the other types of rocks is mainly due to the amount of magnetite perceptible.

In thin sections they appear homogeneously and varying their granulation from thin to thick (crystal size varying from ≤ 0.01 mm to 3.20 mm). It is composed basically by orthopyroxene (30%), clinopyroxene (20%), hornblende-edenite (24%), quartz (including veinlets, 12%). Secondary minerals are biotite (5%), pyrrhotite (4%), magnetite (3%), chalcopyrite (1%), grunerite (<1%), tremolite-actinolite (<1%), apatite (trace), goethite (trace), carbonate (calcite, trace), graphite (trace), clay minerals (rare, scattered along the rock), ilmenite (rare), rutile (very rare), pentlandite (very rare), and zircon (very rare).

They show a foliation Sn defined by the arrangement of the recrystallized aggregates to locally polygonized pyroxene and amphibole crystals (predominance of the hornblende-edenite series). The amphibole aggregates of the hornblende-edenite series sometimes segregate films/strings, setting up a pseudo banding. Occasionally, pyroxene crystals are also observed truncating the foliation Sn.

There are alterations of orthopyroxene (ferrosilite) and clinopyroxene (diopside-augite series) for the following amphiboles: hornblende-edenite series and, locally, for grunerite and tremolite-actinolite. The pyroxene crystals are also replaced by clays, carbonate, goethite or directly to brownish-green biotite. The amphibole crystals of the hornblende-edenite series, in turn, change to brown biotite. Some biotite crystals show inclusions of zircon with formation of pleochroic halos.

Opaques are represented by sulphides, oxides, and graphite, all isolated or associated with each other. Opaque minerals of non-foliation character are crystalline/blasts idiomorphic to hypidiomorphic, spread along the rock and

concentrated, mainly, in the portions where the crystals of hornblende-edennite segregate films. The main oxide is magnetite, that appears as crystalline idiomorphic to hypidiomorphic dispersed through the rock, either isolated or associated with the sulfides. Locally, fine pyrite-substituted ilmenite crystals scattered over the rock are found. There are rare pyrrhotite sulphides, occasionally with inclusions or borders of chalcopyrite and rarely with pentlandite flames. Fine crystals of sulphides, magnetite, and ilmenite partially substituted by rutile are products of exsolutions of pyroxene crystals.

4.2.2.3.2 Pyroxene Skarns

They are presented in thin sections as a homogeneous and granular rock varying from fine to medium (crystal size ranging from ≤0.01 mm to 7.5 mm).

This type of skarn presents basic minerals, such as clinopyroxene (hedenbergite, 71; diopside, 77%), plagioclase (3-22%), and potassic feldspar (microcline, 12%). Secondary mineralogy is represented by quartz (1-5%), epidote (trace), amphibole (tremolite-actinolite series, 5%), titanite (trace-1%), opaque minerals (1%), and allanite (trace).

Clinopyroxene (diopside-hedenbergite) are altered to amphibole (tremolite-actinolite), opaque minerals, and titanite. They are arranged in a discontinuous foliation Sn which contour granoblastic aggregates of pyroxene itself, suggesting recrystallization in high temperatures (superior amphibolite facies).

Plagioclase occurs in hypidiomorphic (tabular) to xenomorphic crystals, whether segmented or not by albite/Carlsbad and pericline. Some crystals are clear, others are incipiently changed to saussurite. It presents clinopyroxene inclusions and may be aligned with the foliation Sn in discontinuous way with exuded features.

Potassic feldspar (microcline) is arranged in exuded aggregates transposed to foliation Sn showing jigsaw shape contact with pyroxene matrix. Quartz is xenomorphic, aligned with the foliation Sn presenting undulose extinction. Amphibole, titanite, opaque minerals, and epidote are product of alteration/substitution between clinopyroxene and plagioclase. Opaque minerals

are xenomorphic, fine crystals that either occupy the spaces between pyroxene blasts or are products of exsolutions of pyroxene.

4.2.2.3.3 Garnet-Pyroxene Skarns

This type of skarn presents lepidoblastic, poikiloblastic, and granoblastic texture; fine to coarse granulation (crystal size ranges from ≤ 0.01 mm to 10.40 mm), with a predominance of the average value.

It presents as main mineralogy quartz (including venules, 7-20%), garnet (3-30%), biotite (1-29%), clinopyroxene (<1-44%); and as accessories potassic feldspar (7%), magnetite (trace-12%), plagioclase (3-13%), amphiboles (tremolite-actinolite, rare-3%, hornblende-edenite, <1-16%, grunerite , <1% -2%), chlorite (trace-2%), orthopyroxene (2-10%), carbonate (calcite, trace-2%), white mica/sericite (2%), goethite (trace-1%), ilmenite (trace-6%), titanite (2%), ulvospinel (trace, <1%), zircon (trace), allanite (trace), apatite (trace), clay mineral (trace), rutile (trace), hematite (rare), goethite (trace), pyrrhotite (trace-2%), pyrite (trace), epidote (trace), chalcopyrite (trace- <1%), pentlandite (trace).

Quartz is interstitial and a product of recrystallization and fluid supply. Biotite occurs as recrystallized aggregates arranged in foliation Sn and defined by discrete foliation C. They also represent a product of fluid input and pyroxene alteration (retromorphosis). Biotite changes to chlorite and white mica. The garnet occurs as crystals/aggregates of crystals and blasts growing along Sn foliation and encompasses the other minerals that make up the rock. It also occurs dispersed through the rock.

Plagioclase occurs in idiomorphic to hypidiomorphic crystals, whether twined or not, according to albite/Carlsbad and pericline occasionally. Some crystals show deformed scales, reactions with quartz (simplectites) and usually saussuritized. K-feldspar occurs locally represented by microcline, constituting clear to clayed xenomorfic blasts/crystals and associated-streaked with pyroxene + amphibole + biotite films. K-feldspar blasts suggest the supply of potassium-rich fluids to the system.

Orthopyroxene (ferrosilite) and clinopyroxene (likely diopside-augite series) change locally to the following amphiboles: grunerite, hornblende-edenite,

61

and tremolite-actinolite. Pyroxene crystals are also replaced by clay mineral, carbonate, goethite or directly to reddish brown biotite. Sometimes it is arranged along the foliation Sn.

Some amphibole crystals are also replaced by brown biotite. Zircon and metamytic allanite scores are included in biotite crystals. Developed crystals of titanite and apatite in the form of fine euhedral crystals are scattered throughout the rock.

Opaque minerals (syn-foliation character) are scattered throughout the rock and included in garnet blasts. They are represented by oxides and sulfides, isolated or associated with each other. They are products of exsolutions of mafic minerals.

Among the oxides stand out crystals/blasts, hypidiomorphic to xenomorphic, of magnetite locally with ulvospinel exsolutions and association with preserved or incipiently changed to rutile ilmenite. Ilmenite crystals are idiomorphic (tabular) to hypidiomorphic, preserved or in various stages of alteration to rutile, including total pseudomorphosis. Some crystals show hematite exsolutions.

Among the sulfides, hypifiomorohic to idiomorphic fine crystals of pyrrhotite (dominant sulphide), chalcopyrite, and pyrite occur, either alone or in association with each other. Also occurs pentandlite, included in pyrrhotite.

Hydrothermal fluid input and subsequent deformations eventually obliterated the original features of the rock. These fluids are responsible for precipitation mainly of quartz, garnet, and biotite in the system.

The rock is cut by millimetric quartz lenses preferably arranged according to the Sn foliation plane. Sn foliation transposed by discrete C foliation, even locally, indicates shear zone.

The association of clinopyroxene + orthopyroxene + plagioclase indicates that the protolith is a metamorphosed gabbroic affiliation rock in the amphibolite facies and conferred by the assembly: amphibole + biotite + garnet + magnetite + ulvospinel.

Garnet nucleation can occur from reactions involving substitutions of mafic primary minerals (pyroxenes) associated with aluminum surplus in the system.

The localized occurrence of chlorite and white mica indicates specific conditions of the greenschist facies. It is likely that this rock was formed by contact metamorphism and indications of retromorphosis suggest distal retrogradation zone, therefore an exoskarn.

The carbonate + clinopyroxene paragenesis is likely generated from the input of fluids derived from a gabbroic rock intrusion (Protolithic) in marble (contact metamorphism), reached amphibolite facies temperature conditions.

4.2.2.3.4 Marbleization/Carbonate Alteration

Drill cores revealed portions (or zones) of strong carbonate alteration. These zones are not always constant, ranging from centimetric to metric bands. They are easily detectable using hydrochloric acid. They occur in two ways, not only as white bands, but also as darker bands, the latter containing magnetite and phlogopite/biotite.

In thin section (Figure 13), marbleization process is shown in a homogeneous way and granulation varying from fine to medium (size of the crystals ranging from ≤0.01 mm to 7.20 mm), with a predominance of medium grain size (crystal size around 3,20 mm). The texture in general is characterized as granoblastic.

Figure 13 - Photomicrograph of sample DDH0004PET002 – 50.20 m - Hole: DH-04. Granules of carbonate (Cb) and quartz (Qz) associated mainly with pyroxene (Cpx) and biotite (Bt) crystals. Transmitted light, crossed nicols, 2.5x objective, 10x eyepieces.
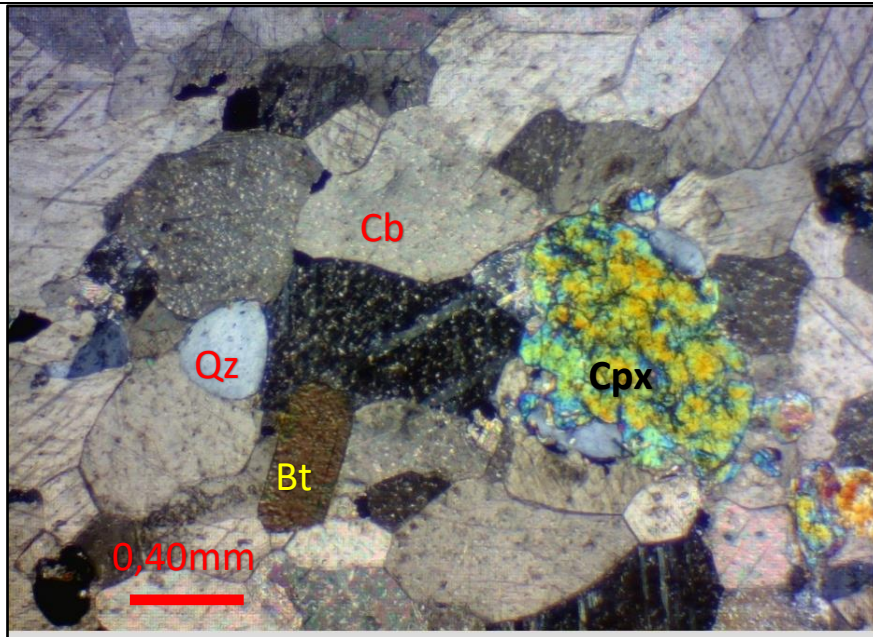
The basic mineralogy includes calcite (37-60%), olivine (8-15%), amphibole (4-6%), pyroxene (diopside, 9-22%; ferrossilite, 1%), biotite/phlogopite (6-23%) and serpentine (7-12%). The secondary minerals are magnetite (2-3%), sulfides (pyrrhotite, trace 2%; pyrite, trace; chalcopyrite, trace), chlorite (trace), graphite (3%), and hercynite (4%). The magnetite, in this case, is a product of serpentinized olivine exsolution and occurs either along the planes of fractures of olivine or phyllosilicates. It presents a foliation Sn.

The carbonate + olivine + clinopyroxene paragenesis indicates conditions of contact metamorphism compatible with high amphibolite facies. The presence of graphite, magnetite, and hercynite are also indicative of the rock reaching granulite facies. The retro metamorphism is marked by the change of: (a) olivine for serpentine + phlogopite; (b) clinopyroxene for amphibole and probable phlogopite; and (c) phlogopite for chlorite. The presence of white mica formed mainly from hercynite indicates late fluid performance in the system. The amount of graphite observed in veinlets may be associated with hydrothermal events.

4.2.2.3.5 Magnetite-Pyroxene Skarns

They are rocks rich in magnetite (about 15 to 25%, may achieve more than 30 % locally). Represents the intermediate member of the Serra Caiada Complex unit (Roig and Dantas, 2013). Its origin is not clear, but it has a close relation with marbles, igneous rocks and granulitic gneisses. They are elongated, according to their major axis, to NE-SW direction, in discontinuous (surface) bodies, having dimensions between 1.2 and 1.5 km in length and 200 to 300 m in thickness (Figure 14). They are in the NW and SE portions of the area.

Figure 14 – (A) Outcrop of Magnetite-Pyroxene Skarn, on the W portion of study area. (B) Outcrop of Pyroxene-Magnetite Skarn, on the E portion of study area.
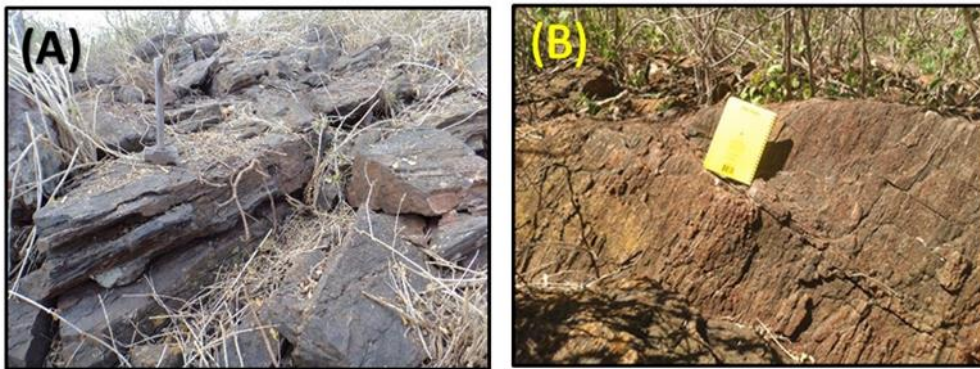
In thin section, this rock presents textured characteristics ranging from granoblastic to nematoblastic, and poikiloblastic textures can occur locally. Its granulation varies between fine and coarse (crystals ranging from ≤0.01 mm to 5.00 mm, up to 9.60 mm).

The basic mineralogy consists of quartz (23-46%), pyroxene (ferrossilite, 6-27%; diopside, 3-15%), amphibole (grunerite, trace-15%; hornblende, trace-12%), and magnetite (15-34%). The accessory minerals are potassic feldspar (2-12%), plagioclase (trece-5%), biotite (trace-5%), carbonate (trace-3%), chlorite (trace), apatite (trace), clay minerals (trace), oxides (ilmenite, trace; rutil, trace; goethite, trace-1%; ulvuspnel, trace-1%), and sulfides (mainly pyrrhotite, trace-4%). Pyroxene (ferrosilite) changes to amphibole (hornblende-edenite). Amphibole, in turn, changes to biotite. The magnetite is fine (predominant) to medium size (the average size of the crystals ranging from ≤ 0.01 mm to 1.00 mm), as crystals idiomorphic to hypidiomorphic and sleek. Exsolutions of

ulvospinel occurs in magnetite crystals and the same occurs inclusively in the ganga crystals.

The paragenesis observed in the description suggests that the rock reached the granulite facies and retro metamorphized to amphibolite facies. The occurrence of chlorite (localized) indicates the onset of retro metamorphism for greenschist facies.

4.2.3 Granites

Granitic rocks are associated with the context of study area, identified as biotite granite, leuco granitic dykes fine to medium, aplites and pegmatites, locally presenting magnetite. They also have unclear relationships with the skarns of the region.

Compositionally, the granites are classified as monzo to sienogranites, equigranular, grain size is fine to medium, having the biotite as main mafic and less often amphibole. On the surface, they are found throughout the area as small bodies and stocks.

Granite dykes occur throughout the area. The leucogranite dikes have medium to fine grain, containing biotite, usually undeformed, being predominantly of NS direction, as well as pegmatitic and aplitic rocks, some with NS directions, and varying sizes (from small centimeter to metric dikes). Pegmatitic rocks are directly related to calcissilicatic rocks. In drill cores, these rocks intersect all other lithologies.

4.3 Magnetic Susceptibility

By integrating data from Magnetic susceptibility, SATMAGAN and geological mapping, based on the parameterization of Clark & Emerson (1991) and Hunt et al (1995), it was possible to distinguish eight lithological groups that are presented here and described later.

Magnetic Susceptibility ($x10^{-3}$SI) is presented through means (Table 2). Magnetite Skarn rocks present the major values to Magnetic Susceptibility with average of 589.43 x 10^{-3}(SI). Pyroxene Skarns present an average of Magnetic Susceptibility of 108.6 x 10^{-3}(SI). Gneisses show lower values as 3.65 x 10^{-3}(SI) while Granites present 5.92 x 10^{-3}(SI).

Magnetic Minerals analysis by Saturation Magnetization Analyser displayed respective values for fore mentioned rocks, respectively named: 22.92 (%), 5.61 (%), 1.07 (%) e 0.9 (%). These four values ranges can be correlated with the anomaly intensity ranges found in Figure 4, respectively. The skarn relations will be better discussed in detail following.

Table 2 – Mean values of Magnetic Susceptibilities (SI x 10-3) and percentage of Magnetites by Saturation of Magnetization Analyser.

Parameters	Rock Type			
	Mgt Skarns	Skarns*	Granites	Gneisses**
Magnetic Susceptibility $(SI \times 10^{-3})$	557.87	22.59	5.92	3.59
% Magnetic Minerals by Saturation of Magnetization Analyser (Magnetite)	22.49	1.92	1.07	0.9

Garnet Pyroxene Skarns, Pyroxene Skarns and Pyroxene Amphibole Skarns Included.
** Garnet Biotite Gneisses and Hornblende Pyroxene Gneisses included.*

The skarn rocks presented previously are distinguished from each other not only by their mineralogical content, and therefore, there is a chemical relationship, as a physical relation highlighted by the contrast of observed magnetic properties, in addition to the contact relations, weather abrupt or gradational, between these rocks. From the observation of features in macro, meso, and micro scale it is possible to highlight some of these relationships.

Among these relationships, the main one is between Magnetic Susceptibility and depth (discussed below), which is intrinsically linked to the amount of magnetite in the rock, especially Magnetite Skarn and Garnet-Pyroxene Skarn. Looking at these rocks under a microscope, it is possible to observe that between 20 and 65 meters deep, a greater percentage of magnetite is observed (between 20 and 30%), while at depths above 65 meters the amount of magnetite falls (below 20%). Figure 15 briefly shows these observed relationships.

The behavior of magnetite grains/blasts is arranged differently between these depth ranges. Between 20 and 65 meters deep, the rocks present intense ruptile-ductile deformation, with formation of strong Sn foliation and banding; alternating mafic, magnetite, among others, in addition to felsic minerals, the latter characterized mainly by interstitial recrystallized quartz. Sometimes it is also possible to observe a transposed S-C foliation, typical of shear zones. Mineral interactions are also more intense in this depth range, with greater mineral transformations, especially involving pyroxenes and amphiboles. Garnets is also formed from pyroxene in this depth range.

Carbonate alterations occur intensely in the range between 20 and 65 meters, obliterating previous structures (foliation and banding) and forming new ones.

At depths above 65 meters it is possible to observe the minerals with more hypidiomorphic to idiomorphic characteristics, arranged in a Sn foliation and larger magnetite grain/blast size compared to the other skarn rocks in study area, with a more cumulative texture, suggesting a disposition isotropic as the rock pack deepens.

Figure 15 – Skarn relations showing variations in size, amount (percentage), and arrangement of grains/blasts, into depth from drill cores undertaken in study area. In (a,b) thin section - nicols parallel and crossed, respectively - shows magnetite crystals/blasts disposed in foliation Sn and interacting with pyroxene, in Magnetite-Pyroxene Skarn. In (c) magnetite crystals/blasts are higher in size, than in previous picture; (d) the same picture in crossed nicols. (e) Magnetite in minor size and following foliation Sn. Magnetite are also interacting pyroxene and garnet crystals/blasts in Garnet-Pyroxene Skarn; crossed nicols in (f). (g) Thin section shows intense deformation and magnetite crystals/blasts presenting minor size; crossed nicols in (h); (i) Thin section and drill core showing crystals/blasts higher than in other rocks in this plate; arrangement seems more isotropical. Depths and Magnetic Susceptibility are available along this picture.
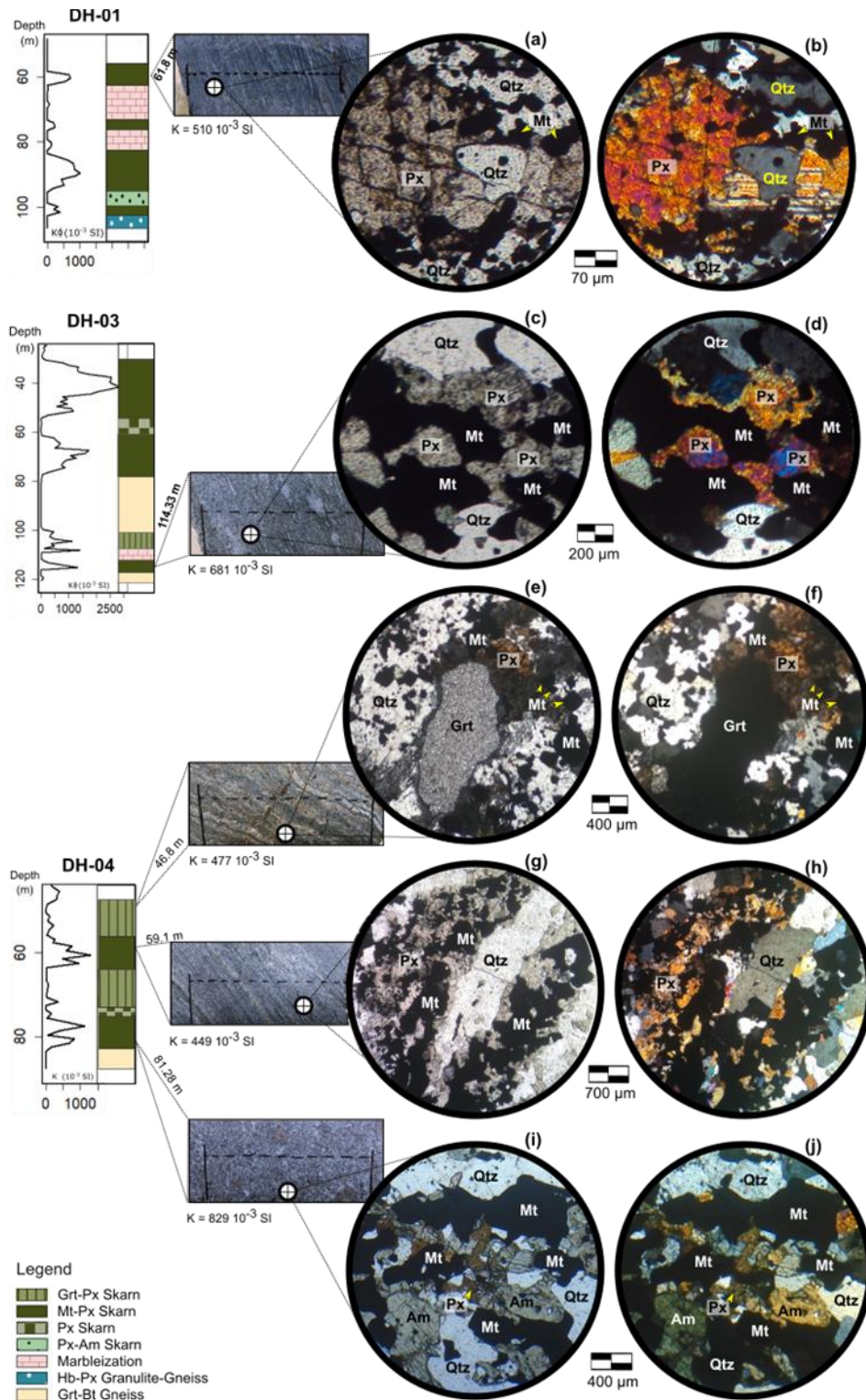
4.3.1. Integration between Anomaly Intensity and Magnetic Susceptibility Signatures of Lithotypes

The ASA Filter used for contour demarcation showed similar patterns of anomalies intensity (Figure 5), hence it can be suggested a local arrangement of lithologies based on magnetic susceptibility data and geological mapping.

Using the color scale of magnetic products, high-amplitude ASA zones in Red are recognized in the field as mineralized zones, because they contain unusual amounts of magnetite for the area. The drill cores feature magnetic susceptibility signatures compatible with Fe-Skarns (Clark & Emerson, 1991) and are classified as Magnetite Skarns. Zones in Orange can be classified as pyroxene skarns in the Central and East-Southeast Areas. In the NW part of the study area, Basic Granulitic Gneisses are more present. Magnetic Susceptibility signatures for both lithologies are similar.

For intermediate anomalies, in yellow, field information shows that these features are associated with small stocks and granite and/or pegmatitic intrusions. Magnetic Susceptibility signatures show values, between 0,03 and 21,87 x 10^{-3} SI, compatible with these rocks.

The low-amplitude ASA zones are shown in the colours Light Green and Dark Green, and this one is the weakest response among all of them. In the field, garnet-biotite Gneisses (Serra Caiada Complex) are observed in the places that correspond to the areas of Light Green tones and are the most found lithology in the area. The areas in Dark Green correspond to Monzogranites Orthogneisses (President Juscelino Complex). The Gneisses were not discriminated by magnetic susceptibility measurements, so their signatures are presented together and correspond to those measured by Clark and Emerson (1991) and Hunt et al. (1995).

The integration between Magnetic data and Surface mapping (Figure 16a) helped to generate the final geological interpretative map (Figure 16b). Skarns occurs under stretched lens shape, in Garnet-Biotite gneiss intruded by granites, associated with Hornblende-Oligoclase orthogneisses and Hornblende-Pyroxene granulite-gneisses.

Figure 16 – Integration of magnetic data and surface mapping: (a) Analytical Signal Amplitude map showing a geologic sketch; (b) Final Geologic Map of the area made from the integration of geophysical and geological data.
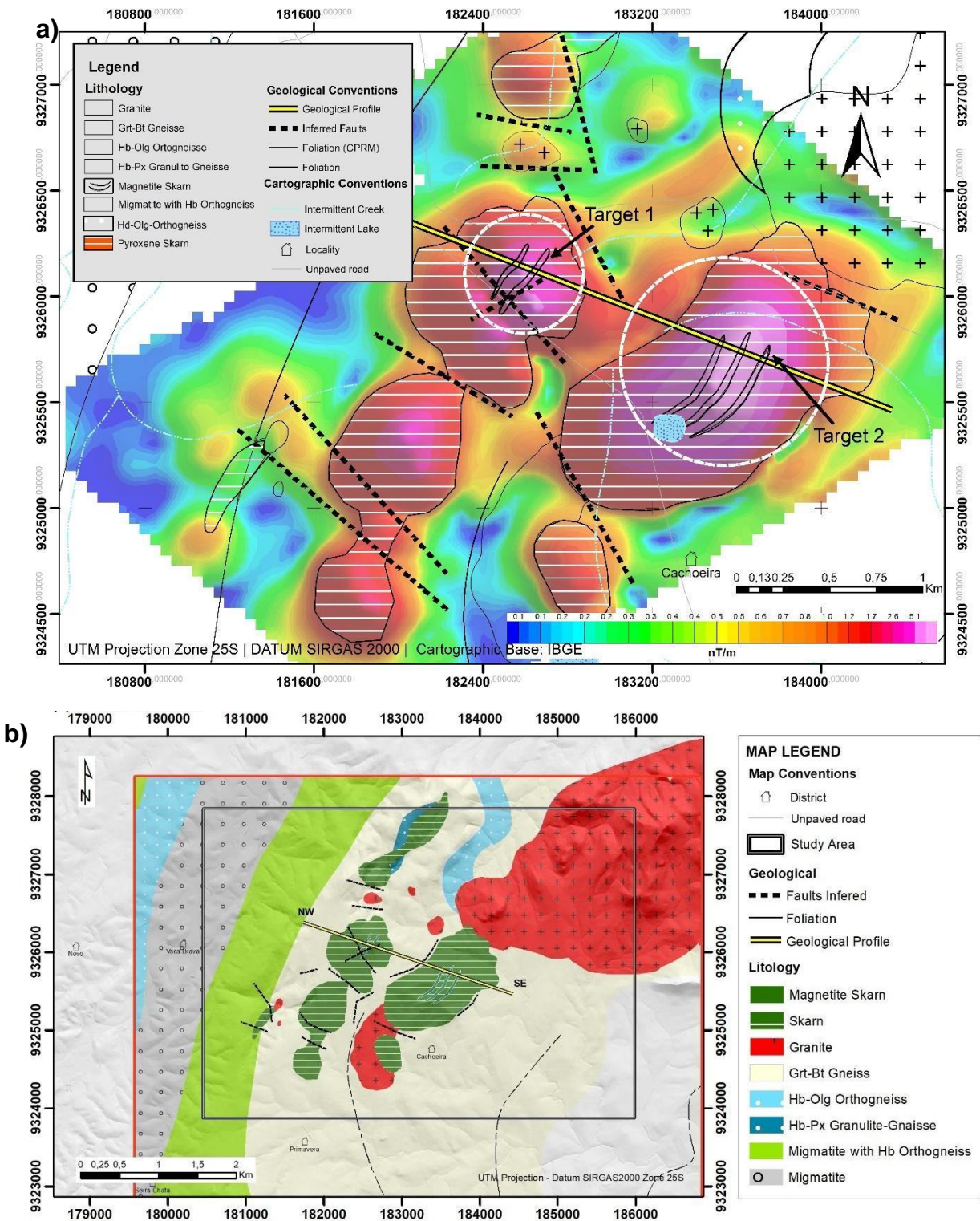
The NW-SE profile crosscut the main magnetic anomalies (anomalous bodies indicated with white circles - Fig. 16a). In magnetic inversion these are the main anomalous bodies to be addressed next.

4.4 Multivariate Data Analysis

By integrating values of magnetic susceptibility with Satmagan data and geochemical data was possible classifying skarn lithologies and one hydrothermal alteration, Marbleization. Geochemical data was released by XRF analysis of Major elements which Fe (w%) t and CaO (w%) t with FeO (w%) (Determination by Volumetric methodology), magnetite determined by SATMAGAN, and Magnetic Susceptibility were chosen as the best variable for this classification.

An Exploratory Data Analysis was performed in results of chemical analysis of 741 fresh rock samples using Fe (w%) t, CaO (w%) t, FeO (w%), and magnetite determined by SATMAGAN, against Magnetic Susceptibility values. This analysis could identify 04 groups of data which were interpreted as 04 Skarn Rocks and 01 hydrothermal zonation. They are presented in 4 tables below (Tables 3 to 6).

Table 3 – Exploratory Data Analysis for Magnetite (Mt) Skarn. All parameters against Magnetic Susceptibility.

	Mt Skarn				
Validate Parameter	Mag. (%)	Mag_Sus. (x 10^{-3} SI)	FeO (%)	Fe (%)	CaO (%)
Count	217	217	217	217	217
Min	5.12	101.26	13.70	19.62	0.88
Max	33.75	1403.33	36.30	35.58	12.35
Mean	18.34	452.52	21.46	26.06	3.53
Median	18.59	395.88	21.50	25.73	2.90
1st Quartile	14.35	226.74	18.40	23.46	2.06
3rd Quartile	21.94	632.44	24.00	28.33	4.30
Std Deviation	6.02	279.20	4.03	3.41	2.18
Variance	36.30	77950.59	16.21	11.60	4.76
CoVariance	852.26	852.26	46.38	400.97	-72.46

Table 4 – Exploratory Data Analysis for Hydrothermal Alteration, Marbleization. All parameters against Magnetic Susceptibility.

	Marbleization				
Validate Parameter	Mag. (%)	Mag_Sus. (x 10-3 SI)	FeO (%)	Fe (%)	CaO (%)
Count	243	243	243	243	243
Min	0.31	0.00	0.43	2.48	10.20
Max	25.23	571.48	25.10	27.36	40.00
Mean	1.64	23.35	9.74	9.11	22.82
Median	1.05	5.66	8.77	7.94	23.00
1st Quartile	0.67	0.65	5.53	16.53	16.53

3rd Quartile	1.70	19.56	13.30	11.78	28.90
Std Deviation	2.42	61.05	5.23	4.43	7.59
Variance	5.87	3726.83	27.30	19.63	57.54
CoVariance	133.21	133.21	101.47	139.47	-106.00

Table 5 – Exploratory Data Analysis for Grt-Px Skarn. All parameters against Magnetic Susceptibility.

	Grt-Px Skarn				
Validate Parameter	Mag. (%)	Mag_Sus. (x 10-3 SI)	FeO (%)	Fe (%)	CaO (%)
Count	84	84	84	84	84
Min	0.60	10.26	2.42	2.64	1.85
Max	11.29	93.00	24.50	19.94	39.20
Mean	2.19	31.17	11.08	10.22	22.29
Median	1.71	22.79	10.83	9.76	23.80
1st Quartile	1.27	17.17	6.62	6.46	15.45
3rd Quartile	2.31	42.78	15.19	13.50	29.18
Std Deviation	1.79	20.06	5.56	4.55	9.26
Variance	3.20	402.53	30.95	20.71	85.79
CoVariance	19.21	19.21	37.14	39.56	-70.03

Table 6 – Exploratory Data Analysis for Px Skarn and Px-Am Skarn. All parameters against Magnetic Susceptibility.

	Px Skarn/Px-Am Skarn				
Validate Parameter	Mag. (%)	Mag_Sus. (x 10-3 SI)	FeO (%)	Fe (%)	CaO (%)
Count	131	131	131	131	131
Min	0.31	0.00	0.43	2.48	2.48
Max	2.81	9.87	12.10	9.85	40.00
Mean	0.80	2.02	6.48	6.34	22.13
Median	0.71	0.36	6.79	6.46	24.00
1st Quartile	0.52	0.00	4.45	4.69	13.68
3rd Quartile	1.01	3.58	8.05	7.78	29.35
Std Deviation	0.39	2.83	2.64	1.89	9.48
Variance	0.15	8.01	6.96	3.56	89.87
CoVariance	0.61	0.61	-0.74	-0.69	6.34

Through boxplots, it is possible to verify quartiles values and the mean distribution of variables (Figure 17). Magnetite Skarn (Figure 17-a) has the highest percentage of magnetite, total iron, FeO, and Magnetic Susceptibility results, among the lithologies of interest, in contrast with CaO values. Boxplot related to Magnetite (Mt) shows median line in 18.55 (%) indicating a soft negative asymmetric distribution of values meaning most of them are above of this line. Dispersion values are represented by samples found between first and third quartiles, respectively, 14.35 (%) and 21.94 (%). Lower fence and upper

fence values are, respectively, 5.12 and 32.55 (%). One outlier is presented with value of 33.75 (%), above the upper fence line. Boxplot for Fe (Fe_{total}) show soft positive asymmetric distribution presenting first and third quartiles in 23.4 and 28.33 (%). Lower and upper fences are 19.62 and 28.33 (%). Fe shows one outlier, below lower fence, with value of 15.9 (%). FeO is the only boxplot presenting symmetric distribution where first quartile is 18.4 (%) and third quartile is 24 (%). Lower and Upper fence lines are 13.7 and 31.6 (%), respectively. There is one outlier plotting above upper fence with value of 36.3 (%). CaO Boxplot presented positive asymmetric distribution with first quartile in 2.06 (%) and third quartile in 4.36 (%). Lower Fence limit presented 0.88 (%) and 7.89 (%) for upper fence limit. Several outliers are observed above de upper fence line limit. Boxplot related to Magnetic Susceptibility (MS) shows dispersion of samples are between 224.73 x 10^{-3} SI and 630.19 x 10^{-3} SI (first and third quartiles). Median line, which is equal to 391.84 x 10^{-3} SI, indicates soft positive asymmetric distribution meaning most of the values found are below this line. Lower fence and upper fence are, respectively, 101.26 x 10-3 SI and 1,168.33 x 10^{-3} SI. Outliers are present in three observations above of upper line fence showing values of 1,265.6 x 10^{-3} SI, 1,348.33 x 10^{-3} SI, and 1,403.33 x 10^{-3} SI.

Marbleization Zone (Figure 17-b) represents an intermediate pattern between the pluton/igneous intrusion, responsible for providing the fluids, and marble. Also, this zone, a hydrothermal process, is associated with the skarn formations, especially magnetite skarns. Magnetite (%) by SATMAGAN presented dispersion values near 0 % and positive asymmetric distribution. Several outliers are observed with values reaching between 20 and 30 %. This could indicate neo-formation of magnetite as indicated in petrographic analysis. Fe (w%) t and FeO (w%) presented similar dispersion and positive asymmetric distribution and values of third quartile below to 15 %, suggesting an association of iron-bearing mineral phases. Few outliers are found. CaO (w%) presented higher dispersion than the other variables and soft negative asymmetric distribution. Magnetic Susceptibility presented dispersion values below to 20 x 10^{-3} SI and positive asymmetric distribution. Some outliers are observed above the upper fence.

In Grt-Px Skarns (Figure 17-c), magnetite percentage by SATMAGAN is presented with flat dispersion and values near zero. Negative asymmetric distribution is observed. Some outliers are found above the upper fence. Fe (w%) t and FeO (w%) boxplots showed similar dispersion and symmetric distribution. No outliers are found. This means there are iron bearing silicates in mineralogical content, such as Amphibole (Hornblende, Grunerite), product of destabilization of Clinopyroxene (Diopside, Hedenbergite), Orthopyroxene (Ferrossilite), and Garnet (Andradite?) found in petrographic analysis. CaO (w%) presented high dispersion and asymmetric distribution. No outliers are observed. Dispersion of CaO may be understood as a variety of Ca-bearing silicates including pyroxene, amphibole, and garnet. Magnetic susceptibility presented dispersion with values between 19 and 40 x 10^{-3} SI and asymmetric distribution, meaning most values near 20 x 10^{-3} SI. Some outliers are observed above the upper fence. The presence of small contents of magnetite helps to explain the values of magnetic susceptibility, as well the presence of amphiboles may explain the content of ferrous oxide in this faciology.

The other Skarns has presented the same pattern, however values of Total Iron, FeO, Magnetic Susceptibility, and Satmagan showing decrease, despite of CaO that showed an increased value of its interval with small variations. This can be understood as reactions of iron bearing silicates and formation of iron oxides caused by intrusion or contact metamorphism related to plutonism activities in host rocks, particularly marbles.
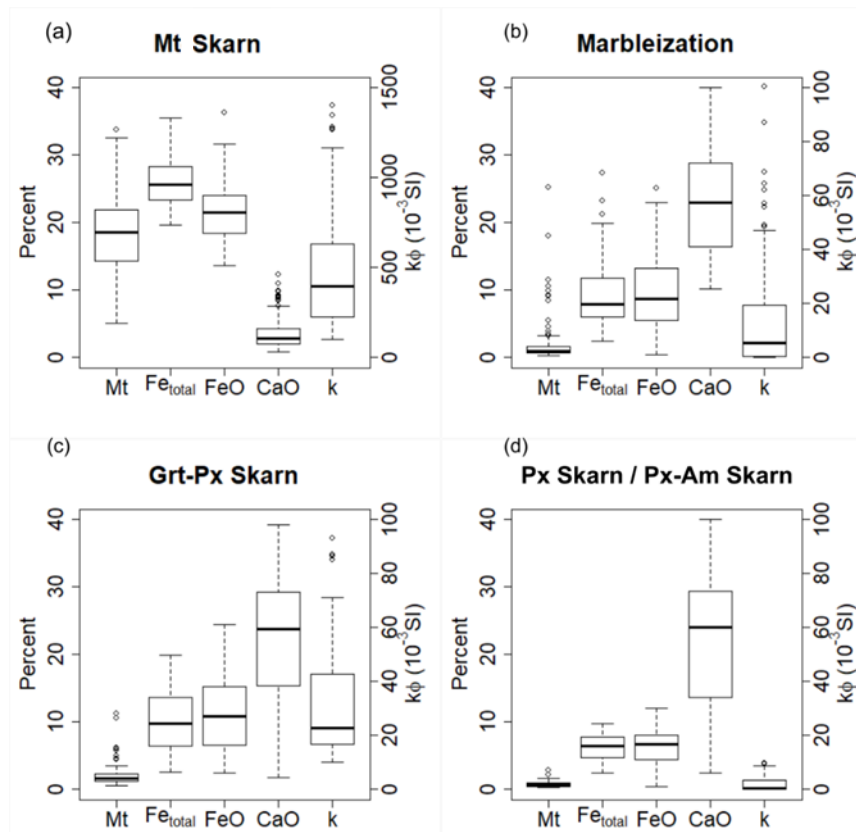
Garnet-Pyroxene Skarns presented magnetic susceptibility intervals between 10 and 99,99 x 10^{-3} SI, values of magnetite by SATMAGAN below 12 %, Fe (w%) t values between 2 % and 20 %, and FeO (w%) below 15 %, helped to delimit this rock.

Granite and gneisses presented values very similar and lower when compared to Skarn lithologies and will not be covered in this section.

Scattergrams of Multiple Linear Regression (Figure 18, below) refer to Skarn lithologies and show characteristics of dispersion among chosen variables. The variables chosen are linked to the processes of formation and mineralogical alteration in these rocks. For Magnetite Skarn, displayed in Figure 18a), there is a relation between Fe (w%) t and FeO (w%) may indicate that a parcell of iron is from iron ferrous meaning this latter may be, not also from another mineral phase or some alteration in Magnetite, but from the Magnetite itself. Relation between Fe (w%) t and Magnetite (%) (by SATMAGAN) indicate 56 % of Fe is from magnetite. Magnetic suceptibility and Magnetite (%) (by SATMAGAN) means

high magnetic susceptibility is from magnetite mineral content. And the inverse linear regression between FeO (w%) and Magnetite (%) (by SATMAGAN) may indicate other mineral phases containing ferrous iron, corroborating the correlation between Fe (w%) t and FeO (w%). The existence of mineral phases including ferrous iron are observed in thin section in the form of pyroxenes such as diopside and/or ferrossilite, and amphiboles, such as hornblende and/or grunerite. Finally, inverse correlation CaO (w%) with the other variable indicates minimum or no content of calcium in this rock type. This information confirms observation in grab sample (with magnifying lenses) and in microscopic analysis that this kind of rock (or faciology) is free of, or is not in contact with, CaO enriched rocks like Marble.

In Figure 18-b), it is observed scattergrams for Marbleization zone, a strong hydrothermal alteration found in drill core samples. Strong linear regression between Fe (w%) t and FeO (w%) indicates the presence of mineral phases with ferrous iron in this faciology. Linear Regression between Magnetic suceptibility and Magnetite (%) (by SATMAGAN) confirms Magnetic Susceptibility is, not also, due to Magnetite content but, in part is due to iron-bearing mineral phases. The inverse regressions between Fe (w%) t and CaO (w%), and FeO (w%) and CaO (w%) may be linked to replacement of Fe^{2+} to Ca^{2+} in amphibole minerals, and/or the non-compatibilization between calcium minerals, like carbonates and iron silicates, like pyroxene and amphibole. At last, but not least, weak linear regression between Magnetic Susceptibility and CaO (w%) means mineral phases containing calcium (e.g., calcite) presents low values of this magnetic property.

Scattergrams for Garnet-Pyroxene Skarns is showed in Figure 18c (below). Linear Regressions between Fe (w%) t x Magnetite (%) (by SATMAGAN), and FeO (w%) x Magnetite (%) (by SATMAGAN), means, respectively, 41 % of iron total is from Magnetite, and 21 % of ferrous iron is content in Magnetite. Strong regression between Fe (w%) t x FeO (w%) refers to ferrous iron and could be related to pyroxene (diopside) and garnet (grossular or andradite), which could be linked to weak and inverse linear regression between FeO (w%) and CaO (w%). This latter regression also may indicate the presence of amphibole. This information is confirmed by petrographic analysis.

The last scattergram set is related to the other two skarn types: Pyroxene-Amphibole Skarns and Pyroxene Skarns (Figure 18d). Both lithotypes are put here together because they present similar values for the chosen variables. The pattern is similar to the other skarn lithotypes when values of Fe (w%) t and FeO are correlated, individually, to CaO (w%) may indicate the presence of pyroxene and amphiboles, especially those which includes CaO and Fe^{2+} into their composition (like tremolite) corroborating the results of the petrographic analyses that show this mineral phase and reaffirm the conditions of hydrothermal activity in these lithologies. Fe and FeO, when analyzed against each other is concerned, once more, about ferrous iron in mineral phases like pyroxene and amphibole. Magnetic susceptibility against the others variable is displayed very dispersive in diagrams and this is attributed to low values (near zero) of the magnetic property.

Figure 18 – Scattergrams between variables input for the multiple linear regression, for the main lithologies of interest in the study area. Abbreviations were generated during R processing: "MAG" refers to magnetite (%) by Satmagan, "SUSCEPT" is equal to magnetic susceptibility (k), "FE" is related to Fe (w%) t, "FeO" is FeO (w%), and CaO means CaO (w%). Pearson correlation coefficients r are given.
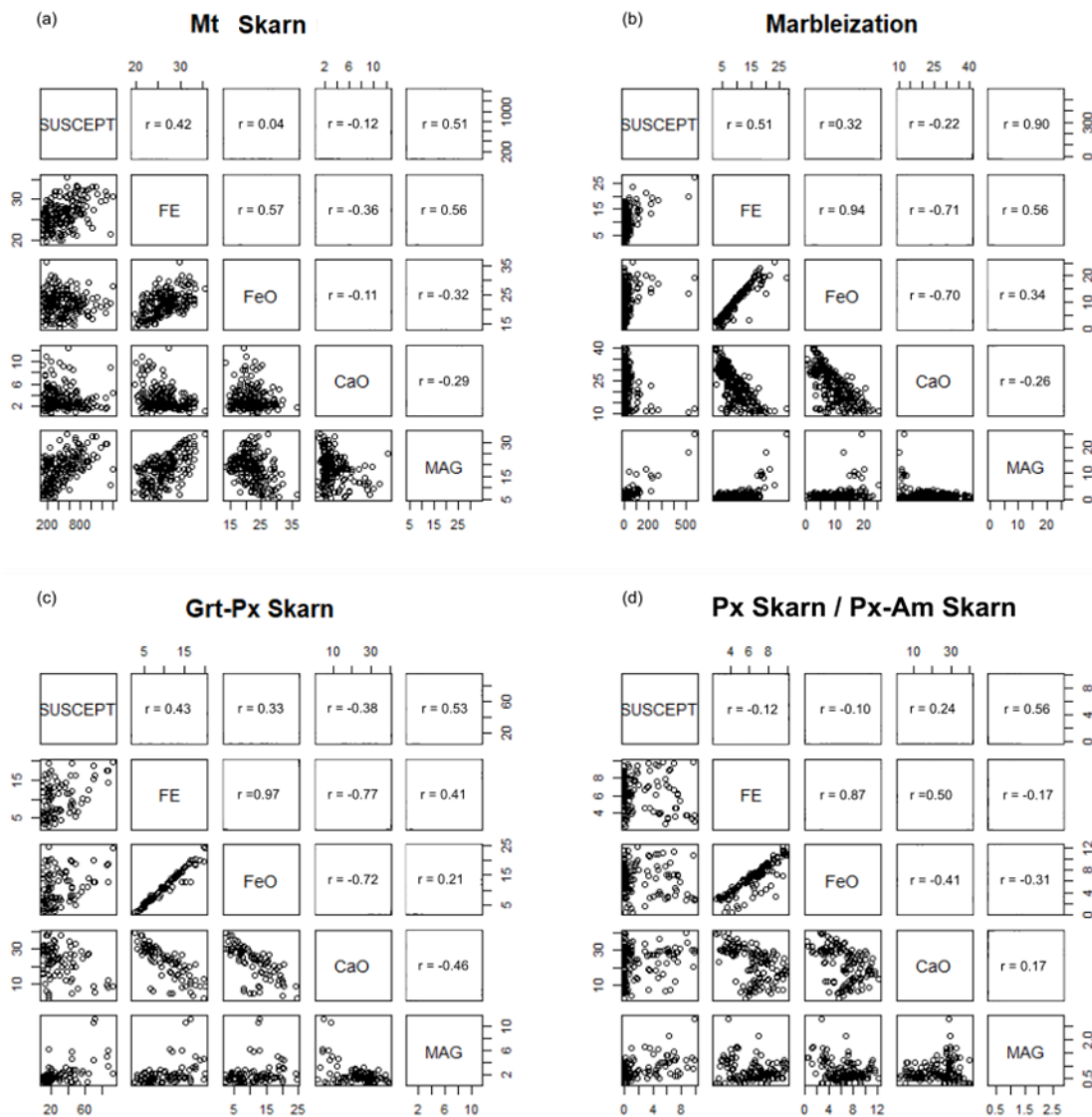
Summaries for model and testes are presented in Table 7.

Not only adjustment of standardized residuals in Q-Q plot but also Shapiro-Wilk normality test didn't reject that residuals for all MLR performed have a normal probability distribution, which is prerogative for the F variance analysis.

ANOVA test rejected null hypothesis H_0 (p-value < 0.05) for MRL, which meant that independent variables could explain the results of k. This situation has happened mainly for Mt and FeO contents – including Mt-Px skarns that have the highest concentration of iron, among lithologies analyzed.

Table 7 - Summaries of multiple linear regression and tests, for the main lithologies of interest in the study area, having k as response variable. Abbreviations: "Mt" refers to magnetite, "Fe" is related to total iron content, "FeO" is ferrous oxide, and CaO means calcium oxide, MLR for multiple linear regression, Df means degrees of freedom.

LITHOLOGY	MODEL/TEST	PARAMETERS			
			Estimate	Std. Error	t value	p value
Mt-Px Skarn	**MLR**	Intercept	-345.63	143.68	-2.41	0.017
		Fe	-52.64	20.58	-2.56	0.011
		FeO	54.65	15.19	3.60	< 0.001
		CaO	8.32	7.78	1.07	0.286
		Mt	52.78	9.98	5.29	< 0.001
		$R^2 = 0.3185$; F-statistic: 26.24 on 4; 212 Df, p-value: < 0.001				
	Shapiro-Wilk	p-value <0.001				
	ANOVA		Df	F value	p value	-
		Fe	1	56.38	<0.001	-
		FeO	1	19.17	<0.001	-
		CaO	1	1.43	0.23	-
		Mt	1	27.96	<0.001	-
Marble-ization	**MLR**		Estimate	Std. Error	t value	p value
		Intercept	-21.08	12.44	-1.69	0.091
		Fe	0.09	1.91	0.05	0.961
		FeO	0.25	1.35	0.18	0.853
		CaO	0.18	0.33	0.55	0.582
		Mt	22.55	1.21	18.63	< 0.001
		$R^2 = 0.8112$, F-statistic: 255.7 on 4, 238 Df, p-value: < 0.001				
	Shapiro-Wilk	p-value <0.001				
	ANOVA		Df	F value	p value	-
		Fe	1	335.21	< 0.001	-
		FeO	1	316.28	< 0.001	-
		CaO	1	24.33	< 0.001	-
		Mt	1	346.98	< 0.001	-
Grt-Px Skarn	**MLR**		Estimate	Std. Error	t value	p value
		Intercept	2.51	13.24	0.19	0.85
		Fe	8.45	5.55	1.52	0.13
		FeO	-5.53	4.25	-1.30	0.20
		CaO	0.06	0.32	0.20	0.84
		Mt	0.98	3.23	0.30	0.76
		$R^2 = 0.3229$, F-statistic: 10.9 on 4; 79 Df, p-value: < 0.001				
	Shapiro-Wilk	p-value <0.001				
	ANOVA		Df	F value	p value	-
		Fe	1	23.01	<0.001	-
		FeO	1	20.46	<0.001	-
		CaO	1	0.02	0.883	-
		Mt	1	0.09	0.762	-
Px Skarn	**MLR**		Estimate	Std. Error	t value	p value
		Intercept	-2.51	1.24	-2.02	0.0452
		Fe	-0.48	0.23	-2.11	0.0371
		FeO	0.46142	0.16	2.89	0.0046
		CaO	0.045	0.02	1.84	0.0682
		Mt	4.49	0.56	8.07	< 0.001
		$R^2 = 0.3582$, F-statistic: 19.14 on 4, 126 DF, p-value: < 0.001				
	Shapiro-Wilk	p-value <0.001				
	ANOVA		Df	F value	p value	-
		Fe	1	3.36	0.069	-
		FeO	1	0.13	0.722	-
		CaO	1	7.91	0.00569	-
		Mt	1	65.16	<0.001	-

Table 8 shows analyzed parameters and its intervals for each skarn lithology in the study area. All intervals presented in the table took into account

the statistical analysis carried out and previously commented, through correlation diagrams and boxplots. The magnetic susceptibility intervals shown in the table were used as a parameter for the geophysical model.

Table 8 - Parameters applied do range values of magnetic susceptibility k and group them for lithology.

Lithology	Analyzed Parameters	Intervals
Mt Skarn	Magnetic Susceptibility	$k > 100 \times 10^{-3}$ SI
	Magnetite % (Satmagan)	5 % > x < 35 %
	Fe(w%) t	15 % > x < 40 %
	FeO(w%) t	10 % > x < 40 %
Grt-Px Skarn	Magnetic Susceptibility	$10 \leq k < 99,99 \times 10^{-3}$ SI
	Magnetite % (Satmagan)	x < 5 %
	Fe(w%) t	2 % > x < 20 %
	FeO(w%) t	2 % > x < 25 %
Px Skarn/Px-Am Skarn	Magnetic Susceptibility	$k < 10 \times 10^{-3}$ SI
	Magnetite % (Satmagan)	x ≤ 3 %
	Fe(w%) t	2 % < x < 10 %
	FeO(w%) t	x < 15 %
Marbleization	Magnetic Susceptibility	$k < 50 \times 10^{-3}$ SI
	Magnetite % (Satmagan)	x ≤ 3 %
	Fe(w%) t	*2 < x < 30%*
	FeO (w%)	*2 < x < 25%*
	CaO(w%) t	10 ≤ x ≤ 40 %

4.5 3D Magnetic Inversion

In this study, the inversion approach was made using Total Magnetic Intensity Field map. The inversion was able to provide depth of magnetic sources, shape, and geometry. The magnetic susceptibility values of anomalies of intensity between Very High to Intermediate were compared with magnetic susceptibility data found in drill core.

The high intensity anomalies studied in this work concerns magnetite-bearing rocks which were called Magnetite Skarns.

Two main bodies worked here are regarding to a central body (called Target 1) and to a larger body to East (Target 2). These bodies will be better presented later.

In the Figure 19 is displayed the main isosurface of high-value range, presented in shades of pink. This isosurface represents the lithological type of Magnetite Skarn with cutoff point in 0.0950 (or 95×10^{-3}SI), for magnetic

susceptibility, aligned with susceptibility measurements in drill core and literature data (Clark & Emmerson, 1991 and Hunt et al. 1995).

Figure 19 – Magnetic inversion isosurface of the two main bodies. It is possible to note the shape and geometry of the bodies: a Dike, Target 1, shallower; and, a Pipe, Target 2, reaching deeper depths. The bodies present dip directions to W. The cutoff point is 0.0950 SI (or 95 x 10-3SI). Blue arrows indicate Geographic North.
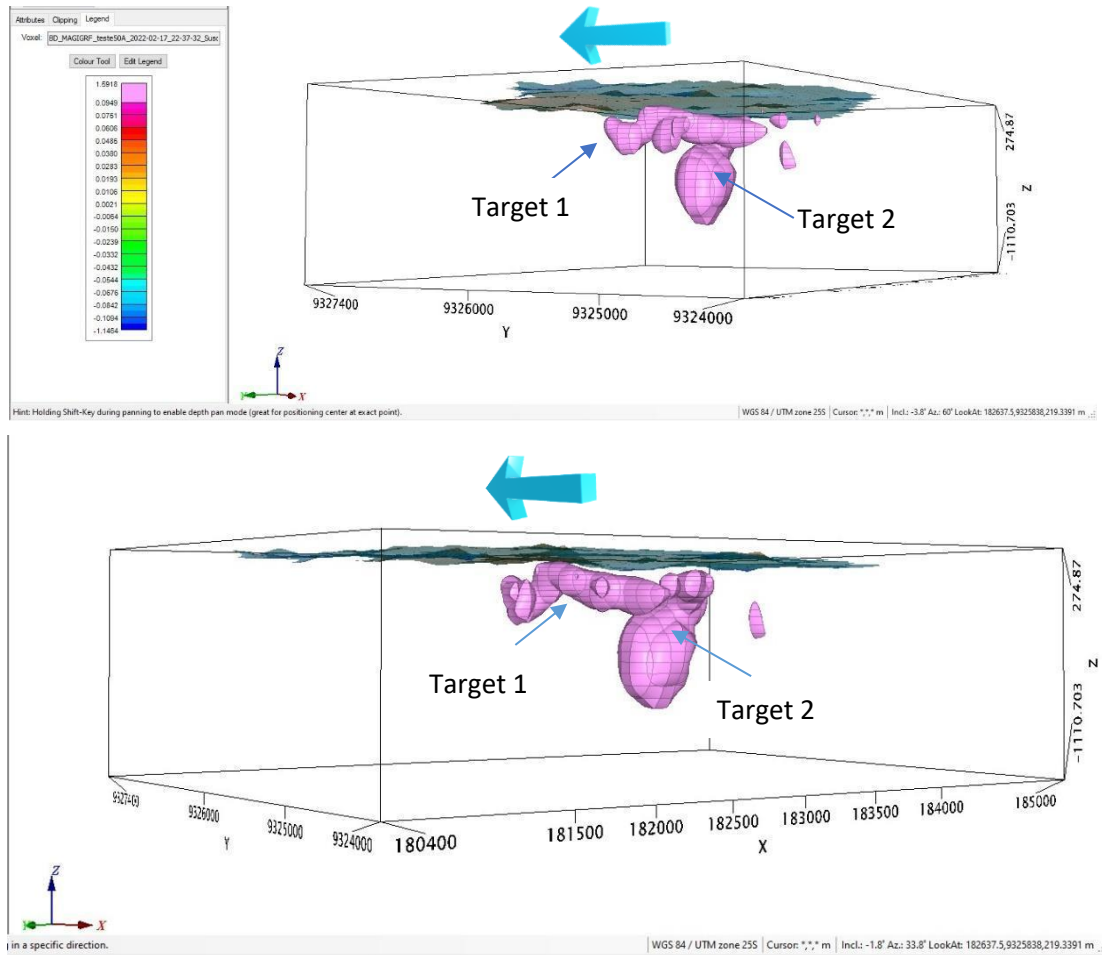
Two larger bodies and proximal smaller bodies may be observed. Target 2 body, positioned to E of the area has cone shape and much of geometry presents itself as Pipe and dives to NW. Target 1 body is in elongated shape and geometrically shows itself as a Dike with direction, approximate, WNW-ESE and vertical diving. These main bodies have maximum depths in order of 730 m and 350 m, respectively. Some smaller bodies have shallower depths (~200 m) and are lined up in the NE-SW direction, in the central part of the area. Other smaller bodies are dispersed at depths close to 800 m. All smaller bodies are circular in shape.

4.5.1. NW-SE Section Analysis

The NW-SE section extracted in the central part of the area shows estimated depths of up to 600 meters for sources with high magnetic susceptibilities, presenting bodies shallower to W and deeper to E of the area.

The section (Figure 20) shows dips in Target 1 and Target 2 bodies, the latter with a moderate to high dip to W (Figure 20, white dashed arrow). Target 1 body presents a high dip angle also to W. The sources show magnetic susceptibility values, at this point, between 63.3 x 10^{-3} (SI) and 942.6 x 10^{-3} (SI), from magnetic inversion data. These magnetic susceptibility values are similar with values measured with the KT-20 susceptibility meter in rock samples from drill core. In general, these values are in accordance to values found in the literature (Clark & Emerson, 1991), when Magnetite Skarns are presented from 120 x 10^{-3} (SI).

Figure 20 – Section from magnetic inversion (112° Az) showing the main causative sources in Geophysical model. Dotted White Arrows shows your dives to W/NW. The white circle shows a possible interaction between anomaly and country rock.
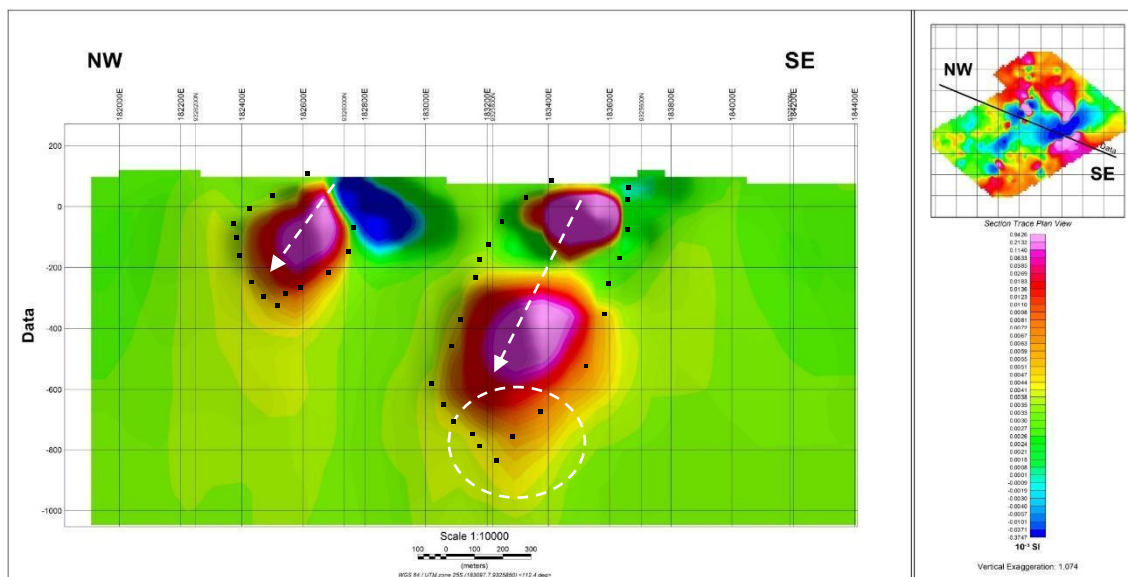
An interaction between different Magnetic Susceptibility products is still noticeable in Target 2 body (Figure 20, white dashed circle), suggesting a link with a deeper magnetic source (not detected) or genetic relationships with tying lithologies.

Target 1 has a higher magnetic susceptibility contrast than Target 2,

indicating contact with a non-magnetite bearing country rock, maybe Monzogranitic OrthoGneisses from Presidente Juscelino/Serra Caiada Complex (Figure 8, blue portion in section).

4.6 Geological Model (Interpretation)

Integrating geophysical data on the surface and in depth with the geological data, it was possible to suggest a geological model. The geological map used the highlighting of the contours of magnetic anomalies in the Amplitude of the Analytical Signal map, to interpret and delimit the lithologies of the area, besides field data on an outcrop and microscope scale. Data from magnetic susceptibility and SATMAGAN helped in the classification of lithologies.

In the geological map (Figure 16b) it is possible to observe a dark green magnetic/geological unit arranged as a range of elongated bodies in the NE-SW direction, approximately 4 km long, and another, smaller, but thicker, also presenting NE-SW direction. This lithology, referred to here as Skarn, presents in the central part of the two bodies, areas enriched in Magnetite, which are referred to as Magnetite Skarns. These bodies are associated with small stocks and granite dikes. All these lithologies lie in an Archean basement composed of Hornblende Orthogneisses, magnetite biotite Gneisses, hornblende Gneisses and Gneisses Granulithic.

The magnetic inversion, based on Magnetic Anomaly map, shows two main bodies, Target 1, in elongated format with Dike geometry and N-S direction. Another, Target 2, with shape of cone and Pipe geometry with dip to NW/W. Smaller bodies appear in the central part of the area, have a circular shape, and are queued with NE-SW orientation. A smaller body, to E, appears to be in line with the Target 1, Dike format body, N-S.

The section generated by inversion remarks the contrast in subsurface, suggesting direction and intensity of dip (Figure 21).

The magnetic intensity of anomalies is confirmed with petrographic information, by Magnetization Saturation Analyses (quantifying Magnetite) and by magnetic susceptibility measurements.
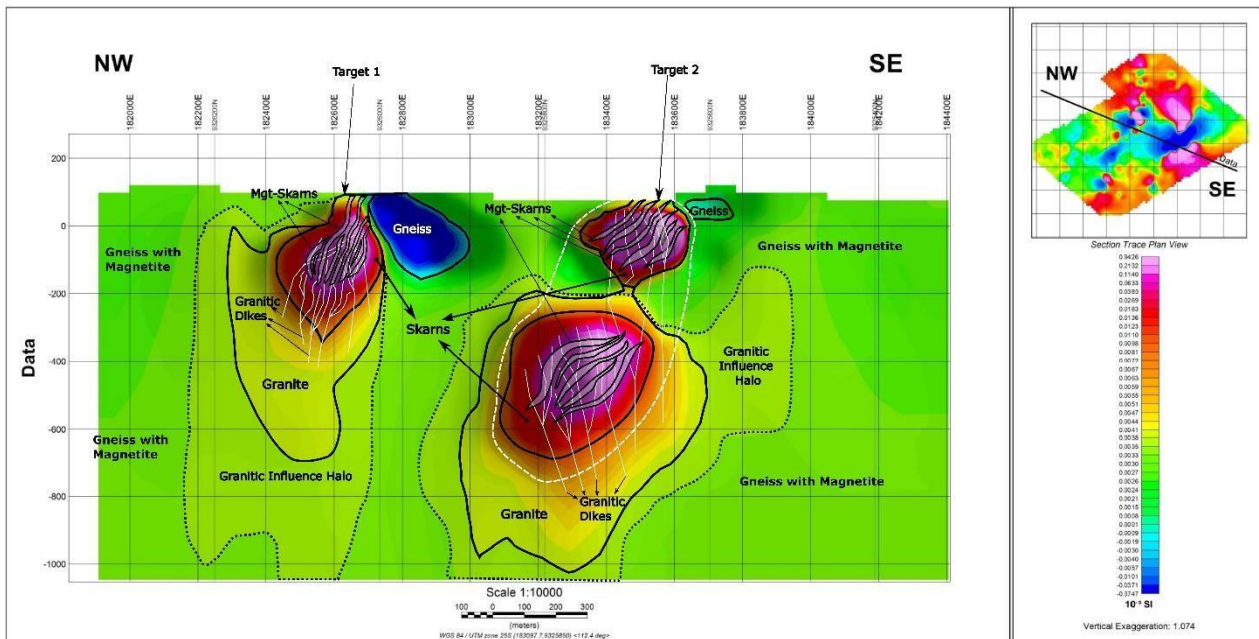
Also in the section, we can relate the graph of the inversion to the geological context of the area in subsurface using geology, SATMAGAN and Magnetic Susceptibility data. The integration of the techniques suggests that anomalous bodies (in pink, in Figure 21) are magnetite-rich rocks and their host rocks have some amount of this mineral.

The exception is the blue part (section center) which would indicate an enclosed lithology with very low concentration or absence of Magnetite.

Magnetic susceptibility model shows that there is a variation within the range and a signature and anomalies contrasting with the country rocks and that there is a direct relationship with the parameters of SATMAGAN and the absolute amount of magnetite in the rock, and that it can be used as a prospective guide to find high-content and mineralized zones.

A few more observations can be made in the section, regarding the interaction between anomalous bodies in pink (magnetite-rich rocks) and intermediate bands in yellow and orange.

These bands may be related to granite rocks, since the Magnetic Susceptibility values presented both in inversion/section and measured in drill core samples and literature values are compatible (Table 9). Thus, the granites observed in the region would be the Magnetite or Type I series,

according to Clark and Emmerson (1991), indicating that the concentrations of Magnetite in the Skarns could be attributed to fluid interactions between the granites and the formation of Magnetite-bearing Skarns or Magnetite Skarns.

Another remarkable point would be the directions of anomalous bodies. The dike-shaped body has almost N-S (NNW-SSE, more precisely) direction while the pipe-shaped body has NE-SW direction. These directions indicate Neoproterozoic relations.

All the information discussed above suggests a non-Classic Model of Fe-Skarn Mineral Deposit for these occurrences of magnetite-rich rocks.

This mixed characteristic gives a hybrid aspect to the deposit, sometimes influencing the immediate classification of the deposit. The iron enrichment paragenesis of these rocks, especially Magnetite, is the main factor for the strong geophysical response in the area. The Magnetic Susceptibility ranges measured in samples and the Magnetite range determined by SATMAGAN are in accordance with those visualized in magnetic inversion (see Table 8). When compared to the literature, these ranges present values measured slightly outside those established and again imply a hybridization. Clark & Emmerson (1991) presented a range between 225 x 10-3 SI to 1180 x 10-3 SI for Magnetite-rich Banded Iron Formation, and this one is inserted in the range found for Magnetite-rich rocks in the studied region, both in the result of the inversion and in the magnetic susceptibility measurements through the KT-20 device (Table 9). Limited and prominent banding rock portions occur at some points in the deposit and are visible in drill cores (Figure 22). Generally, these points display values of magnetic susceptibility compatible with the range suggested in the literature and petrographic aspects hint a classification for BIF. These sections can be interpreted as relicts of BIF's that somehow coexist with the Skarns and may have contributed to their enrichment. This interpretation is consistent with the works of Abrahão Filho (2016) and Dias et al. (2021), however, mineral chemical analyses would be necessary in the samples from the mineralized bodies studied here to ratify it.

Table 9 - Magnetic Susceptibility values and percentage of Magnetite obtained during the study, compared with values obtained in the literature.

Lithologies	Parameters					
	Measured Magnetic Susceptibility by KT-20 device (SI x 10^{-3}) Mean Values	**Magnetic Minerals by SATMAGAN (% Magnetite)**	**3D Magnetic Inversion Magnetic Susceptibility Values (SI x 10^{-3})**	**Section Magnetic Susceptibility Values (SI x 10^{-3})**	**Magnetic Susceptibility SI x 10^{-3} (Clark & Emmerson, 1991)**	**% Magnetite (Clark & Emmerson, 1991)**
Gneisses	0.00 - 94.13	0.41 - 3.48	< 2.1	< 3.8	-	-
Granites	0.03 - 21.87	0.62 - 2.21	2.1 - 48.5	3.8 - 11	0.3 - 70	0.1 - 2
Skarns	0.11 - 144.83	0.31 - 30.00	48.5 - 95	11 - 63.3	0.3 - 105	0.1 - 4
Mgt Skarns	91.25 - 2,867.25	3.68 - 53.45	95 - 1591.8	63.3 -942.6	105 - 1000	4 - 25
Mgt BIF's	-	-	-	-	225-1180	7-20+

Figure 22 - Petrographic and Mineralogical aspects in a rock sample from Target 2 drill core: a) Overview of the drill core; b) A sample of drill core in detail; And c) Petrography of the sample showing band like form alternating quartz (Qz), pyroxene (Py) and magnetite (minerals in black).
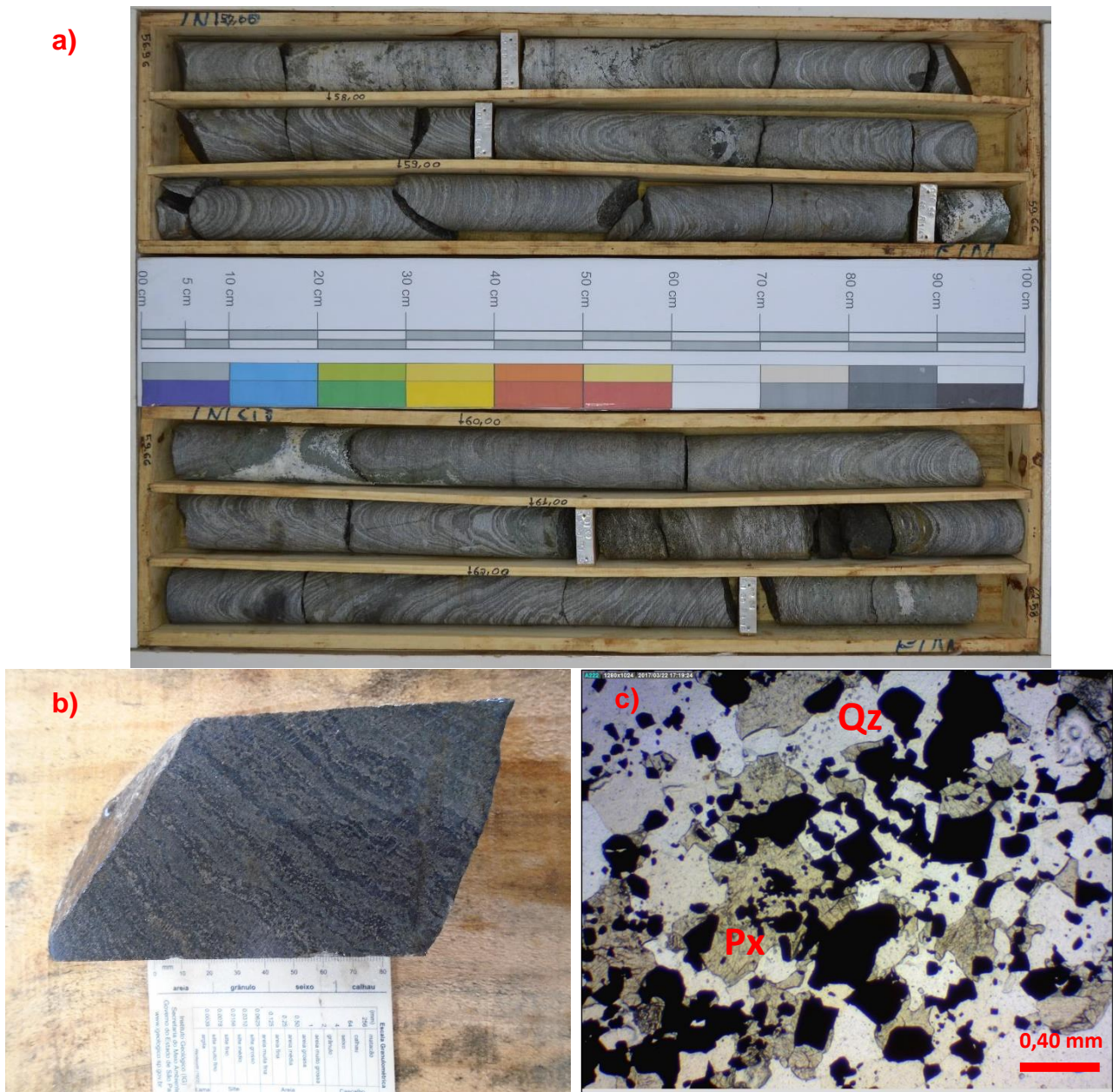
On the other hand, this banded aspect can be a characteristic of the Skarn formation process where the bandings are developed by geochemical dissipative structure, through minerals self-organize according to their chemical affinities forming this type of structure. Generally, bandings are irregular and limited mainly due to the size of veins/veinlets and discontinuities to which metasomatic and hydrothermal fluids percolates and interact with other rocks (marbles, granites, shales,

etc.) (Guy 1993).

Thus, a geological model (Figure 23) is proposed where the Skarns and Magnetite Skarns would have formed from the rework of older rocks under the influence of the Brasiliano Orogeny.

Figure 23 - Interpretation of the Section from Magnetic Inversion. 2D Geologic Model
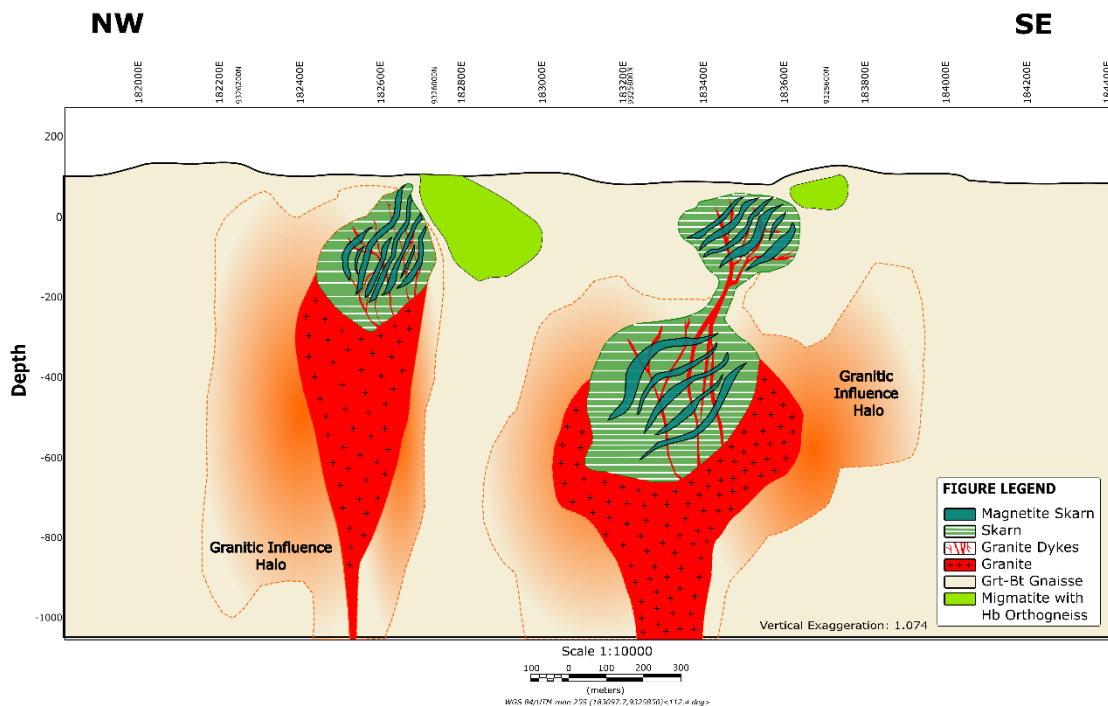
Results indicated a sequence of lithotypes which are compatible with classic Skarn models (Meinert et al., 2005). Mineralogy showed a progradational sequence comprising Amphibole, Pyroxene, Garnet, and Magnetite. A strong carbonate alteration was found, and there is doubt if it can be related to a carbonate rock or to a strong alteration from other rock.

There is a difference in magnetite size along drill core samples. This feature is realized not only by microscope observations but through the susceptibility data. The percentage of magnetite increases in certain zones as the grain size decreases, and the Magnetic Susceptibility vary according to this, suggesting two types of magnetite.

In some points, the Magnetic Susceptibility signature for this magnetite rock is like magnetite rocks classified in other studies, especially

Fe-Skarns (Clark and Emmerson, 1991; Hunt et al., 1995).

By the sections analysed, the following parameters are known: hydrothermalism, such as paragenesis involving carbonate, sulphides, quartz and magnetite, presence of graphite (venules and disseminated) in marbles, formation of garnet from destabilization of other minerals.

The occurrences registered in the region, point to iron ores composed essentially by magnetite, quartz, pyroxene (ferrossilite) and amphibole (grunerite, in less quantities). This mineralogical association is present in all the thin sections studied in the rocks that make up the Skarnitic package. The hydrothermal contribution is confirmed by the presence of huge amount of (CO_2?) fluid which destabilizes the rocks exchanging the mineralogy. The presence of sulphides in some skarns samples also confirms the hydrothermal activity.

The magnetite crystals/blasts observed in the thin sections present various sizes, shapes, and amount, indicating different stages of formation (igneous, metamorphic and/or hydrothermal). Part of this magnetite can be linked to a shear zone process. Exsolutions of ulvospinel are observed included in magnetite crystals and other ganga minerals. Such exsolutions may evidence an Fe-Ti association.

Along drill cores, it is possible to discern zones in the calcissilicatic rocks, however the limits of these zones (or faciologies) are irregular. The susceptibility gauge helped to understand the mineralogy of these zones/faciologies by the contrast of this parameter among intervals. Available Magnetic Susceptibility data in literature confirmed the Mt-Px Skarns intervals.

The Mt Skarn owns the highest magnetic susceptibility values in relation to the other rocks, consequently, it is caused by its greater quantity of magnetite, informed through Satmagan results (Figure 24). Grt-Px Skarn presents intermediate data in comparison to other skarn types, which presented low values to Magnetic Susceptibility.

Figure 24 – *Scale showing different ranges of Magnetic Susceptibility of skarn rocks of the study area, evolved by Clark and Emerson (1991) and adapted for this research.*
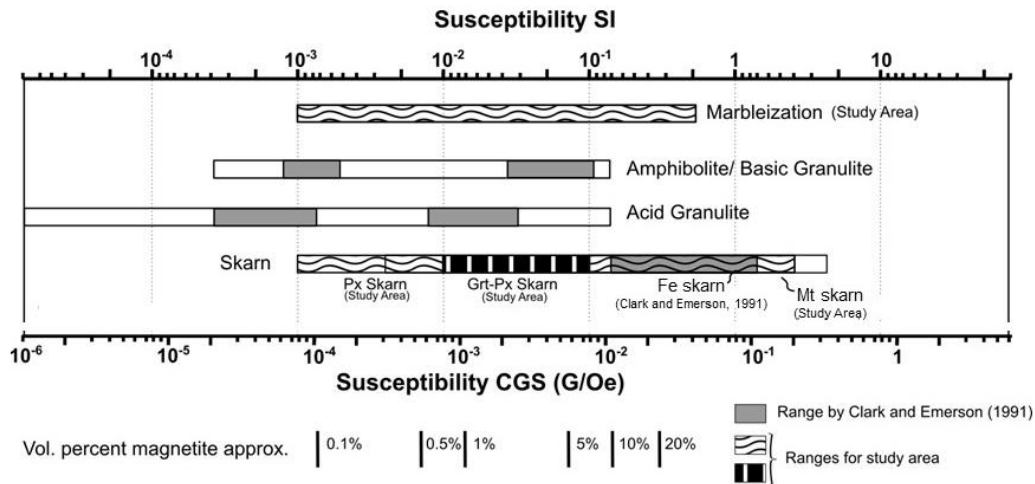
Marbleization facies presented intermediate to low Magnetic Susceptibility values, High values for CaO and the same pattern for FeO and Fe (w%) t, which represents a contribution of a huge amount of fluid interacting with those rocks and exchanging its mineralogy.

Once gathering geological, petrographic, and Magnetic Susceptibility information, a good relation could be seen in Figure 25, which brings magnetic susceptibility profiles related to the drill cores. These pictures represent an integrative approach to provide a delimitation of Skarn rocks and, at least, one Hydrothermal process zone. Graphs shows in detail the interaction of physical parameters in 4 drill holes.

Figure 25 - Profiles above shows relationship among magnetic susceptibility and altered rocks by hydrothermal/metassomatic process. It is noticed the magnetic susceptibility is higher when the amount of magnetite increases. Magnetic signatures in Grt-Px Skarn type is variable, achieving more than 1000 x 10⁻³ SI (DH-03) and near to zero (DH-04). Signature in weathered rocks is almost null and has been avoided in this study. All these values are compatible with the studies of Clark and Emerson (1991) and Hunt et al. (1995).
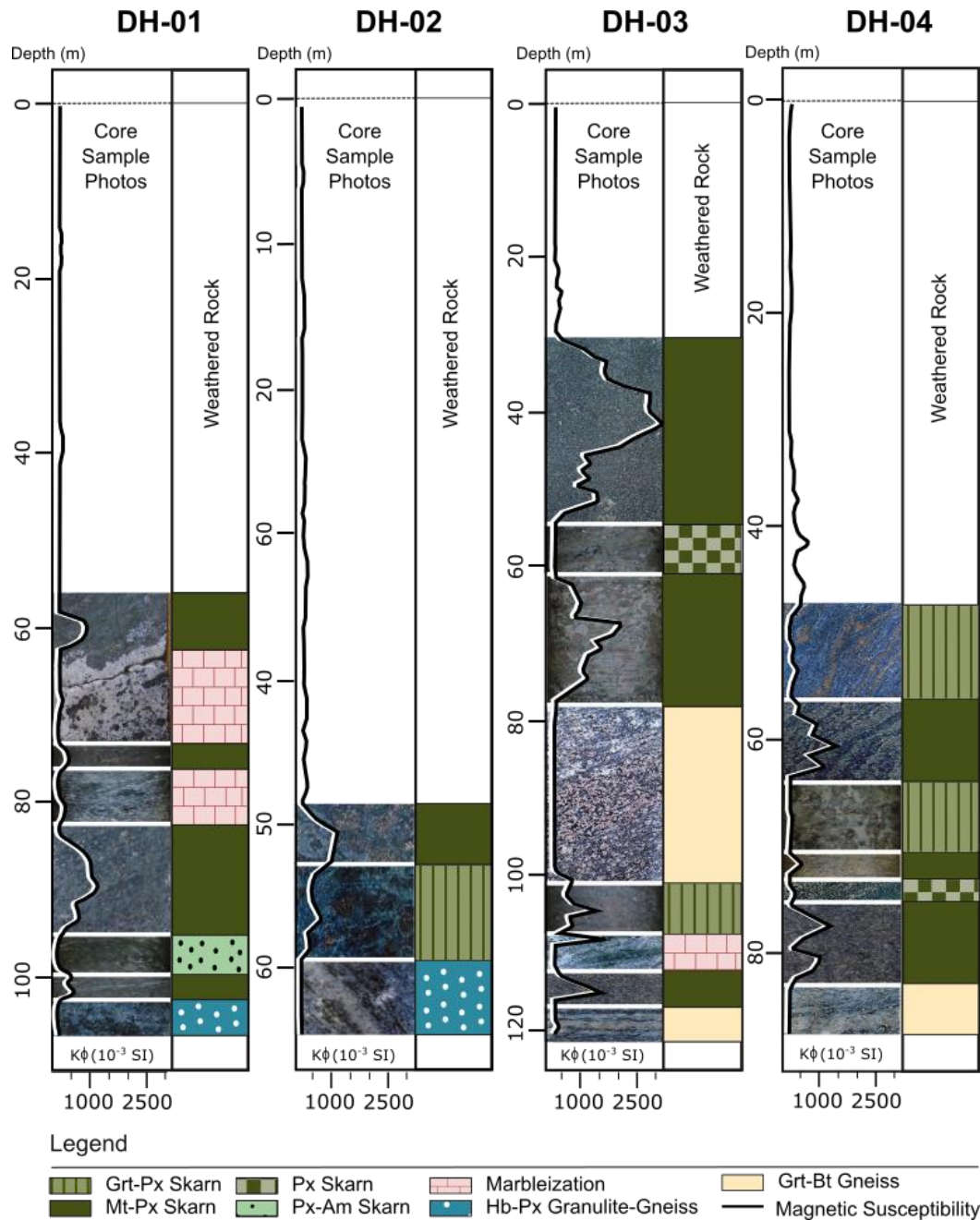
In addition, there is a likely inverse proportion relation between CaO and *k* levels, which suggests that chemical reaction involving alterations of those rocks by hydrothermal fluids, may play an important role in potential iron mineralization in skarns. Those fluids destabilize the rocks providing conditions

to exchange mineralogy. Box plot graphs in section 4.3 show the behavior of those parameters in every skarn rock and marbleization, where CaO values varies from rock to rock and, mostly, in marbleization.

5   CONCLUSIONS

The present work used terrestrial magnetic data combined with surface and subsurface geology information and petrophysical data (Magnetic susceptibility in Probe Holes and Magnetization Saturation Analyses) in addition to a 3D magnetic inversion, to analyse the influence of metamorphic and orogenetic events on magnetite-rich rocks encrusted in Archean terrain. All integrated techniques provided information on the local tectono-structural context and interactions between the Magnetite Skarns and their enduring rocks.

The results shown here demonstrate that:

- There are two major anomalous bodies, Target 1 (W) of shallow depth and a deeper anomaly Target 2 (E).

- Target 1 anomaly, can reach 350 m; and, Target 2 anomaly, can reach 730 m.

- Diamond drilling core suggest that Magnetite bearing Skarn rocks can be found over 100 m deep.

- Statistic Analysis showed the distribution and dispersion of the sample data. It was possible determine 04 Skarn rocks and a Hydrothermal zone. Parametric tests were performed to assess distribution and asses the independence of the parameters.

- Both Anomaly (in depth) suggests the participation of granites in the enrichment of Magnetite Skarns. Granites in region contain magnetite.

- A 2D geological model was generated based on surface mapping and 3D magnetic inversion.

. The results obtained also suggest a lenticular and pod format for the Skarns, to be interlayered between Magnetite bearing and barren Skarns,

giving a pattern of false banding. The classical sequence of progradation and retrogradation is presented in a hybrid way suggesting rock rework and iron remobilization, which may have been mobilized from silicates such as pyroxenes and oxides and deposited as magnetite-rich zones in the form of pockets or lenses. Iron transport may have been controlled via granite Dikes, which served as metal conductors.

ACKNOWLEDGEMENTS

REFERENCES

Abrahão-Filho, E.A. 2016. Rochas piroxeníticas ricas em ferro do Maciço São José do Campestre, Rio Grande do Norte, Brasil. MSc. diss., Brasília Univ.

Al Macky, M., M. Rosid, and A. Jaman. 2020. Mapping of gold mineralization using 3D inversion magnetic data at Zone X, West Java. Journal of Physics Conference Series. doi: 10.1088/1742-6596/1494/1/012034

An, S., K. Zhou, J. Wang, H. Yang, and Z. Zhang. 2018. Integrated analysis of gravity and magnetic fields in the Eastern Tianshan Belt, Xinjiang, Central Asia: Implications for Cu-Au-Fe polymetallic deposits exploration. Journal of Applied Geophysics 159:319-328. doi: 10.1016/j.jappgeo.2018.09.002

Anderson, K., F. Wall, G. Rollinson, and C. Moon. 2014. Quantitative mineralogical and chemical assessment of the Nkout iron ore deposit, Southern Cameroon. Ore Geology Reviews 62:25-39. doi: 10.1016/j.oregeorev.2014.02.015.

Araújo, I. L. 2012. Caracterização do arcabouço tectônico do terreno São José do Campestre, Província Borborema, com base em dados de aerogeofísica. MSc. diss., Brasília Univ.

Archanjo, C.J., M.H.B.M. Hollanda, S.W. Rodrigues, B.B.B. Neves, and R. Armstrong. 2008. Fabrics of pre- and syntectonic granite plutons and chronology of shear zones in the Eastern Borborema Province, NE Brazil. Journal of Structural Geology 30(3):310-336. doi: 10.1016/j.jsg.2007.11.011

Arthaud, M.H., Caby, R., Fuck, R.A., Dantas, E.L., and Parente, C.V. 2008. Geology of the northern Borborema Province, NE Brazil and its correlation with Nigeria, NW Africa. Geological Society, London, Special Publications 294(1):49-67. doi: 10.1144/SP294.4

Bastos, C.F., F.A. Caxito, J.A.R. Vale, D.A. Silveira, J.B. Rodrigues, A.R. Alkmim, C.M. Valeriano, and E.J. Santos. 2019. An Ediacaran back-arc basin preserved in the Transversal Zone of the Borborema

Province: evidence from geochemistry, geochronology and isotope systematics of the Ipueirinha Group, NE Brazil. Precambrian Research 320:213-231. doi: 10.1016/j.precamres.2018.11.002

Barton, M.D., and D.A. Johnson. 1996. Evaporitic-source model for igneous-related Fe oxide-(REE- Cu-Au-U) mineralization. Geology 24(3):259-262.

Bridges, I.C. 1974. Machine contouring using minimum curvature. Geophysics 39:39-48. doi: 10.1190/1.1440410

Brito-Neves, B.B., E.J. Santos, and W.R.Q. Van-Schmus. 2000. Tectonic history of the Borborema province. In Tectonic Evolution of South America, ed. U.G. Cordani, E.J. Milani, A. Thomaz-Filho, and D.A. Campos, 151- 182. 31st International Geological Congress (Rio de Janeiro).

Brito-Neves, B.B., R.A. Fuck, and M.M. Pimentel. 2014. The Brasiliano collage in South America: a review. Brazilian Journal of Geology 44(3):493-518. doi: 10.5327/Z2317-4889201400030010

Brito-Neves, B.B., E.J. Santos, R.A. Fuck, and L.C.M.L. Santos. 2016. A preserved early Ediacaran magmatic arc at the northernmost portion of the Transversal Zone central subprovince of the Borborema Province, Northeastern South American. Brazilian Journal of Geology 46(4):491-508. doi: 10.1590/2317-4889201620160004

Clark, D.A., and D.W. Emerson. 1991. Notes on rock magnetization characteristics in applied geophysical studies. Exploration Geophysics 22: 547-555.

Costa, F.G., E.S.M. Palheta, J.B. Rodrigues, I.P. Gomes, and A.M. Vasconcelos. 2015. Geochemistry and U–Pb zircon ages of plutonic rocks from the Algodões granite-greenstone terrane, Tróia Massif, northern Borborema Province, Brazil: Implications for Paleoproterozoic subduction- accretion processes. Journal of South American Earth Sciences 59:45-68. doi: 10.1016/j.jsames.2015.01.007

Dantas E.L. 1997. Geocronologia U-Pb e Sm-Nd de terrenos Arqueanos e paleoproterozóicos do Maciço Caldas Brandão, NE do Brasil. PhD Thesis, Paulista State Univ.

Dantas, E.L., W.R. Van-Schmus, P.C. Hackspacher, A.H. Fetter, B.B. Brito-Neves, U. Cordani, A.P. Nutman, and I.S. Williams. 2004. The 3.4–3.5 Ga São José do Campestre massif, NE Brazil: remnants of the oldest crust in South America. Precambrian Research 130:113-137. doi: 10.1016/j.precamres.2003.11.002

Dantas, E.L., Z.S. Souza, E. Wernick, P.C. Hackspacher, H. Martin, D. Xiadong, and J.W. Li. 2013. Crustal growth in the 3.4-2.7 Ga São José do Campestre Massif, Borborema Province, NE Brazil. Precambrian Research 227:120-156. doi: 10.1016/j.precamres.2012.08.006

Deer, W.A.; R.A. Howie; and J. Zussman. 2005. Minerais constituintes das rochas: uma introdução. 2nd ed. Lisbon: Fundação Calouste Gulbenkian.

Figueiredo, B.S. 2012. Geoquímica e gênese das formações ferríferas e metacarbonatos da porção sul do Maciço São José do Campestre, Província Borborema. MSc diss., Brasília Univ.

Fries, M., M.M. Zago, and F.G. Silva. 2020. A geophysical study contributing to analysis and characterization of a localized copper occurrence. Journal of Applied Geophysics 179: 104129. doi: 10.1016/j.jappgeo.2020.104129.

Fruchting, A. 2017. Estratégias para utilização de dados geofísicos na exploração de mineralizações do tipo Ni-Cu-PGE: a descoberta do depósito de limoeiro, PE. MSc diss., Brasília Univ.

Gonçalves, L. C. 2009.Contribuição geofísica à análise do arcabouço tectônico do domínio Rio Grande do Norte, Província Borborema - NE Brasil. MSc diss., Brasília Univ.

Gonçalves, B.F., and E.E.S. Sampaio. 2013. Interpretation of airborne and ground magnetic and gamma-ray spectrometry data in prospecting for base metals in the central-north part of the Itabuna-Salvador-Curaçá Block, Bahia, Brazil. Interpretation 1:T85-T100. doi: 10.1190/INT- 2012-0002.1

Gorczyk, W., and K. Vogt. 2018. Intrusion of magmatic bodies into the continental crust: 3-D numerical models. Tectonics 37:705–723. doi: 10.1002/2017TC004738

Guy, B. 1993. Banded skarns, an example of geochemical dissipative structure. https://hal.science/hal-00523251/ (accessed February 9th, 2023).

Honsho, C., T. Yamazaki, T. Ura, K. Okino, H. Morozumi, and S. Ueda. 2016, Magnetic anomalies associated with abundant production of pyrrhotite in a sulfide deposit in the Okinawa Trough, Japan. Geochemistry, Geophysics, Geosystems 17:4413– 4424. doi:10.1002/2016GC006480.

Hunt, C., B.M. Moskowitz, and S.K. Banerje. 1995. Magnetic properties of rocks and minerals. In A Handbook of Physical Constants, ed. T.J. Ahrens, 189-204, vol. 3. Washington: American Geophysical Union.

Jiang, D., Z. Zeng, S. Zhou, Y. Guan, T. Lin, and P. Lu. 2020. Three-Dimensional Magnetic Inversion Based on an Adaptive Quadtree Data Compression. Applied Sciences 10(21):7636. doi: 10.3390/app10217636

Khesin, B., S. Feinstein, Y. Vapnik, S. Itkis, and R. Leonhardt. 2005. Magnetic study of metamorphosed sedimentary rocks of the Hatrurim formation, Israel. Geophysical Journal International 162: 49- 63. doi: 10.1111/j.1365-246X.2005.02630.x

Kim, E. J., D. Shin, S. Shin, H.T. Nam, and S. Park. 2015. Skarn zonation and rock physical properties of the Wondong Fe-Pb-Zn polymetallic deposit, Korea. Geosciences Journal 19:587-598. doi: 10.1007/s12303-015-0017-2

Landim, P.M.B. 2011. Análise estatística de dados geológicos multivariados. São Paulo: Oficina de Textos.

Lima, H., M. Pimentel, L. Santos, and E. Dantas. 2019. Isotopic and geochemical characterization of the metavolcano-sedimentary rocks of the Jirau do Ponciano dome: A structural window to a Paleoproterozoic continental ARC root within the Southern Borborema province, Northeast Brazil. Journal of South American Earth Sciences 90:54-69. doi: 10.1016/j.jsames.2018.12.002

Lino, L.M., F.A. Cavallaro, S.R.F. Vlach, and D.C. Coelho. 2018. 2D magnetometric modeling of a basic-intermediate intrusion geometry: geophysical and geological approaches applied to the Limeira intrusion, Paraná Magmatic Province (SP, Brazil). Brazilian Journal of Geology 48(2):305-315. doi: 10.1590/2317-4889201820180099

Lishchuk, V., C. Lund, P. Koch, B. Pålsson, and M. Gustafsson. 2019. Geometallurgical characterisation of Leveäniemi iron ore – unlocking the patterns. Minerals Engineering 131:325-335. doi: 10.1016/j.mineng.2018.11.034

Lishchuk, V., C. Lund, and Y. Ghorbani. 2019. Evaluation and comparison of different machine-learning methods to integrate sparse process data into a spatial model in geometallurgy. Minerals Engineering 134:156-165. doi: 10.1016/j.mineng.2019.01.032

Liu, S., M. Fedi, X. Hu, Y. Ou, J. Baniamerian, B. Zuo, Y. Liu, and R. Zhu. 2018. 3D inversion of magnetic data in the simultaneous presence of significant remanent magnetization and self-demagnetization: example from Daye iron-ore deposit, Hubei province, China. Geophysical Journal International 215(1):614-634. doi: 10.1093/gji/ggy299.

Markowski, A., J. Vallance, M. Chiaradia, and L. Fontboté. 2006. Mineral zoning and gold occurrence in the Fortuna skarn mine, Nambija district, Ecuador. Mineralium Deposita 41:301-321. doi: 10.1007/s00126-006-0062-x

Mazhari, Nazi, A. Malekzadeh-Shafaroudi, and M. Ghaderi. 2017. Detecting and mapping different types of iron mineralization in Sangan mining region, NE Iran, using satellite image and airborne geophysical data. Geosciences Journal 21:137-148. doi: 10.1007/s12303-016-0018-9.

McGladrey, A.J., G.R. Olivo, A.M. Silva, G.D. Oliveira, B.B. Neto, and S. Perrouty. 2017. The integration of physical rock properties, mineralogy and geochemistry for the exploration of large zinc silicate deposits: a case study of the Vazante zinc deposits, Minas Gerais, Brazil. Journal of Applied Geophysics 136:400-416. doi: 10.1016/j.jappgeo.2016.11.013

Meinert, L.D. 1992. Skarns and skarn deposits. Geoscience Canada 19(4):145-162.

Meinert, L.D. 2000. Gold skarns related to epizonal plutons. Rev Econ Geol 13:347–375.

Meinert, L.D., G.M. Dipple, and S. Nicolescu. 2005. World skarn deposits. Economic Geology 100th Anniversary SI:299-336. doi: 10.5382/AV100.11

Miller, H.G., and V. Singh. 1994 Potential Field Tilt a New Concept for Location of Potential Field Sources. Journal of Applied Geophysics 32:213-217. doi: 10.1016/0926-9851(94)90022-1

Moraes, J.D.S. 2020. Gênese das formações ferríferas da porção central do Maciço São José do Campestre, Rio Grande do Norte, Nordeste do Brasil. MSc diss., Brasília Univ.

Moraes, J.D., P.F. Cordeiro, E. Abrahão-Filho, J.R. Oliveira, and C.V. Silva Filho. 2022. Metamorphic disturbances of magnetite chemistry and the Sm-Nd isotopic system of reworked Archean iron formations from NE Brazil. Geoscience frontiers 13(5), 101131. doi: 10.1016/j.gsf.2020.11.018

Mueller, A.G. 1997. The Nevoria gold skarn deposit in Archean iron-formation, Southern Cross greenstone belt, Western Australia; I, Tectonic setting, petrography, and classification. Economic Geology 92(2):181–209. doi: 10.2113/gsecongeo.92.2.181

Nabighian M.N., V.J.S. Grauch, R.O. Hansen, T. Lafehr, W. Pearson, and J.D. Phillips. 2005. The historical development of the magnetic method in exploration. Geophysics 70(6):33ND-61ND. doi: 10.1190/1.2133784

Neves, S.P., O. Bruguier, A. Vauchez, D. Bosch, J.M.R. Silva, and G. Mariano, 2006. Timing of crustal formation, deposition of supracrustal sequences and Transamazonian and Brasiliano metamorphism in easter Borborema Province (BE Brazil): Implications for western Gondwana assembly. Precambrian Research 149(3-4):197-216. doi: 10.1016/j.precamres.2006.06.005

Neves, S.P., O. Bruguier, J.M. Silva, G. Mariano, A.F. Filho, and C.M. Teixeira. 2015. From extension to shortening: Dating the onset of the Brasiliano Orogeny in eastern Borborema Province (NE Brazil). Journal of South American Earth Sciences 58:238-256. doi: 10.1016/j.jsames.2014.06.004

Nielsen, B.M., and T.M. Rasmussen. 2002. Geological correlation of magnetic susceptibility and profiles from Nordre Strømfjord, southern West Greenland. Geology of Greenland Survey Bulletin 191:48–56. doi: 10.1016/S0301-9268(98)00098-9

NOAA. 2019. International Geomagnetic Reference Field. https://www.ngdc.noaa.gov/IAGA/vmod/igrf.html (accessed February 9th, 2023).

Parente C.V., C.U.V. Veríssimo, N.F. Botelho, T.J.S. Santos, C.G. Oliveira, J.A. Lira-Júnior, and D.T. Martins. 2015. Fe-Cu skarns deposits in the Santa Quiteria magmatic arc, Borborema Province, Brazil. Brazilian Journal of Geology 45:359-382. doi: 10.1590/2317- 488920150030264

Pereira, L.C.L., L.C.M.L. Santos, and T.A. Carrino. 2019. The role of airborne geophysics in the investigation of gold occurrences in the Itapetim Region, Borborema Province, Northeast Brazil. Brazilian Journal of Geology 49(3):1-17. doi: 10.1590/2317-4889201920190028

Pérez-Barnuevo, L., S. Lévesque, and C. Bazin. 2018. Drill core texture as geometallurgical indicator for the Mont-Wright iron ore deposit (Québec, Canada). Minerals Engineering 122:130-141. doi: 10.1016/j.mineng.2018.03.020.

Pilkington, M., and Z. Bardossy. 2015. Dsim 3d: Software to Perform Unconstrained 3d Inversion of Magnetic Data. Natural Resources Canada.

http://oaresource.library.carleton.ca/wcl/2016/20160718/M183-2-7749-eng.pdf (accessed February 9th, 2023).

Raju, P.V.S., and K.S. Kumar. 2020. Magnetic Survey for Iron-Oxide-Copper-Gold (IOCG) and Alkali Calcic Alteration Signatures in Gadarwara, M.P, India: Implications on Copper Metallogeny. Minerals 10(8):671. doi: 10.3390/min10080671

Roig, H.L., and E.L. Dantas. 2013. Folha SB.25-Y-A-I São José do Campestre: carta geológica - escala 1:100.000. Brasília, Serviço Geológico do Brasil - CPRM. color map. http://rigeo.cprm.gov.br/jspui/handle/doc/17669 (accessed February 9th, 2023).

Santos, E.J., and V.C. Medeiros. 1999. Constraints from granitic plutonism on Proterozoic crustal growth of the transverse zone, Borborema province, NE-Brazil. Revista Brasileira de Geociências 29(1):73-84. doi: 10.25249/0375-7536.1999297384

Santos, L.C.M.L., E.L. Dantas, E.J. Santos, R.V. Santos, and H.M. Lima. 2015. Early to late Paleoproterozoic magmatism in NE Brazil: The Alto Moxotó Terrane and its tectonic implications for the pre-Western Gondwana assembly. Journal of South American Earth Sciences 58:188- 209. doi: 10.1016/j.jsames.2014.07.006

Santos, L.C.M.L., E.L. Dantas, P.A. Cawood, E.J. Santos, and R.A. Fuck. 2017. Neoarchean crustal growth and Paleoproterozoic reworking in the Borborema Province, NE Brazil: insights from geochemical and isotopic data of TTG and metagranitic rocks of the Alto Moxotó Terrane. Journal of South American Earth Sciences 79:342-363. doi: 10.1016/j.jsames.2017.08.013

Santos, L.C.M.L., E.L. Dantas, P.A. Cawood, G.A. Lages, H.M. Lima, and E.J. Santos. 2018. Accretion tectonics in western Gondwana deduced from Sm- Nd isotope mapping of terranes in the Borborema Province, NE Brazil. Tectonics 37(8):2727-2743. doi: 10.1029/2018TC005130

Shafiei, B., and J. Shahabpour. 2008. Gold Distribution in Porphyry Copper Deposits of Kerman Region, Southeastern Iran. Journal of Sciences Islamic Republic of Iran 19:247-260.

Shapiro, S.S., and M.B. Wilk. 1965. An analysis of variance test for normality (complete samples). Biometrika 52(3-4):591–611. doi: 10.1093/biomet/52.3-4.591

Sheibi, M., H. Mirnejad, and M. Moghaddama. 2016. Magnetic susceptibility anisotropy as a predictive exploration tool of metasomatic iron oxide deposits: Example from the Panj-Kuh iron ore body, NE Iran. Ore Geology Reviews 72:612–628. doi: 10.1016/j.oregeorev.2015.08.024.

Sial, A., and V. Ferreira. 2016. Magma associations in Ediacaran granitoids of the Cachoeirinha– Salgueiro and Alto Pajeú terranes, northeastern Brazil: Forty years of studies. Journal of South American Earth Sciences 68:113-133. doi: 10.1016/j.jsames.2015.10.005

Silva-Filho, C.V.R. 2012. Isótopos de Nd aplicados à datação direta de formações ferríferas paleoarqueanas do maciço São José do Campestre, Rio Grande do Norte-RN. MSc diss., Brasília Univ.

Souza, Z.S., F. Kalsbeek, X. Deng, R. Frei, E.L. Dantas, J. Li, M.M. Pimentel, and A.C. Galindo. 2016. Generation of continental crust in the northern part of the Borborema Province, northeastern Brazil, from Archaean to Neoproterozoic. Journal of South American Earth Sciences 68:68-96. doi: 10.1016/j.jsames.2015.10.006

Souza-Neto, J.A., J.M. Legrand, M. Volfinger, M.L. Pascal, and P. Sonnet. 2008. W-Au skarns in the Neo- Proterozoic Seridó Mobile Belt, Borborema Province in northeastern Brazil: an overview with emphasis on the Bonfim deposit. Mineralium Deposita 43(2):185-205. doi: 10.1007/s00126-007-0155-1

Storch, HV, and F.W. Zwiers. 2003. Analysis of Variance. In Statistical analysis in climate research, 171-192, 2nd edn. Cambridge: Cambridge University Press.

Stradling, A.W. 1991. Development of a mathematical model of a crossbelt magnetic separator. Minerals Engineering 4:733-745.

Sun, S., and C. Chao. 2016. A self-constrained inversion of magnetic data based on correlation method. Journal of Applied Geophysics 135:8-16. doi: 10.1016/j.jappgeo.2016.09.022.

Yang, Y.S., Y.Y. Li, T.Y. Liu, Y.L. Zhan, and J. Feng. 2011. Interactive 3D forward Modeling of Total Field Surface and Three-Component Borehole Magnetic Data for the Daye Iron-Ore Deposit (Central China). Journal of Applied Geophysics 75:254-263. doi: 10.1016/j.jappgeo.2011.07.010

Van-Schmus, W.R., B.B. Brito-Neves, P.C. Hackspacher, and M. Babinski. 1995. U/Pb and Sm/Nd geochronologic studies of the eastern Borborema Province, Northeast Brazil: initial conclusions. Journal of South American Earth Sciences 8(3-4):267-288. doi: 10.1016/0895- 9811(95)00013-6

Van-Schmus, W.R., E.P. Oliveira, A.F. Silva-Filho, F. Toteu, J. Penaye, and I.P. Guimarães. 2008. Proterozoic links between the Borborema province, NE Brazil, and the central African fold belt. Geological Society of London 294(1):66-69. doi: 10.1144/SP294.5

Van-Schmus, W.R., M. Kozuch, and B.B. Brito-Neves. 2011. Precambrian history of the Zona Trasnversal of the Borborema Province, NE Brazil; Insights from Sm-Nd and U-Pb geochronology. Journal of South American Earth Sciences 31(2-3):227-252. doi: 10.1016/j.jsames.2011.02.010

Verduzco, B., J. Fairhead, C Green., and C. MacKenzie. 2004. New Insights into magnetic derivatives for structural imaging. The Leading Edge 23:116-119. doi: 10.1190/1.1651454

CAPÍTULO 3
DISCUSSÕES E CONCLUSÃO

CAPÍTULO 3 – DISCUSSÕES E CONCLUSÃO

Observações de campo mostraram que os corpos mineralizados possuem direções NE-SW com mergulho acentuado para NW. Através dessas observações, nota-se o controle estrutural desses corpos por zonas de cisalhamento dextrais. Tal controle estrutural por zonas de cisalhamento é observado em análises petrográficas através de estruturas S-C e minerais deformados e recristalizados (e.g. quartzo com extinção ondulante). Essas feições estruturais são compatíveis com a configuração tectono-estrutural da Orogênese Brasiliana.

As relações mineralógicas em análises petrográficas mostram quatro zonas principais, sendo uma zona distal rica em piroxênio e uma zona proximal rica em granada. A mineralogia apresentada está de acordo com a mineralogia encontrada em trabalhos clássicos sobre *skarn*. As alterações encontradas dizem respeito a silicificação e carbonatação, predominantemente.

Ainda, é possível notar em superfície e em furos de sonda a influência de tectônica rúptil e intrusões de diques graníticos com magnetita em rochas calcissilicáticas. Diques de monzogranito, a magnetita, cortam todas as estruturas. A assinatura de susceptibilidade magnética para esses granitos acusa tipologia I, juntamente com a sua correspondente, relativamente alta porcentagem em minerais de magnetita, determinadas por SATMAGAN.

Aos diques de granito da região estudada são atribuídas idades ediacaranas e caráter pós tectônico a tardimagmático com base em relações de campo (Pinheiro, 2009) e Geoquímica de rocha total, química mineral e datações em plutons correlatos (Cavalcante et al., 2014, Antunes 2000, Dias, 2006).

Os resultados físicos apresentados estão de acordo com classificações de literatura onde apontam para assinatura de susceptibilidade magnética e porcentagem de magnetita, determinadas por SATMAGAN, correlacionadas a Fe-*Skarns*.

A análise estatística mostrou a distribuição e dispersão dos dados amostrais. Foi possível determinar 04 faciologias de Skarn e uma zona Hidrotermal. Testes paramétricos foram realizados para avaliar a distribuição e a independência entre os parâmetros.

A geofísica terrestre identificou duas anomalias principais apresentando direções NE-SW, delimitadas por Amplitude do Sinal Analítico (ASA). Também foi possível distinguir três domínios (A, B e C) onde as anomalias aumentam sua intensidade de Oeste para Leste.

Através da inversão magnética por suscetibilidade magnética foi possível identificar dois corpos principais, o *Target* 1 em forma de dique e o *Target* 2 em forma de pipa. De acordo com Gorczyk & Vogt (2018), corpos em formato de pipa e diques ocorrem em níveis de crosta superior. Além disso, uma das anomalias (*Target* 1) se apresenta rotacionada no modelo magnético mostrando direção N-S. A inversão sugere ainda uma provável interação em subsuperfície com granitos não exumados, demonstrando continuidade da mineralização em profundidades superiores a 800 m. Essa interação levou a retrabalhamento da crosta pré-existente remobilizando Ferro de minerais silicatados e óxidos, re-precipitando como magnetita. O principal condutor dessas magnetitas neo-formadas seriam diques graníticos.

Levando-se em consideração o conjunto de informações acima é possível atribuir a participação de diques graníticos ao enriquecimento em magnetita das rochas ricas em Fe e, portanto, na formação dos depósitos de Fe-*Skarn* no NASJC.

REFERÊNCIAS

Abrahão-Filho E.A. 2016. Rochas piroxeníticas ricas em ferro do Maciço São José do Campestre, Rio Grande do Norte, Brasil. Dissertação de Mestrado, Instituto de Geociências, Universidade de Brasília, Brasília, 197 p.

Aksyuk A.M., Zharikov V.A. 1988. The phlogopite skarn deposits: physical- chemical conditions of formation, in Zachrisson, E., ed., Proceedings of the 7th Quadrennial IAGOD Symposium: Stuttgart, E. Schweizer-bart'sche Verlagsbuchhandlung, p. 321–326.

Al Macky M., Rosid M., Jaman A. 2020. Mapping of gold mineralization using 3D inversion magnetic data at Zone X, West Java. Journal of Physics: Conference Series. DOI: 1494. 012034. 10.1088/1742-6596/1494/1/012034.

Almeida F.F.M., Hasuy Y., Brito Neves B.B., Fuck R.A. 1977. Províncias estruturais brasileiras. In: Simpósio de Geologia do Nordeste, 8, Campina Grande, 1977. Atas. Campina Grande, SBG, p.363-391.

Almeida F.F.M., Hasui Y., Brito Neves B.B.; Fuck R.A. 1981. Brazilian structural provinces: an introduction. Earth-Science Reviews, Amsterdam: Elsevier, v. 17, n. 1/2, p. 1-29.

An, S., Zhou, K., Wang, J., Yang, H., & Zhang, Z. 2018. Integrated analysis of gravity and magnetic fields in the Eastern Tianshan Belt, Xinjiang, Central Asia: Implications for Cu-Au-Fe polymetallic deposits exploration. Journal of Applied Geophysics.

Anderson K., Wall F., Rollinson G., Moon C. 2014. Quantitative mineralogical and chemical assessment of the Nkout iron ore deposit, Southern Cameroon. Ore Geology Reviews. 62. 25–39. 10.1016/j.oregeorev.2014.02.015.

Angelim, L.A.A., Medeiros, V.C., Nesi, J.R. 2006. Programa Geologia do Brasil –PGB. Projeto Geologia e Recursos Minerais do Estado do Rio Grande do Norte. Mapa geológico do Estado do Rio Grande do Norte. Escala. 1:500.000. Recife: CPRM/FAPERN, 2006. 1mapa color

Antunes, A. F. 2000. Cinemática de Alojamento e Petrografia do Pluton de Monte das Gameleiras, Porção SE do Estado do Rio Grande do Norte. Trabalho de Conclusão de Curso em Geologia, Universidade Federal do Rio Grande do Norte. 90 p.

Araujo, I. L. de. 2012. Caracterização do arcabouço tectônico do terreno São José do Campestre, Província Borborema, com base em dados de aerogeofísica. 2012. ix, 98 f., il. Dissertação (Mestrado em Geociências Aplicadas) —Universidade de Brasília, Brasília.

Araújo, M. G. S., Brito Neves, B. B., Archanjo, C. J. 2001. Idades 40Ar/39Ar do magmatismo básico Meso-Cenozóico da Província Borborema Oriental, nordeste do Brasil. In: Anais do 19° Simpósio de Geologia do Nordeste, Natal. P .260-261.

Archanjo C.J., Hollanda M.H.B.M., Rodrigues S.W., Neves B.B.B., Armstrong R. 2008. Fabrics of pre- and syntectonic granite plutons and chronology of shear zones in the Eastern Borborema Province, NE Brazil. Journal of Structural Geology, 30(3):310-336. DOI: 10.1016/j.jsg.2007.11.011

Archanjo C., Viegas, L. & Hollanda, H. & Souza L., Liu D.. 2012. Timing of the HT/LP transpression in the Neoproterozoic Seridó Belt (Borborema Province, Brazil): Constraints from U\Pb (SHRIMP) geochronology and implications for the connections between NE Brazil and West Africa. Gondwana Research. 10.1016/j.gr.2012.05.005.

Arthaud, M.H., Caby, R., Fuck, R.A., Dantas, E.L., & Parente, C.V. 2008. Geology of the northern Borborema Province, NE Brazil and its correlation with Nigeria, NW Africa.

Bastos C.F., Caxito F.A., Vale J.A.R., Silveira D.A., Rodrigues J.B., Alkmim A.R., Valeriano C.M., Santos E.J. 2019. An Ediacaran back-arc basin preserved in the Transversal Zone of the Borborema Province: Evidence from geochemistry, geochronology and isotope systematics of the Ipueirinha Group, NE Brazil. Precambrian Research, 320:213-231. DOI: 10.1016/j.precamres.2018.11.002

Barton M.D., Johnson D.A. 1996. Evaporitic-source model for igneous-related Fe oxide-(REE- Cu-Au-U) mineralization. Geology, 24(3):259-262.

Bridges I.C. 1974. Machine contouring using minimum curvature. Geophysics, 39:39-48. DOI: 10.1190/1.1440410

Brito-Neves B.B., Santos E.J., Van-Schmus W.R.Q. 2000. Tectonic history of the Borborema province. In: Cordani U.G., Milani E.J., Thomaz-Filho A., Campos D.A. (eds.). Tectonic Evolution of South America. 31st International Geological Congress. Rio de Janeiro, p. 151- 182.

Brito neves, B. B.; Campos neto, M. C.; Schmus, W. R. V.; Santos, E. J. 2001. O Sistema Pajeú-Paraíba e o maciço São José do Campestre no leste da Borborema. Revista Brasileira de Geociências. São Paulo, v.31(2), p. 173-184.

Brito-Neves B.B., Fuck R.A., Pimentel M.M. 2014. The Brasiliano collage in South America: a review. Brazilian Journal of Geology, 44(3):493-518. DOI: 10.5327/Z2317-4889201400030010

Brito-Neves B.B., Santos E.J., Fuck R.A., Santos L.C.M.L. 2016. A preserved early Ediacaran magmatic arc at the northernmost portion of the Transversal Zone central subprovince of the Borborema Province, Northeastern South American. Brazilian Journal of Geology, 46(4):491- 508. DOI: 10.1590/2317-4889201620160004

Bucher, K., Grapes, R., 2011. Petrogenesis of Metamorphic Rocks. Berlin (Germany): Ed. Springer. 8th Edition.

Cavalcante, R., Galindo, A. C., Silva, F. C. A., De Souza, R. F. 2014. Química mineral e condições de cristalização do Pluton Granítico Barcelona, extremo nordeste da Província Borborema, Nordeste do Brasil. Pesquisas em Geociências, 41(3), 257-272.

Clark D.A., Emerson D.W. 1991. Notes on rock magnetization characteristics in applied geophysical studies. Exploration Geophysics, 22: 547-555.

Corrêa R.,Oliveira C., Dantas E., Schutesky M., Hollanda, M. B. M. de. 2021. The root zones of the Seridó W-skarn system, northeastern Brazil: Constraints on the metallogenesis of a large Ediacaran tungsten Province. Ore Geology Reviews. 128. 10.1016/j.oregeorev.2020.103884.

Corrêa R.S., Oliveira C., Dantas E., Botelho N.F. 2020. Hydrothermal footprint related to regional-scale shear zone-controlled scheelite mineralization, Seridó W-skarn system, northeastern Brazil. Journal of South American Earth Sciences. 103. 102755. 10.1016/j.jsames.2020.102755.

Correa, R. T., Vidotti, R. M., Oksum, E. (2016). Curie surface of Borborema province, Brazil. Tectonophysics, 679, 73-87.

Costa F.G., Palheta E.S.M., Rodrigues J.B., Gomes I.P. Vasconcelos A.M. 2015. Geochemistry and U–Pb zircon ages of plutonic rocks from the Algodões granite-greenstone terrane, Tróia Massif, northern Borborema Province, Brazil: Implications for

Paleoproterozoic subduction- accretion processes. Journal of South American Earth Sciences, 59:45-68. DOI: 10.1016/j.jsames.2015.01.007

Dantas E.L. 1997. Geocronologia U-Pb e Sm-Nd de terrenos Arqueanos e paleoproterozóicos do Maciço Caldas Brandão, NE do Brasil. PhD Thesis, Instituto de Geociências e Ciências Exatas, Universidade Estadual Paulista, São Paulo, 208 p.

Dantas E.L., Van-Schmus W.R., Hackspacher P.C., Fetter A.H., Brito-Neves B.B., Cordani U., Nutman A.P., Williams I.S. 2004. The 3.4–3.5 Ga São José do Campestre massif, NE Brazil: remnants of the oldest crust in South America. Precambrian Research, 130: 113-137. DOI: 10.1016/j.precamres.2003.11.002

Dantas E.L., Souza Z.S., Wernick E., Hackspacher P.C., Martin H., Xiadong D., Li J.W. 2013. Crustal growth in the 3.4-2.7 Ga São José do Campestre Massif, Borborema Province, NE Brazil. Precambrian Research, 227:120-156. DOI: 10.1016/j.precamres.2012.08.006

Deer, W.A.; Howie, R.A.; Zussman, J. Minerais constituintes das rochas: uma introdução. Macedo, C.A.R. (Trad.). 2nd ed. Lisboa: Fundação Calouste Gulbenkian. ISBN: 972-31- 084-1.

Dentith, M. C., & Mudge, S. 2014. Geophysics for the Mineral Exploration Geoscientist. Cambridge University Press.

Dias, L. G. D. S. 2006. Caracterização geológica, geoquímica e geocronológica da suíte plutônica enoproterozóica da região de Serrinha, porção centro-leste do maciço São José de Campestre, sudeste do RN. Dissertação de Mestrado (PPGG/UFRN), Universidade Federal do Rio Grande do Norte.

Einaudi, M.T., Meinert, L.D., Newberry, R.J., 1981. Skarn deposits. Econ. Geol., Seventy-fifth Anniversary Volume, 317-391

Einaudi, M.T., Burt, D.M., 1982. Introduction - Terminology, Classification and Composition of Skarn Deposits. Econ. Geol. 77, 745-754.

Figueiredo B.S. 2012. Geoquímica e gênese das formações ferríferas e metacarbonatos da porção sul do Maciço São José do Campestre, Província Borborema. MS Dissertation, Instituto de Geociências, Universidade de Brasília, Brasília, 109 p.

Fries M., Zago M. M., da Silva F. G., 2020. A geophysical study contributing to analysis and characterization of a localized copper occurrence, Journal of Applied Geophysics, Volume 179, , 104129, ISSN 0926-9851, https://doi.org/10.1016/j.jappgeo.2020.104129.

Fruchting, A. 2017. Estratégias para utilização de dados geofísicos na exploração de mineralizações do tipo Ni-Cu-PGE: a descoberta do depósito de limoeiro, PE. 2017. ix, 89 f., il. Dissertação (Mestrado em Geologia) —Universidade de Brasília, Brasília.

Ganade de Araújo, C. E., Weinberg, R. F., Cordani, U. G. 2014. Extruding the Borborema Province (NEBrazil): a two-stage Neoproterozoic collision process. Terra Nova, 26(2), 157-168.

Gonçalves, L. C. 2009.Contribuição geofísica à análise do arcabouço tectônico do domínio Rio Grande do Norte, Província Borborema - NE Brasil. 2009. xi, 100 f., il. Dissertação (Mestrado em Geologia) -Universidade de Brasília, Brasília.

Gonçalves B.F., Sampaio E.E.S. 2013. Interpretation of airborne and ground magnetic and gamma-ray spectrometry data in prospecting for base metals in the central-north part of the Itabuna-Salvador-Curaçá Block, Bahia, Brazil. Interpretation, 1: T85-T100. DOI: 10.1190/INT- 2012-0002.1

Gorczyk, W., & Vogt, K. 2018. Intrusion of magmatic bodies into the continental crust: 3-D numerical models. Tectonics, 37, 705–723. https://doi.org/10.1002/2017TC004738

Guy, B. 1993. Banded skarns, an example of geochemical dissipative structure.

Hall, D.L., Cohen, L.H., and Schiffman, P., 1988, Hydrothermal alteration associated with the Iron Hat iron skarn deposit, eastern Mojave Desert, San Bernardino County, California: ECONOMIC GEOLOGY, v. 83, p. 568–587.

Hao, H. Lentz, D. Jianwei, L. Hall, D., 2014. Re-equilibration processes of magnetite from iron skarn deposits. Acta Geologica Sinica (English Edition), 88 (supp. 22): 354-356.

Hollanda, M. H. B. M. D., Souza Neto J., Archanjo C., Stein H., Maia A. 2017. Age of the granitic magmatism and the W-Mo mineralizations in skarns of the Seridó belt (NE Brazil) based on zircon U-Pb (SHRIMP) and Re-Os determinations. Journal of South American Earth Sciences. 79. 10.1016/j.jsames.2017.07.011.

Hollanda, M. H. B. M. D., Archanjo, C. J., Macedo Filho, A. A., Fossen, H., Ernst, R. E., de Castro, D. L., Melo, A. C., Oliveira, A. L. 2019. The Mesozoic Equatorial Atlantic Magmatic Province (EQUAMP). In Dyke Swarms of the World: A Modern Perspective (pp. 87-110). Springer, Singapore.

Honsho, C., Yamazaki, T., Ura, T., Okino, K., Morozumi, H., and Ueda, S. 2016, Magnetic anomalies associated with abundant production of pyrrhotite in a sulfide deposit in the Okinawa Trough, Japan, Geochem. Geophys. Geosyst., 17, 4413– 4424, doi:10.1002/2016GC006480.

Hunt C., Moskowitz B.M., Banerje S.K. 1995. Magnetic properties of rocks and minerals. In: Ahrens T.J. (ed.). A Handbook of Physical Constants vol. 3. Washington: American Geophysical Union, p. 189-204. DOI: 10.1029/RF003p0189

Jardim de Sá, E. F., 1994. A Faixa Seridó (Província Borborema, NE do Brasil) e o seu significado geodinâmico na Cadeia Brasiliana/Pan-Africana. Instituto de Geociências da Universidade de Brasília, Brasília, Tese de Doutorado, 804p.

Jesus B. A.-de. 2011. Rochas máficas e ultramáficas do Complexo Riacho da Telha, Maciço São José do Campestre, Província Borborema - NE do Brasil. MS Dissertation, Instituto de Geociências, Universidade de Brasília, Brasília, 80 p.

Jiang D, Zeng Z, Zhou S, Guan Y, Lin T, Lu P. 2020. Three-Dimensional Magnetic Inversion Based on an Adaptive Quadtree Data Compression. Applied Sciences. 10(21):7636. https://doi.org/10.3390/app10217636

Khesin B., Feinstein S., Vapnik Y., Itkis S., Leonhardt R. 2005. Magnetic study of metamorphosed sedimentary rocks of the Hatrurim formation, Israel. Geophysical Journal International, 162: 49- 63. DOI: 10.1111/j.1365-246X.2005.02630.x

Kim E. J., Shin D., Shin S., Nam H.T., Park S. 2015. Skarn zonation and rock physical properties of the Wondong Fe-Pb-Zn polymetallic deposit, Korea. Geosciences Journal, 19:587-598. DOI: 10.1007/s12303-015-0017-2

Landim, P. M. B. Análise estatística de dados geológicos multivariados. São Paulo:Oficina de Textos, 2011. 208 p. ISBN: 978-85-7975-032-8.

LASA Engenharia e Prospecções S/A, PROSPECTORS Aerolevantamentos e Sistemas LTDA. 2009. Projeto Aerogeofísico Paraíba - Rio Grande do Norte; Pernambuco - Paraíba: relatório final do levantamento e processamento dos dados magnetométricos e gamaespectométricos. Internal report. Rio de Janeiro: Lasa Engenharia e Prospecções; Prospectors Aerolevantamentos e Sistemas. Programa Geologia do Brasil (PGB). 401 p.

Lima H., Pimentel M., Santos L., Dantas, E. 2019. Isotopic and geochemical characterization of the metavolcano-sedimentary rocks of the Jirau do Ponciano dome: A structural window to a Paleoproterozoic continental ARC root within the Southern Borborema province, Northeast Brazil. Journal of South American Earth Sciences, 90:54-69. DOI: 10.1016/j.jsames.2018.12.002

Lino L.M., Cavallaro F.A., Vlach S.R.F., Coelho D.C. 2018. 2D magnetometric modeling of a basic-intermediate intrusion geometry: geophysical and geological approaches applied to the Limeira intrusion, Paraná Magmatic Province (SP, Brazil). Brazilian Journal of Geology, 48(2):305-315. DOI: 10.1590/2317-4889201820180099

Lishchuk V., Lund C., Koch, P., Pålsson B., Gustafsson M. 2018. Geometallurgical characterisation of Leveäniemi iron ore – unlocking the patterns. Minerals Engineering, Volume 131, 2019, Pages 325-335, ISSN 0892-6875, https://doi.org/10.1016/j.mineng.2018.11.034.

Lishchuk, V.; Lund, C.; Ghorbani, Y. 2019. Evaluation and comparison of different machine-learning methods to integrate sparse process data into a spatial model in geometallurgy. Minerals Engineering, v. 134, p. 156-165. https://doi.org/10.1016/j.mineng.2019.01.032

Liu, Shuang & Fedi, Maurizio & Hu, Xiangyun & Ou, Yang & Baniamerian, Jamaledin & Zuo, Boxin & Liu, Yuegao & Zhu, Rixiang. 2018. 3D inversion of magnetic data in the simultaneous presence of significant remanent magnetization and self-demagnetization: example from Daye iron-ore deposit, Hubei province, China. Geophysical Journal International. 215. 10.1093/gji/ggy299.

Markowski A., Vallance J., Chiaradia M., Fontboté L. 2006. Mineral zoning and gold occurrence in the Fortuna skarn mine, Nambija district, Ecuador. Mineralium Deposita, 41:301-321. DOI: 10.1007/s00126-006-0062-x

Mazhari, Nazi & Malekzadeh Shafaroudi, Azadeh & Ghaderi, Majid. (2017). Detecting and mapping different types of iron mineralization in Sangan mining region, NE Iran, using satellite image and airborne geophysical data. Geosciences Journal. 21. 137-148. 10.1007/s12303-016-0018-9.

McGladrey A.J., Olivo G.R., Silva A.M., Oliveira G.D., Neto B.B., Perrouty S. 2017. The integration of physical rock properties, mineralogy and geochemistry for the exploration of large zinc silicate deposits: a case study of the Vazante zinc deposits, Minas Gerais, Brazil. Journal of Applied Geophysics, 136:400-416. DOI: 10.1016/j.jappgeo.2016.11.013

Medeiros, V. C. D. 2004. Evolução geodinâmica e condicionamento estrutural dos terrenos Piancó-Alto Brígida e Alto Pajeú, domínio da Zona Transversal, NE do Brasil. Tese de Doutorado (PPGG/UFRN), Universidade Federal do Rio Grande do Norte. 199 p.

Medeiros, V. C., Cavalcante, R., Cunha, A. L. C., Dantas, A. R., Costa, A. P., Brito, A. A., Rodrigues, J. B., Silva, M. A. 2017. O furo estratigráfico de Riacho Fechado (Currais Novos/RN), domínio Rio Piranhas-Seridó (província Borborema, NE Brasil): procedimentos e resultados. Estudos Geológicos, 27(3), 3-44.

Meinert L.D. 1992. Skarns and skarn deposits. Geoscience Canada, 19(4):145-162.

Meinert LD 2000. Gold skarns related to epizonal plutons. Rev Econ Geol v 13:347–375

Meinert L.D., Dipple G.M., Nicolescu S. 2005. World skarn deposits. Economic Geology 100th Anniversary Volume, SI:299-336. DOI: 10.5382/AV100.11

Meinert, Lawrence. (2020). Meinert GP v9n11.

Miller H.G. and Singh V. 1994 Potential Field Tilt a New Concept for Location of Potential Field Sources. Journal of Applied Geophysics, 32, 213-217. https://doi.org/10.1016/0926-9851(94)90022-1

Mizusaki, A. M. P., Thomaz-Filho, A., Milani, E. J., De Césero, P. 2002. Mesozoic and Cenozoic igneous activity and its tectonic control in northeastern Brazil. Journal of South American Earth Sciences, 15(2), 183-198.

Moraes, J. D. dos S. de. 2020. Gênese das formações ferríferas da porção central do Maciço São José do Campestre, Rio Grande do Norte, Nordeste do Brasil. 2020. 52 f., il. Dissertação (Mestrado em Geologia) — Universidade de Brasília, Brasília.

Moraes J.D., Cordeiro P.F., Abrahão Filho E., Oliveira J.R. & Silva Filho C.V. 2020. Metamorphic disturbances of magnetite chemistry and the Sm-Nd isotopic system of reworked Archean iron formations from NE Brazil. Geoscience frontiers, 101131.

Mueller A.G., 1997. The Nevoria gold skarn deposit in Archean iron-formation, Southern Cross greenstone belt, Western Australia; I, Tectonic setting, petrography, and classification. Economic Geology, 92(2):181–209. DOI: 10.2113/gsecongeo.92.2.181

Nabighian M.N., & Grauch V.J.S., Hansen R.O., Lafehr T.,Pearson W & Phillips J.D. 2005. The historical development of the magnetic method in exploration. Geophysics. 70. 10.1190/1.2133784.

Nadoll, P., Angerer, T., Mauk, J.L., French, D., Walshe, J., 2014. The chemistry of hydrothermal magnetite: A review. Ore Geology Reviews 61, 1–32.

Neves S.P., Bruguier O., Vauchez A., Bosch D., Silva J.M.R., Mariano G. 2006. Timing of crustal formation, deposition of supracrustal sequences and Transamazonian and Brasiliano metamorphism in easter Borborema Province (BE Brazil): Implications for western Gondwana assembly. Precambrian Research, 149(3-4):197-216. DOI: 10.1016/j.precamres.2006.06.005

Neves, S. P. 2011. Atlantica revisited: new data and thoughts on the formation and evolution of a longlived continent. International Geology Review, 53(11-12), 1377-1391.

Neves S.P., Bruguier O., Silva J.M., Mariano G., Filho A.F., & Teixeira C.M. 2015. From extension to shortening: Dating the onset of the Brasiliano Orogeny in eastern Borborema Province (NE Brazil). Journal of South American Earth Sciences, 58, 238-256.

Ngonge, E. D., de Hollanda, M. H. B. M., Archanjo, C. J., de Oliveira, D. C., Vasconcelos, P. M. P., Muñoz, P. R. M. 2016. Petrology of continental tholeiitic magmas forming a 350-km-long Mesozoic dyke swarm in NE Brazil: constraints of geochemical and isotopic data. Lithos, 258, 228-252.

Nielsen B.M., Rasmussen T.M. 2002. Geological correlation of magnetic susceptibility and profiles from Nordre Strømfjord, southern West Greenland. Geology of Greenland Survey Bulletin, 191:48–56. DOI: 10.1016/S0301-9268(98)00098-9

NOAA. 2019. International Geomagnetic Reference Field. Available on: <https://www.ngdc.noaa.gov/IAGA/vmod/igrf.html>. Accessed in: Oct. 2020.

Oliveira, R. G., Medeiros, W. E. 2018. Deep crustal framework of the Borborema Province, NE Brazil, derived from gravity and magnetic data. Precambrian Research, 315, 45-65.

Padilha, A. L., Vitorello, Í., Pádua, M. B., Bologna, M. S. 2014. Electromagnetic constraints for subduction zones beneath the northwest Borborema province: Evidence for Neoproterozoic Island arc–continent collision in northeast Brazil. Geology, 42(1), 91-94.

Padilha, A. L., Vitorello, Í., Pádua, M. B., Fuck, R. A. 2016. Deep magnetotelluric signatures of the early Neoproterozoic Cariris Velhos tectonic event within the Transversal sub-province of the Borborema Province, NE Brazil. Precambrian Research, 275, 70-83.

Padilha, A. L., Vitorello, I., Pádua, M. B., Fuck, R. A. 2017. Cryptic signatures of Neoproterozoic accretionary events in northeast Brazil imaged by magnetotellurics: Implications for the assembly of West Gondwana. Tectonophysics, 699, 164-177.

Parente C.V., Veríssimo C.U.V., Botelho N.F., Santos T.J.S., Oliveira C.G., Lira-Júnior J.A., Martins D.T. 2015. Fe-Cu skarns deposits in the Santa Quiteria magmatic arc, Borborema Province, Brazil. Brazilian Journal of Geology, 45:359-382. DOI: 10.1590/2317- 488920150030264

Pereira L.C.L., Santos L.C.M.L., Carrino T.A. 2019. The role of airborne geophysics in the investigation of gold occurrences in the Itapetim Region, Borborema Province, Northeast Brazil. Brazilian Journal of Geology, 49(3):1-17. DOI: 10.1590/2317-4889201920190028

Pérez-Barnuevo L., Lévesque S. & Bazin C. 2018. Drill core texture as geometallurgical indicator for the Mont-Wright iron ore deposit (Québec, Canada). Minerals Engineering. 122. 10.1016/j.mineng.2018.03.020.

Pilkington M. 2015. Dsim 3d: Software to Perform Unconstrained 3d Inversion of Magnetic Data. Place of publication not identified: Natural Resources Canada. http://oaresource.library.carleton.ca/wcl/2016/20160718/M183-2-7749-eng.pdf. Accessed August 23, 2022.

Pinheiro, H. M. D. 2009. Caracterização petrográfica e textural de diques graníticos e suas encaixantes em uma porção central do Núcleo Arqueano, Maciço São José de Campestre, RN, nordeste do Brasil. Trabalho de Conclusão de Curso, Universidade Federal do Rio Grande do Norte.

Pirajno, Franco. 2009. Hydrothermal Processes and Mineral Systems. 10.1007/978-1-4020-8613-7_10.

Purtov, V.K., Kholodnov, V.V., Anfilogov, V.N., and Nechkin, G.S., 1989, The role of chlorine in the formation of magnetite skarns: International Geology Review, v. 31, p. 63–71.

Raju, P.V. Sunder, and K. Satish Kumar. 2020. "Magnetic Survey for Iron-Oxide-Copper-Gold (IOCG) and Alkali Calcic Alteration Signatures in Gadarwara, M.P, India: Implications on Copper Metallogeny" Minerals 10, no. 8: 671. https://doi.org/10.3390/min10080671

Ray, G.E., Webster, I.C.L., 1991. Geology and Mineral Occurences of the Merry Widow Skarn Camp, Northern Vancouver Island, 92L/6. B.C. Ministry of Energy, Mines and Petroleum Resources, Open File 1991-8.

Roig H.L., Dantas E.L. 2013. Folha SB.25-Y-A-I São José do Campestre: carta geológica - escala 1:100.000. Brasília, Serviço Geológico do Brasil - CPRM. color map. Available on: <http://rigeo.cprm.gov.br/jspui/handle/doc/17669>. Accessed in: Oct. 2020.

Santos E.J., Medeiros V.C. 1999. Constraints from granitic plutonism on Proterozoic crustal growth of the transverse zone, Borborema province, NE-Brazil. Revista Brasileira de Geociências, 29(1):73-84. DOI: 10.25249/0375-7536.1999297384

Santos L.C.M.L., Dantas E.L., Santos E.J., Santos R.V., Lima H.M. 2015. Early to late Paleoproterozoic magmatism in NE Brazil: The Alto Moxotó Terrane and its tectonic implications for the pre-Western Gondwana assembly. Journal of South American Earth Sciences, 58:188- 209. DOI: 10.1016/j.jsames.2014.07.006

Santos L.C.M.L., Dantas E.L., Cawood P.A., Santos E.J., Fuck R.A. 2017. Neoarchean crustal growth and Paleoproterozoic reworking in the Borborema Province, NE Brazil: insights from geochemical and isotopic data of TTG and metagranitic rocks of the Alto Moxotó Terrane. Journal of South American Earth Sciences, 79:342-363. DOI: 10.1016/j.jsames.2017.08.013

Santos L.C.M.L., Dantas E.L., Cawood P.A., Lages G.A., Lima H.M., Santos E.J. 2018. Accretion tectonics in western Gondwana deduced from Sm- Nd isotope mapping of terranes in the Borborema Province, NE Brazil. Tectonics, 37(8):2727-2743. DOI: 10.1029/2018TC005130

Shafiei, Behnam & Shahabpour, J. 2008. Gold Distribution in Porphyry Copper Deposits of Kerman Region, Southeastern Iran. Journal of Sciences Islamic Republic of Iran. 19. 247-260.

Shapiro, S. S., Wilk, M. B. 1965. An analysis of variance test for normality (complete samples), Biometrika, Volume 52, Issue 3-4, December, Pages 591–611, https://doi.org/10.1093/biomet/52.3-4.591

Sheibi M., Mirnejad, H. & Moghaddama, M. 2016. Magnetic susceptibility anisotropy as a predictive exploration tool of metasomatic iron oxide deposits: Example from the Panj-Kuh iron ore body, NE Iran. Ore Geology Reviews. 72. 612–628. 10.1016/j.oregeorev.2015.08.024. Sial A., Ferreira V. 2016. Magma associations in Ediacaran granitoids of the Cachoeirinha– Salgueiro and Alto Pajeú terranes, northeastern Brazil: Forty years of studies. Journal of South American Earth Sciences, 68:113-133. DOI: 10.1016/j.jsames.2015.10.005

Sial, A.N., & Ferreira, V.P. 2016. Magma associations in Ediacaran granitoids of the Cachoeirinha–Salgueiro and Alto Pajeú terranes, northeastern Brazil: Forty years of studies. Journal of South American Earth Sciences, 68, 113-133.Souza et al., 2016

Silva-Filho C.V.R. 2012. Isótopos de Nd aplicados à datação direta de formações ferríferas paleoarqueanas do maciço São José do Campestre, Rio Grande do Norte-RN. MS Dissertation, Instituto de Geociências, Universidade de Brasília, Brasília, 86 p.

Sokolov, G.A., and Grigorev, V.M., 1977, Deposits of iron, in Smirnov, V.I., ed., Ore deposits of the USSR: London, Pittman, v. 1, p. 7–113.

Souza-Neto J.A., Legrand J.M., Volfinger M., Pascal M.L., Sonnet P. 2008. W–Au skarns in the Neo-Proterozoic Seridó Mobile Belt, Borborema Province in northeastern Brazil: an overview with emphasis on the Bonfim deposit. Mineralium Deposita, 43(2):185-205. DOI: 10.1007/s00126-007-0155-1

Souza, Z. S.; Vasconcelos, P. M.; Nascimento, M. A. L.; Silveira, F. V.; Paiva, H. S.; Dias, L. G. S.; Thied, D.; Carmo, I. O. 2003. 40Ar/39Ar geochronology of Mesozoic and Cenozoic magmatism in NE Brazil. In: Proceedings of IV South American Symposium on Isotope Geology, Salvador.

Souza, Z. S., Martin, H., Peucat, J. J., Jardim De Sá, E. F., Macedo, M. H. D. F. 2007. Calc-alkaline magmatism at the archean–proterozoic transition: the caicó complex basement (NE Brazil). Journal of Petrology, 48(11), 2149-2185.

Souza Z.S., Kalsbeek F., Deng X., Frei R., Dantas E.L., Li J., Pimentel M.M., & Galindo A.C. 2016. Generation of continental crust in the northern part of the Borborema Province, northeastern Brazil, from Archaean to Neoproterozoic. Journal of South American Earth Sciences, 68, 68-96.

Storch HV, Zwiers F.W. 2003. Analysis of Variance. In: Storch HV, Zwiers FW Statistical analysis in climate research, 2nd edn. Cambridge University Press, Cambridge, pp 171-192.

Stradling A W. 1991. Development of a mathematical model of a crossbelt magnetic separator. Minerals Engineering 4:733-745

Sun S, & Chao C. 2016. A self-constrained inversion of magnetic data based on correlation method. Journal of Applied Geophysics. 135. 10.1016/j.jappgeo.2016.09.022.

Yang Y. S., Li Y. Y., Liu T. Y., Zhan Y. L., & Feng J. 2011. Interactive 3D forward Modeling of Total Field Surface and Three-Component Borehole Magnetic Data for the Daye Iron-Ore Deposit (Central China). Journal of Applied Geophysics, 75, 254-263. http://dx.doi.org/10.1016/j.jappgeo.2011.07.010

Uieda L., Oliveira V.C., Barbosa V.C.F. 2014. Geophysical tutorial: Euler deconvolution of potential-field data. The Leading Edge, 33(4):361-476. DOI: 10.1190/tle33040448.1

Van-Schmus W.R., Brito-Neves B.B., Hackspacher P.C., Babinski M. 1995. U/Pb and Sm/Nd geochronologic studies of the eastern Borborema Province, Northeast Brazil: initial conclusions. Journal of South American Earth Sciences, 8(3-4):267-288. DOI: 10.1016/0895- 9811(95)00013-6

Van-Schmus W.R., Oliveira E.P., Silva-Filho A.F., Toteu F., Penaye J., Guimarães I.P. 2008. Proterozoic links between the Borborema province, NE Brazil, and the central African fold belt. Geolical Society of London, 294(1):66-69. DOI: 10.1144/SP294.5

Van-Schmus W.R., Kozuch M., Brito-Neves B.B. 2011. Precambrian history of the Zona Trasnversal of the Borborema Province, NE Brazil; Insights from Sm-Nd and U-Pb geochronology. Journal of South American Earth Sciences, 31(2-3):227-252. DOI: 10.1016/j.jsames.2011.02.010

Vauchez, A.; Neves, S.; Caby, R.; Corsini, M.; Silva, M. R.; Arthaud, M.; Amaro, V. 1995. The Borborema Shear Zone system, NE Brazil. Journal of South American Earth Sciences, 8: p. 247-266.

Verduzco B., Fairhead J., Green, C., & MacKenzie, C. 2004. New Insights into magnetic derivatives for structural imaging. The Leading Edge. 23. 116-119. 10.1190/1.1651454.